DOTTORATO DI RICERCA IN SCIENZE CHIMICHE

CICLO XXVIII

COORDINATORE Prof. ANDREA GOTI

INNOVATIVE METHODS WITH LOW ENERGY CONSUMPTION FOR

EFFICIENT CO_2 CAPTURE AND ITS RE-USE AS A BUILDING BLOCK

FOR THE SYNTHESIS OF USEFUL CHEMICALS

Settore Scientifico Disciplinare CHIM/03

Dottorando	**Tutore**
Dott. Francesco Barzagli	Prof. Fabrizio Mani
_____	_____
Coordinatore	**Co-Tutore**
Prof. Andrea Goti	Dott. Maurizio Peruzzini
_____	_____

Anni 2012/2015

Contents

Chapter 3. The Formulation of New Liquid Sorbents and the Experimental Methodologies Used for their Test

Chapter 4. CO_2 Absorption with Non-Aqueous Solvents Based on 2-amino-2-methyl-1-propanol (AMP)

Chapter 5. Carbon Dioxide Removal for Biogas Upgrading

Chapter 6. CO₂ Absorption with Solvent-Free Secondary Amines

Chapter 7. Biphasic Systems in the CO₂ Capture Processes

Chapter 8. CO₂ Capture and Utilization: Production of Urea and 1,3-Disubstituted Ureas

Chapter 9. The Chemistry of Resorcinol Carboxylation and its Possible Application to CO$_2$ Removal from Exhaust Gases

1. Introduction

1.1. Background

The removal of carbon dioxide from gas mixtures is an important operation, which can find application in numerous industrial processes. CO_2 capture is exploited to clean up the exhaust gases from fossil-fuel fired power plants, steel mills, cement factories and petrochemical and chemical plants, where huge quantities of CO_2 are produced. Another important application relates to the production of ammonia and hydrogen, where CO_2 is produced as a byproduct, and to the natural gas sweetening, because carbon dioxide present in natural gas will reduce the heating value of the gas. Moreover, environmental concerns, such as the global climate change, are now focused amongst the most important and challenging issues facing the world community, and have motivated intensive research on CO_2 capture and sequestration.

The main concern is the world demand for primary energy which is currently more than doubled in the last 40 years (Figure 1.1) and it is expected to increases by 37% between 2013 and 2035 [1-3].
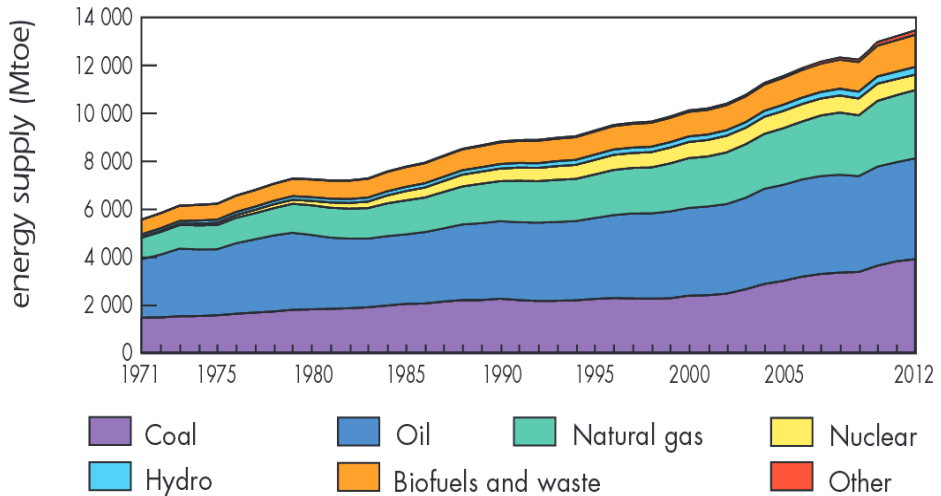
Figure 1.1. World total primary energy supply from 1971 to 2012 by fuel (Mtoe = Million tonnes of oil equivalent). In these graphs, peat and oil shale are aggregated with coal. "Other" includes geothermal, solar, wind, heat, etc [4].

A high percentage of this demand is covered by fossil fuels: today's share of fossil fuels in the global mix is 82%, the same as it was 25 years ago, and the strong rise of renewable energy sources will only reduce the percentage to around 75% in 2035 [1-3]. Similar trends are forecasted by various studies; most of them indicate that fossil fuels will continue to play an important role for many decades to come [4-7]. The use of fossil fuels unfortunately has two important drawbacks. First, most of the conventional oil and gas reserves are located in a few world regions. Consequently, many countries are dependent on few other countries for their energy supplies [8]. Second, the combustion of fossil fuels is responsible for the largest emission of anthropogenic greenhouse gas (GHG), and its massive release into the atmosphere can significantly contribute to the acceleration of natural global warming and the related climate changes [9-13].

1.2.   Climate Changes and their Causes

Human influence on the climate system is clear, and recent anthropogenic emissions of greenhouse gases are the highest in history. Recent climate changes have had widespread impacts on human and natural systems.
Intergovernmental Panel on Climate Change (IPCC), Fifth Assessment Report (AR5), 2014.

1.2.1.   Observed Changes in the Climate System

The Earth's climate has changed throughout history. Just in the last 650,000 years there have been seven cycles of glacial advance and retreat, with the abrupt end of the last ice age about 7,000 years ago marking the beginning of the modern climate era — and of human civilization. Most of these climate changes are attributed to very small variations in Earth's orbit that change the amount of solar energy our planet receives. The current warming trend (Figure 1.2) is of particular significance because most of it is very likely human-induced and proceeds at a rate that is unprecedented in the past 1,300 years [9-13]. Earth-orbiting satellites and other technological devices have enabled scientists to collect many different types of information about our planet and its climate on a global scale. The study of these climate data collected over many years reveals the signals of a changing climate. There are several evidences of rapid climate change taking place in our days.
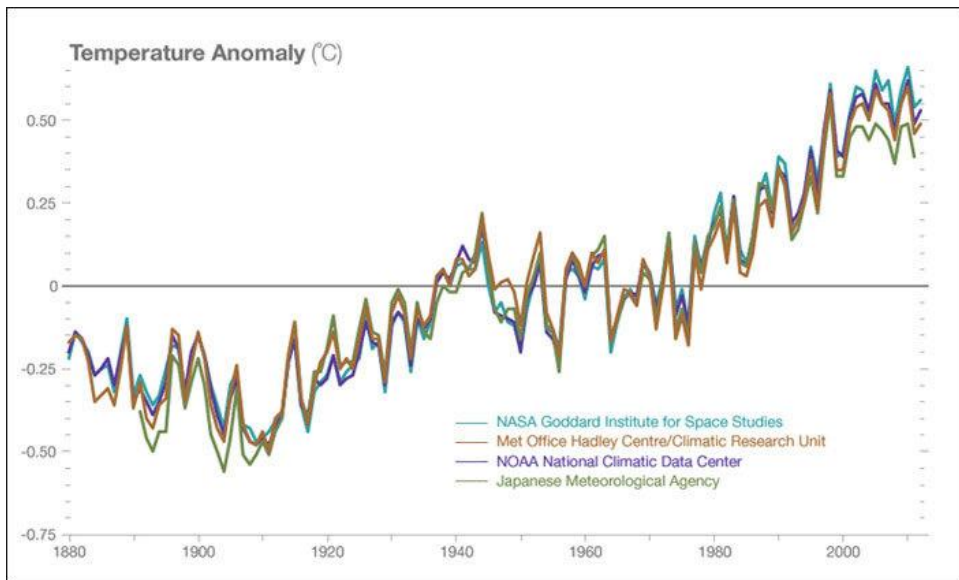
Figure 1.2. Temperature data from four international science institutions. All show rapid warming in the past few decades and that the last decade has been the warmest on record.

The period from 1983 to 2012 was likely the warmest 30-year period of the last 1400 years in the Northern Hemisphere, where such assessment is possible [14-18]. The globally averaged combined land and ocean surface temperature data, as calculated by a linear trend, show a warming of 0.85 °C over the period 1880 to 2012, when several independently produced datasets exist (Figure 1.2).

The oceans have absorbed much of this increased heat, with the top 700 meters of ocean showing warming of 0.17 °C since 1969 [19]. Global sea level rose about 17 centimeters in the last century, and the rate in the last decade is nearly double that of the last century [20]. The Greenland and Antarctic ice sheets have decreased in mass. Data from NASA's Gravity Recovery and Climate Experiment show Greenland lost 150 to 250 cubic kilometers of ice per year between 2002 and 2006, while Antarctica lost about 152 cubic kilometers of ice between 2002 and 2005. Both the extent and thickness of Arctic sea ice has rapidly decreased over the last several decades [21]. Glaciers are retreating almost everywhere around the world, including in the Alps (Figure 1.3), Himalayas, Andes, Rockies, Alaska and Africa [22]. The number of extreme events recorded is increasing since 1950; the number of cold days and nights has decreased and the number of warm days and nights has increased on the global scale, the frequency of heat waves has increased in large parts of Europe, Asia and Australia [14].

Figure 1.3. Two pictures taken at 100 years of difference (1906 - 2003) of Rhône Glacier (Valais, Switzerland) from Furka Pass show the effects of the increase in average temperature of the recent years.

1.2.2. Causes of Climate Change

Most climate scientists agree the main cause of the current global warming trend is human expansion of the "greenhouse effect" [9,23,24] — warming that results when the atmosphere traps heat radiating from Earth toward space. The heat-trapping nature of carbon dioxide and other gases such as methane, nitrous oxide, water vapor and chlorofluorocarbons, was demonstrated in the mid-19th century. In the 1860s, physicist John Tyndall recognized the Earth's natural greenhouse effect and suggested that slight changes in the atmospheric composition could bring about climatic variations. In 1896, Swedish scientist Svante August Arrhenius first speculated that changes in the levels of carbon dioxide in the atmosphere could substantially alter the surface temperature through the greenhouse effect [25]. There is no question that increased levels of greenhouse gases must cause the Earth to warm in response. Ice cores drawn from Greenland, Antarctica, and tropical mountain glaciers show that the Earth's climate responds to changes in greenhouse gas levels. They also show that in the past, large climate changes occurred in tens of years, very quickly geologically-speaking [26].

Anthropogenic greenhouse gas (GHG) emissions since the industrial era have driven large increases in the atmospheric concentrations of carbon dioxide (CO_2), methane (CH_4) and nitrous oxide (N_2O) (Figure 1.4). Total anthropogenic GHG emissions have continued to increase over 1970 to 2010 with larger absolute increases between 2000 and 2010, despite a growing number of climate change mitigation policies. Anthropogenic GHG emissions in 2010 have reached 49 $GtCO_2$-eq/yr. Emissions of CO_2 from fossil fuel combustion and industrial processes contributed about 76% of the total GHG emissions increase from 1970 to 2010, with a similar percentage contribution for the increase during the period 2000 to 2010 (Figure 1.5) [9].

4
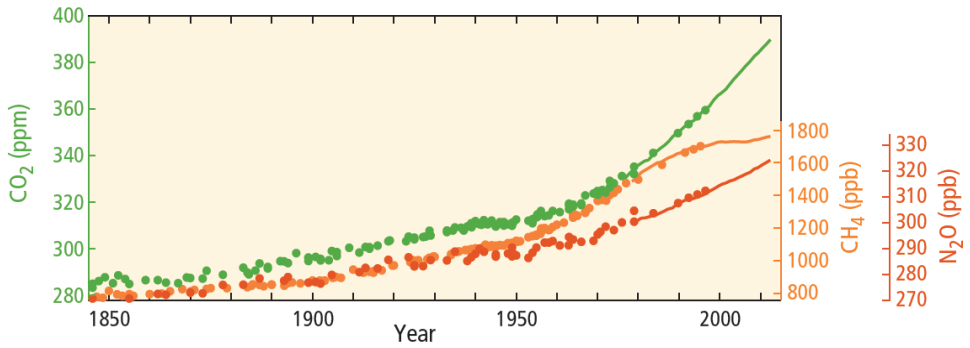
Figure 1.4. Atmospheric concentrations of the greenhouse gases carbon dioxide (CO$_2$, green), methane (CH$_4$, orange) and nitrous oxide (N$_2$O, red) determined from ice core data (dots) and from direct atmospheric measurements (lines).
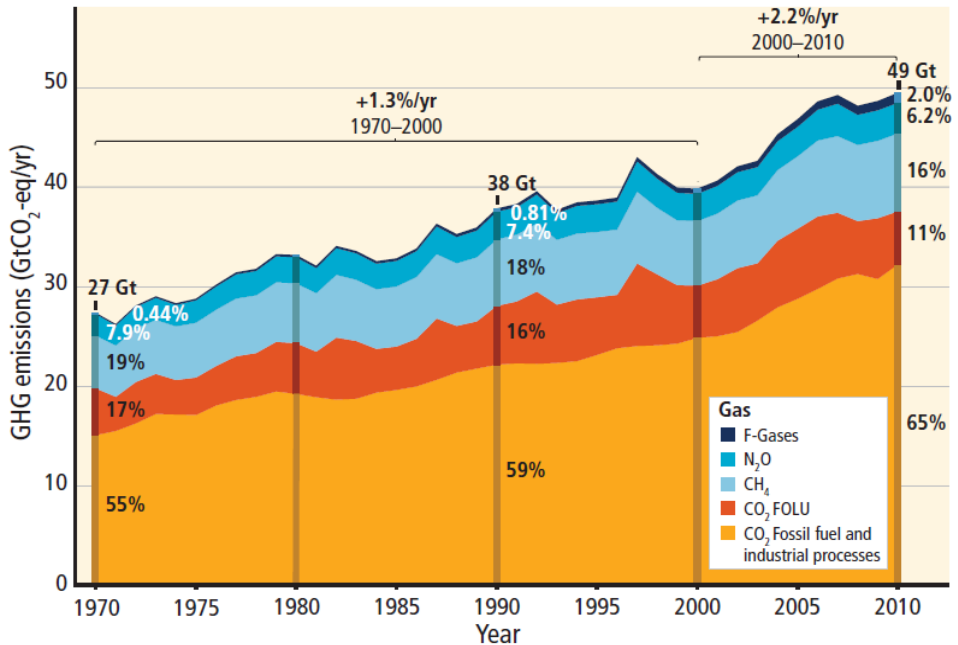
Figure 1.5. Total annual anthropogenic greenhouse gas (GHG) emissions (gigatonne of CO$_2$-equivalent per year, GtCO$_2$-eq/yr) for the period 1970 to 2010 by gases: CO$_2$ from fossil fuel combustion and industrial processes; CO$_2$ from Forestry and Other Land Use (FOLU); methane (CH$_4$); nitrous oxide (N$_2$O); fluorinated gases covered under the Kyoto Protocol (F-gases).

Globally, economic and population growth continued to be the most important drivers of the increase of CO$_2$ emissions from fossil fuel combustion. The contribution of population growth between 2000 and 2010 remained roughly identical to the previous three decades, while the contribution of economic growth has risen sharply. Increased

5

use of coal has reversed the long-standing trend of gradual decarbonization (i.e., reducing the carbon intensity of energy) of the world's energy supply. As reported in the IPCC Fifth Assessment Report (AR5) "*It is extremely likely that more than half of the observed increase in global average surface temperature from 1951 to 2010 was caused by the anthropogenic increase in GHG concentrations and other anthropogenic forcings together*". Multiple studies published in peer-reviewed scientific journals [27-30] show that 97 percent, at least, of actively publishing climate scientists agree: climate-warming trends over the past century are very likely due to human activities. In addition, most of the leading scientific organizations worldwide have issued public statements endorsing this position. The best estimate of the human-induced contribution to warming is similar to the observed warming over the period 1951–2010 as shown in Figure 1.6 [9].
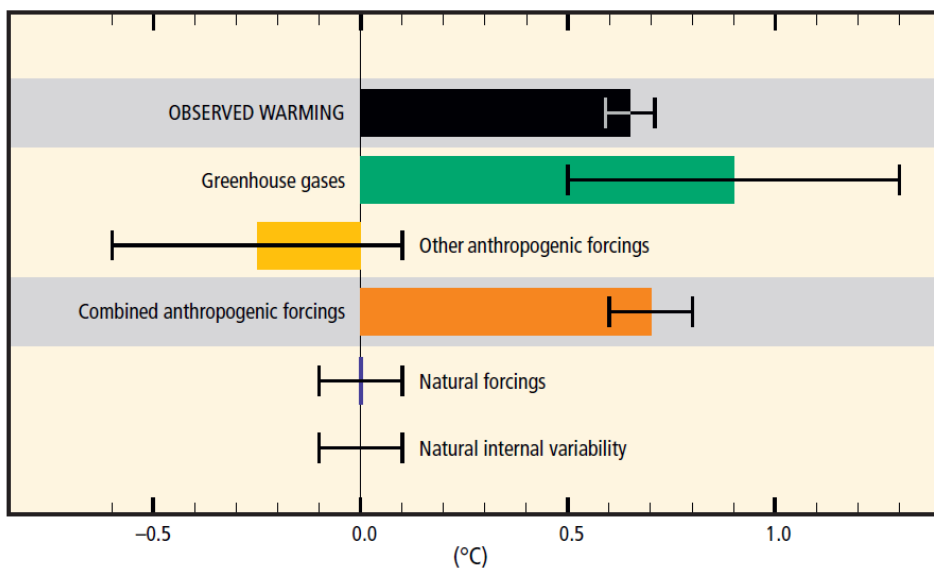
Figure 1.6. Contributions to observed surface temperature change over the period 1951–2010. Assessed likely ranges (whiskers) and their mid-points (bars) for warming trends over the 1951–2010 period from well-mixed greenhouse gases, other anthropogenic forcings (including the cooling effect of aerosols and the effect of land use change), combined anthropogenic forcings, natural forcings and natural internal climate variability (which is the element of climate variability that arises spontaneously within the climate system even in the absence of forcings). The observed surface temperature change is shown in black.

The United Nations Framework Convention on Climate Change provides a structure for intergovernmental efforts to tackle the challenge posed by climate change. The Convention's ultimate objective is to stabilize GHG concentrations in the atmosphere at a level that would prevent dangerous anthropogenic interference with the climate system. The Conference of Parties (COP) further recognized that deep cuts in global GHG

emissions are required, with a view <u>to hold the increase in global average temperature below 2°C above preindustrial levels,</u> and that Parties should take urgent action to meet this long-term goal, consistent with science and on the basis of equity [31].

1.3. CO$_2$ Emissions

Between 1750 and 2011, cumulative anthropogenic CO$_2$ emissions to the atmosphere were appraised to be 2040 GtCO$_2$. About 40% of these emissions has remained in the atmosphere (880 GtCO$_2$); the balance was removed from the atmosphere and stored on land (in plants and soils) and in the ocean. About half of the anthropogenic CO$_2$ emissions between 1750 and 2011 have occurred in the last 40 years (Figure 1.7) [9].
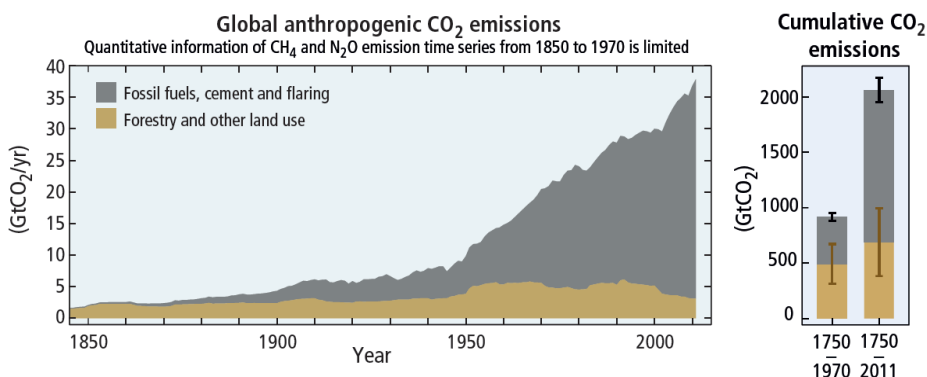
Figure 1.7. Global anthropogenic CO$_2$ emissions from forestry and other land use as well as from burning of fossil fuel, cement production and flaring. Cumulative emissions of CO$_2$ from these sources and their uncertainties are shown as bars and whiskers, respectively, on the right hand side.

Climate scientists have observed that carbon dioxide concentrations in the atmosphere has increased significantly over the past century, compared to the rather steady level of the pre-industrial era (about 280 parts per million in volume, or ppm). The November 2015 concentration of CO$_2$ (400 ppm) was about 40% higher than in the mid-1800s, with an average growth of 2 ppm/year in the last ten years (Figure 1.4).

Some impacts of the increased CO$_2$ concentrations may become slowly apparent since stability is an inherent characteristic of the interacting climate, ecological and socio-economic systems. Even after stabilization of the atmospheric concentration of CO$_2$, anthropogenic warming and sea level rise would continue for centuries due to the time scales associated with climate processes and feedbacks. Some changes in the climate

system would be irreversible in the course of a human lifespan [31]. Carbon dioxide has a variable atmospheric lifetime, estimated of the order of 30–95 years [32]. Given the long lifetime of CO_2 in the atmosphere, stabilizing concentrations of greenhouse gases at any level would require large reductions of global CO_2 emissions from current levels. The lower the chosen level for stabilization, the sooner the reduction of the global CO_2 emissions would need to begin, or the deeper the emission reduction would need to be over time.

1.3.1. The Growing Importance of Energy-Related Emissions

Among the many human activities that produce greenhouse gases, the use of energy represents by far the largest source of emissions [31], as shown in Figure 1.8.
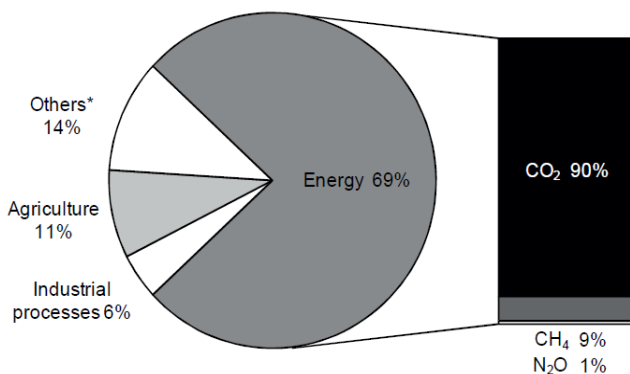
*Figure 1.8. Shares of global anthropogenic GHG, 2010. * Others include large-scale biomass burning, post-burn decay, peat decay, indirect N_2O emissions from non-agricultural emissions of NOx and NH$_3$, Waste, and Solvent Use.*

Smaller shares correspond to agriculture, producing mainly CH_4 and N_2O from domestic livestock and rice cultivation, and to industrial processes not related to energy (steel and cement production, chemical and petrochemical etc.). Within the energy sector, CO_2 produced by fossil fuel combustion dominates the total GHG emissions. CO_2 from energy production represents about three quarters of the anthropogenic GHG emissions for Annex I countries[1], and almost 70% of global emissions. This percentage varies

---

[1] The Annex I Parties to the 1992 UN Framework Convention on Climate Change (UNFCCC) are: Australia, Austria, Belarus, Belgium, Bulgaria, Canada, Croatia, the Czech Republic, Denmark, Estonia, European Economic Community, Finland, France, Germany, Greece, Hungary, Iceland, Ireland, Italy, Japan, Latvia, Liechtenstein, Lithuania, Luxembourg, Malta, Monaco, the Netherlands, New Zealand, Norway, Poland, Portugal, Romania, Russian Federation, the Slovak Republic, Slovenia, Spain, Sweden, Switzerland, Turkey, Ukraine, United Kingdom and United States.

greatly by country, due to diverse national structures. Increasing demand for energy comes from worldwide economic growth and development. Global total primary energy supply (TPES) is more than doubled between 1971 and 2012, mainly represented by fossil fuels (Figure 1.1). Despite the growth of non-fossil energy the share of fossil fuels within the world energy supply is relatively unchanged over the past 40 years. In 2012, fossil sources accounted for 82% of the global TPES [31].

1.3.2. Recent Emissions Trends

Emissions by region. In 2012, global CO_2 emissions were 31.7 $GtCO_2$. This represents a 1.2% year-on-year increase in emissions. Emissions in non-Annex I countries continued to increase (3.8%), although at a lower rate than in 2011, while emissions in Annex I countries decreased by 1.5%. In absolute terms, global CO_2 emissions increased by 0.4 $GtCO_2$ in 2012, driven primarily by increased emissions from coal and oil in non-Annex I countries [31]. Non-Annex I countries, collectively, represented 55% of global CO_2 emissions in 2012. Nearly two-thirds of global emissions in 2012 originated from just ten countries, with the shares of China (26%) and the United States (16%) far surpassing those of all others. The top-10 emitting countries include five Annex I countries and five non-Annex I countries (Figure 1.9).
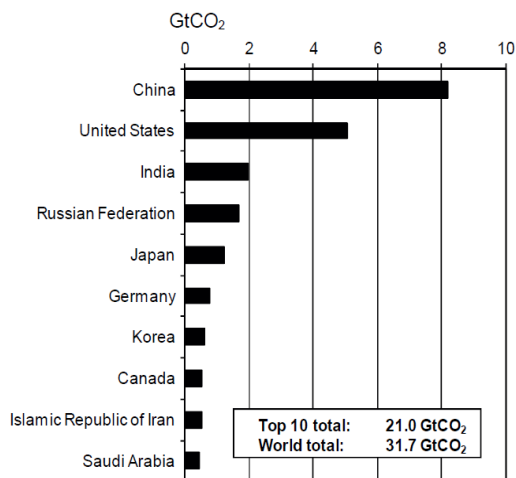
Figure 1.9. Top 10 emitting countries in 2012.

Emissions by fuel. Although coal represented 29% of the world TPES in 2012, it accounted for 44% of the global CO_2 emissions due to its heavy carbon content per unit of energy released, and to the fact that 18% of the TPES derives from carbon-neutral fuels (Figure 1.10). As compared to gas, coal is nearly twice as emission intensive on

average. In 2012, CO_2 emissions from the combustion of coal increased by 1.3% to 13.9 $GtCO_2$. Currently, coal fills much of the growing energy demand of those developing countries (such as China and India) where energy-intensive industrial production is growing rapidly and large coal reserves exist with limited reserves of other energy sources [31].

Percent share
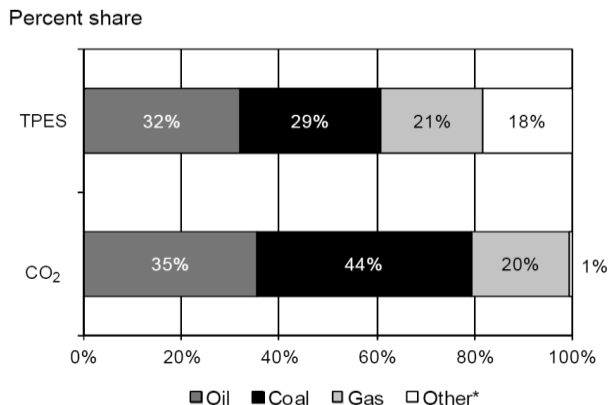
*Figure 1.10. World primary energy supply and CO_2 emissions: shares by fuel in 2012. * Other includes nuclear, hydro, geothermal, solar, tide, wind, biofuels and waste.*

Emissions by sector. Generation of electricity and heat is the main contributor to the CO_2 emissions and responsible for 42% of the world CO_2 emissions in 2010 (Figure 1.11). Worldwide, the electricity and heat production relies heavily on coal, which is the most carbon-intensive fossil fuels.
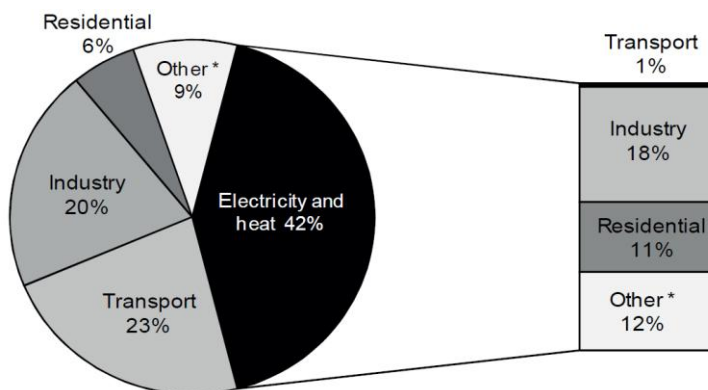
*Figure 1.11. World CO_2 emissions by sector in 2012 and allocation of electricity and heat to end-use sectors.*Other includes commercial/public services, agriculture/forestry, fishing, energy industries other than electricity and heat generation, and other emissions not specified elsewhere.*

Countries such as Australia, China, India, Poland and South Africa produce between 69% and 94% of their electricity and heat through the combustion of coal [31].

The future emission intensity of the electricity and heat sector strongly depends on the fuel that will be used to generate the electricity and on the share of non-emitting sources from renewable sources and nuclear energy. By 2035 the demand for electricity will be almost twice as high as the current one [1]. These trends underline the demand to develop technologies to reduce CO_2 emission associated with the use of fossil fuels.

1.4. CO_2 Capture Strategies

Because of the rise of population and increasing average standard of living more primary energy is required. There are only few possibilities to reduce global emissions of CO_2.

The first option is energy saving, improving technologies that use fossil fuels and avoiding waste: there is a large potential to increase the efficiency of energy conversion processes that needs to be targeted.

The second option is to use fossil energy sources which are less carbon-intensive or to switch to renewable energy sources. This includes switching from fossil fuels to renewable and nuclear energy sources, but also from coal to natural gas. A third option is to capture the CO_2 directly from the large emission sources. This is the field of CCS (Carbon dioxide Capture and Storage) and CCU (Carbon dioxide Capture and Utilization) technologies.
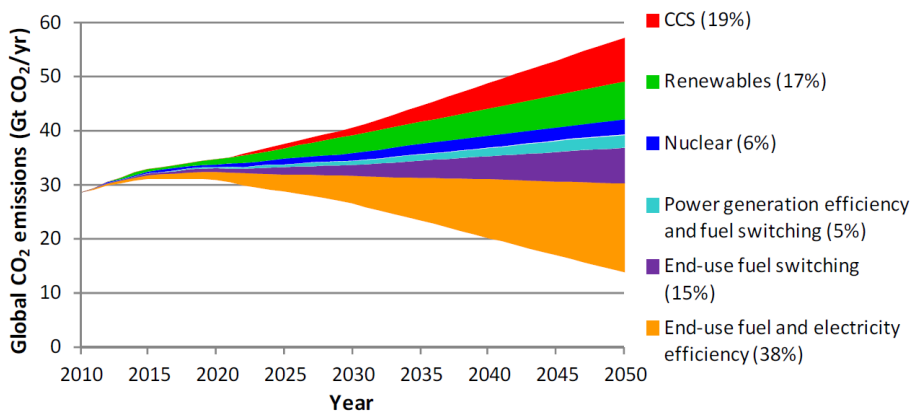
Figure 1.12. Contribution of different CO_2 mitigation strategies in the IEA Blue map scenario, aiming at stabilizing atmospheric GHG emissions at 450 ppm CO_2-eq [3].

It is important to underline that none of the three options by itself can reach the 2 °C target, and a portfolio of mitigation options has to be implemented in order to meet the GHG emission mitigation targets (Figure 1.12) [2-9,33].

1.5.   CCS : Carbon Capture and Storage

Carbon capture and storage (CCS) (or carbon capture and sequestration) is the general term for the processes that reduces the CO_2 emission in the atmosphere from large stationary sources, such as fossil fueled power plants, by means of its capture and its storage usually in an underground geological formation [34,35]. This technique allows the use of fossil fuels but with significantly lower CO_2 emissions. For this reason CCS can be seen as a transition mitigation option until the current fossil fuel based energy infrastructure will be replaced , at least in part, by an infrastructure based mainly on renewable sources. The widespread utilization of the CCS technology mostly depends on its efficiency improvements and climate policies. It is estimated that, depending on the scenario, CCS could account for 19-32% of the total mitigated CO_2 emissions in the power sector, and avoids 18 Gt CO_2 equivalent emissions every year [36,37]. Although the total mitigation costs are uncertain, it has been projected that large-scale deployment of CCS could reduce global mitigation costs by up to 40% [35,38-41]. However, to fully realize this potential it is required that deployment of CCS takes off this decade. In 2011, there were only 8 demonstration projects of integrated commercial scale CCS in the world [42] and, according to the IEA Technology roadmap on CCS, the number of projects needs to increase to around 100 by 2020 and to almost 3500 by 2050 to fulfill the CCS contribution to CO_2 mitigation (see Figure 1.13) [38].

The CCS chain is composed of three steps: capture, transport and storage. Each stage of CCS is technically available and has been used commercially for many years [35,36]. However, several technologies, with different degrees of maturity, are competing to be the low-cost solution for each stage within the CCS value chain. The purpose of CO_2 capture is to separate it from a gas stream and to produce a concentrated stream of CO_2 at high pressure that can readily be transported to a storage site. Although, in principle, the entire gas stream containing low concentrations of CO_2 could be transported and injected underground, energy costs and other associated costs generally make this approach impractical. It is therefore necessary to produce a nearly pure CO_2 stream, that is subsequently compressed and transported by a pipeline into sequestration sites that

include underground geological locations, such as depleted gas or oil fields or saline aquifers [35]. Alternatively, captured CO_2 could be used for enhanced oil recovery (EOR) and enhanced natural gas recovery (EGR).
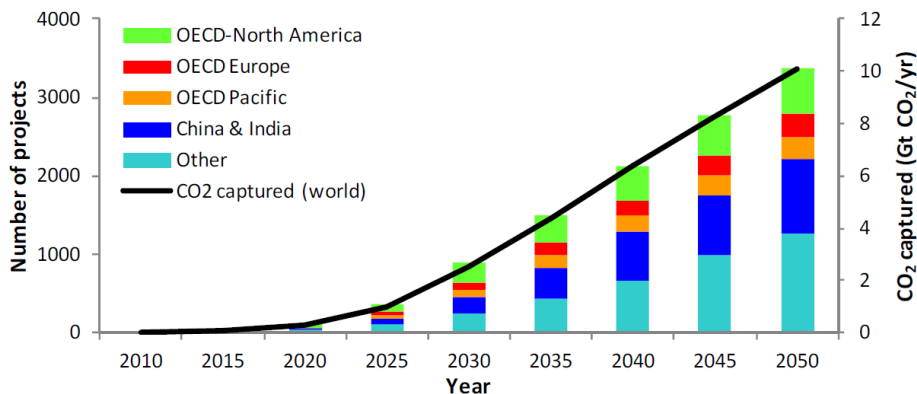
Figure 1.13. IEA Technology roadmap for global development and distribution of CCS [38].

1.5.1. CO₂ Capture Methods

Several methods are available to capture CO_2 from fossil fuel power plant. These include mainly physical and chemical absorption, adsorption, cryogenic and membrane processes [43].

Absorption occurs within the bulk of the material via a chemical reaction or physical interaction. Chemical absorbents react with CO_2, forming thermally unstable compounds. The absorbent is then regenerated by heating and captured CO_2 is released. Typical compounds used in this process are aqueous amines, ammonia-based solutions or carbonate solutions.

Physical absorbents obey Henry's law, where gas solubility is directly proportional to the partial pressure of the said gas in equilibrium, at a constant temperature. The interaction between CO_2 and the solvent is of van der Waals type. Regeneration of the solvent is achieved by increasing the temperature and lowering the pressure of the system [44]. The selective capture is guaranteed by the different solubility of the acid gas (such as CO_2) and carrier (air, methane, nitrogen) in the appropriate solvent. Selexol and Rectisol (trade names for acid gas removal processes that uses respectively dimethyl ethers of polyethylene glycol and methanol as a solvent) are examples of physical absorbents that have been used in natural gas sweetening and synthesis gas treatment.

Adsorption, as opposed to absorption, takes place at the surface of a solid material. This interaction can occur chemically (covalent bonding) or physically (van der Waals). Typical adsorbers are solid materials with large surface areas, such as zeolites, activated carbons, metal oxides, silica gel, and ion-exchange resins, which can interact selectively with acid gases. The flue gas is put in contact with a bed of these adsorbers, allowing the CO_2 separation from the other gases which pass through. When the bed is fully saturated with CO_2, the flue gas is directed to a clean bed and the saturated bed is regenerated [45]. Two techniques can be employed to the adsorption mechanism:

– pressure swing adsorption (PSA), where the flue gas is introduced at high pressure until the concentration of CO_2 reaches equilibrium, then the pressure is lowered to regenerate the adsorbent;

– temperature swing adsorption (TSA), where the regeneration is obtained by increases the temperature of the absorbent;

Adsorption is not yet considered attractive for large-scale separation of CO_2 from flue gas because the capacity and CO_2 selectivity of available adsorbents is low. However, recently new sorbents are being investigated such as metal-organic frameworks and functionalised fibrous matrices that show some promise for the future of this particular technique.

Membrane separation technology is based on the interaction of specific gases with the membrane material by a physical or chemical interaction. Through modifying the material, the rate at which the gases pass through can be controlled. There are wide varieties of membranes available for gas separation, including polymeric membranes, zeolites, and porous inorganic membranes, some of which are used in an industrial scale and have the possibility of being implemented into the process of CO_2 capture. However achieving high degrees of CO_2 separation in one single stage has so far proved to be difficult; therefore, having to rely on multiple stages has led to increasing energy consumption and cost. An alternative approach is to use porous membranes as platforms for absorption and stripping. Here a liquid (typically aqueous amine solutions) provides the selectivity towards the gases. As the flue gas moves through the membrane, the liquid selects and captures the CO_2 [46].

Cryogenic Separation is a technique where the components of a mixture can be separated by cooling and condensation, carried out on the basis of the differences among the phase

transition properties of these components. Cryogenic separation is widely used commercially for streams that already have high CO_2 concentrations (typically > 90%) but it is not used for more dilute CO_2 streams. A major disadvantage of cryogenic separation of CO_2 is the amount of energy required to provide the refrigeration necessary for the process, particularly for dilute gas streams. Another disadvantage is that some components, such as water, have to be removed before the gas stream is cooled, to avoid blockages. Cryogenic separation has the advantage that it enables direct production of liquid CO_2, which is needed for certain transport options, such as transport by ship [47]. Cryogenics would only be applied to high concentration, high pressure gases, such as in pre-combustion capture processes or oxygen fired combustion.

1.5.2. Capture from Large Stationary Plants

Depending on the process or power plant application, there are three main approaches to capture the CO_2 generated from a primary fossil fuel (coal, natural gas or oil), biomass, or mixtures of these fuels: post-combustion capture by chemical absorption, pre-combustion capture, and oxyfuel combustion (Figure 1.14) [35,48].
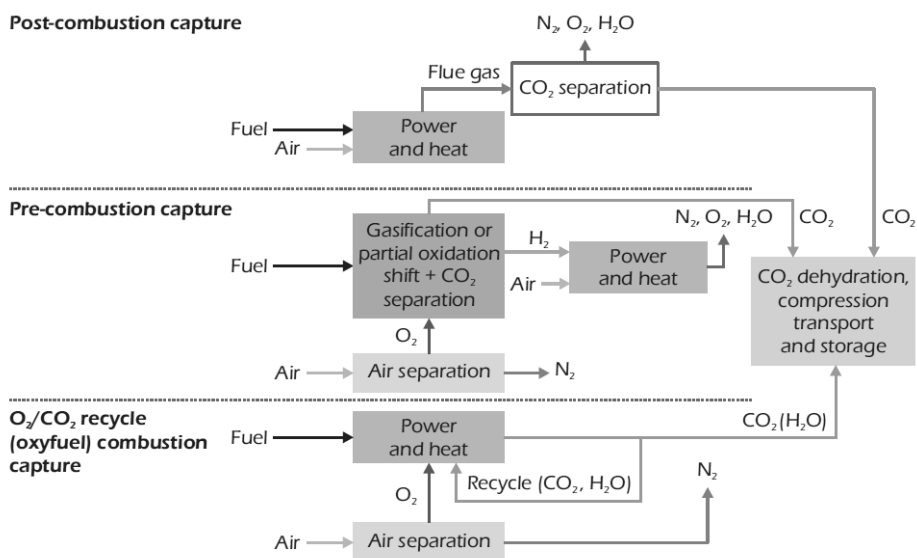
Figure 1.14. CO_2 Capture Processes. Source IPCC 2005 [35].

Post-combustion process refers to separation of CO_2 from the flue gas at the exit of the combustion process: this system normally uses a liquid absorbent to capture the small fraction of CO_2 (typically 3–15% by volume) present in a flue gas stream in which the

main constituent is nitrogen (from air), and subsequent solvent regeneration. This technology, using amine-based solvents, has been used on an industrial scale for decades for the separation of CO_2 in H_2 and NH_3 production and natural gas purification. An advantage of this technique is that it can be applied to existing power plants (retrofit). Moreover, the CO_2 capture process does not interfere with normal operations, meaning that the availability of the facility is not affected. The disadvantage is the large amounts of energy required by absorbent regeneration.

Pre-combustion capture is a process in which fuel is decarbonised before the combustion, resulting in zero carbon dioxide production during the combustion step. A pre-combustion capture process typically comprises a first stage of reaction producing a mixture of hydrogen and carbon oxide (syngas) from a primary fuel. The two main routes are to add steam (reaction 1), in which case the process is called 'steam reforming', or oxygen (reaction 2) to the primary fuel. In the latter case, the process is often called 'partial oxidation' when applied to gaseous and liquid fuels and 'gasification' when applied to a solid fuel, but the principles are the same.

$$C_xH_y + xH_2O \rightleftharpoons xCO + (x+y/2)H_2 \qquad (1)$$

$$C_xH_y + x/2\ O_2 \rightleftharpoons xCO + (y/2)H_2 \qquad (2)$$
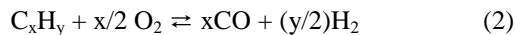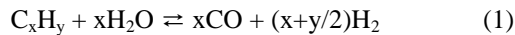
CO then reacts with steam in a catalytic shift reactor to produce CO_2 and additional H_2 (reaction 3).

$$CO + H_2O \rightleftharpoons CO_2 + H_2 \qquad (3)$$
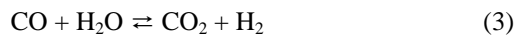
CO_2 is then sequestrated and separated from the hydrogen, which is used as fuel in a combined cycle plant for electricity generation. One of the advantages of pre-combustion capture is the high CO_2 concentration of the flue stream, requiring smaller equipment size. On the other end, this method cannot be retro-fitted to the older pulverised coal power plants that make up much of the world's installed base of fossil fuel power.

Oxy-fuel combustion refers to the ignition of pulverized coal or other carbon-based fuels in a nearly pure O_2 environment and represents a relatively new process for mitigating CO_2 emissions compared with pre-combustion and post-combustion CO_2 capture. The significant advantages of this process arise from the fact that the flue gas is almost entirely CO_2 and therefore it is not necessary to separate it from other components, and

that most existing power plants could be readily equipped with an oxy-fuel combustion system. A main drawback of this option is the need for (currently expensive) pure O_2.

Figure 1.15 provides an overview of current CO_2 capture options and their potential. Among all these options, chemical absorption using aqueous alkanolamine solutions is proposed to be the most applicable technology for CO_2 capture before 2030 [49].
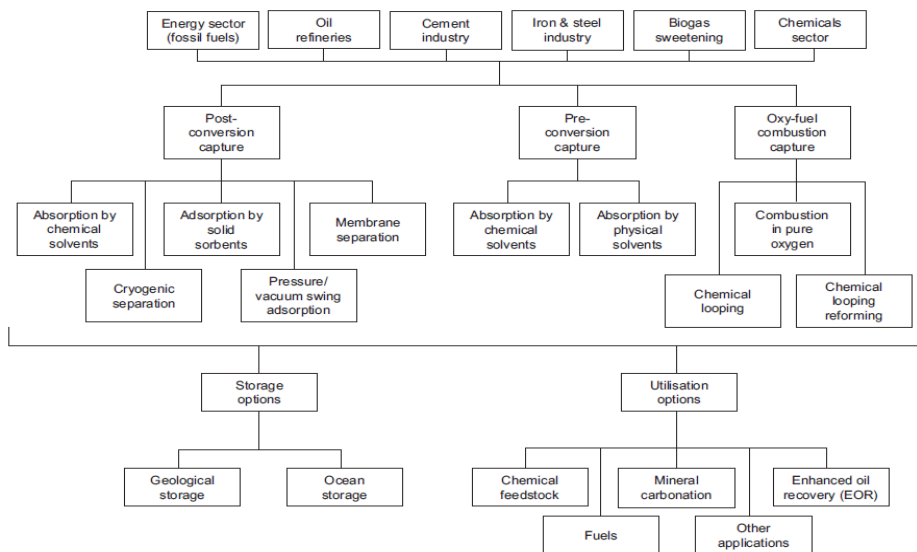
Figure 1.15. Different carbon capture, storage and utilisation options.

1.5.3.   Storage of CO_2 by Injection

While CO_2 capture is likely to represent the major cost, in both money and energy, of the whole CCS process, CO_2 storage poses a great deal of uncertainty. There is uncertainty in the quantification of storage potential, in the confirmation of outline assessments to a standard suitable for investment, the tracking verification and monitoring of injected CO_2, and finally the fail-safe retention of CO_2 [50]. Once captured, CO_2 is compressed and shipped or pipelined to be stored either in the ground, ocean or as a mineral carbonate [35, 51]. Geological storage, involves injecting CO_2 into geological formations such as depleted oil and gas reservoirs, deep saline aquifers and coal bed formations, at depths between 800 and 1000 m [35]. Depending on the characteristics of the site, CO_2 can be stored through different trap mechanisms, including impermeable layers known as ''caprock'' (e.g. mudstones, clays, and shales) which trap CO_2 underneath as well as *in situ* fluids and organic matter where CO_2 is dissolved or

adsorbed [35]. Subject to the reservoir pressure and temperature, CO_2 can be stored as compressed gas, liquid, or in a supercritical condition [51]. The latter (at 31.1 °C and 73.8 bar) makes it denser, increasing the pore space utilisation and making it more difficult to leak [51]. CO_2 storage in geological formations is at present one of the most promising options owing to the previous experience by the oil and gas industry. Deep saline aquifer formations are also a possibility for storage with a large storage capacity estimated at 700–900 Gt CO_2 [35]. Ocean storage relies on the principle that the ocean bed has a huge capacity to store injected CO_2 at great depths. The main concerns with CO_2 storage are its possible leaks and the related damage that a concentrated CO_2 stream would cause if it escaped into the environment. There are several ongoing CCS projects around the world, ranging from the pilot to commercial scale. The latter include the Sleipner and Snøhvit projects in Norway, the Weyburn-Midale in Canada, the In Salah in Algeria and the Salt Creek project in the USA [51]. These projects have been operating in saline aquifer formations (Norway) and depleted oils and gas reservoirs (Canada, Algeria and USA) for more than 10 years. Finally, in the mineral carbonation CO_2 reacts with metal oxides such as magnesium and calcium oxides, to form carbonates. Carbonation, or 'mineral sequestration', can be considered as an utilization option if the carbonates are used in the construction industry [51].

1.6.   CCU : Carbon Capture and Utilization

More recently, a related alternative to CCS – carbon capture and utilization (CCU) – has started to attract attention worldwide because it can turn waste CO_2 emissions into valuable products. CCU combines the CO_2 capture with re-use of CO_2 itself as a technological fluid or as a reagent for the production of chemicals, plastics, or fuels. In a few cases, the re-use can result in a permanent storage of CO_2 from the carbon cycle (e.g. enhanced oil recovery or mineral carbonisation); however, in most cases, the re-use will result in re-emission of CO_2. In the latter case, the lifetime in which CO_2 is removed from the carbon cycle will vary from days to months, as a fuel precursor, to decades if it is used as a precursor for plastics. The primary advantage of CCU compared with CCS is that its end product is of value [50].

1.6.1.   Current Demand of CO_2

Despite the fact that CO_2 is a renewable, widely available, low-cost and low-toxicity carbon feedstock, current industrial demand is relatively low, amounting to around 232 Mt per year, with only a few commercial processes currently using CO_2 as a raw material (Table 1.1). Most of the current demand is met by naturally derived CO_2 with only 40 Mt obtained from anthropogenic sources of which 70% is used for enhanced oil recovery (EOR) and another significant fraction used for urea production [50]. At present, the market for CO_2 is several orders of magnitude smaller than the amount of CO_2 released into the atmosphere each year from anthropogenic sources and approximately 60 times smaller than the amount of CO_2 emitted from large point sources (~14000 Mt per year) [35]. In other words, the use of anthropogenic CO_2 in place of CO_2 derived from natural deposits will offer very small emissions reductions.

Table 1.1. Current CO_2 consuming industrial processes [50].

Process	Industrial mass (Mt/year)	Global CO_2 usage (Mt/year)	Lifetime of storage
Urea	159.4	120	Months
Methanol	55	14	Months
Inorganic carbonates	80	30	Decades/Perm.
Organic carbonates	4	0.2	Decades
Technological	10	10	Days to years
Food	8	8	Days to years
EOR	50	50	Permanent [a]
Total		**232 Mt**	

[a] Whilst EOR offers the potential of permanent storage, most of the CO_2 used for EOR is currently not stored

1.6.2.   Direct Utilization of CO_2

Several industries utilize CO_2 directly. For example, in the food and drink industry, CO_2 (~8 Mt per year) is commonly used as a carbonating agent, preservative, packaging gas and as a solvent for the extraction of flavours and in the decaffeination process [51]. However, these applications are restricted to sources producing CO_2 waste streams of high purity such as ammonia production [51].

EOR (enhanced oil recovery) and ECBM (enhanced coal-bed methane recovery) are other examples of direct utilization of CO_2 where it is used to extract crude oil from an oil field or natural gas from coal deposits, respectively. While the latter is not yet commercially available, the former has been widely practiced for over 40 years in several oil-producing countries, including Norway, Canada and the USA [35]. Also

known as tertiary recovery, EOR is used to extract otherwise unrecoverable oil reserves, and it involves injection of different agents into the reservoir, including CO_2, to remove the oil trapped in the rocks [51]. EOR can extract 30–60% more of the crude originally available in the well, compared to primary and secondary extraction which recover 20–40%. Injected under supercritical conditions, CO_2 mixed with the oil decreases its viscosity, thus helping to increase the extraction yields. However, some CO_2 returns back to the surface with the pumped oil, even if it is recycled for economic reasons. Under special conditions, the injected CO_2 could remain stored underground, similarly to geological storage. EOR offers one of the largest potential markets for CO_2: in a recent report, Advanced Resources International estimated that at least 8 billion tons of CO_2 could be sequestered using EOR in the US alone [50].

1.6.3. Urea and Other Chemicals

A lot of different chemicals could be produced using CO_2 as a carbon feedstock; however, many would either prove impractical on an industrial scale or have limited market potential. Figure 1.16 outlines a number of promising CO_2-derived synthetic targets and their current global market. Of particular interest are alkylene carbonates and polycarbonates, inorganic carbonates (~60 Mt per year), urea (~160 Mt per year), polyurethane (~18 Mt per year), and acrylic acid and acrylates (10 Mt per year) [50].

Urea currently represents the largest market for CO_2 except EOR. In all commercial processes, urea is produced by reacting ammonia and carbon dioxide at elevated temperature and pressure according to the Basaroff reactions:

$$2\,NH_3 + CO_2 \rightleftharpoons NH_2COONH_4 \qquad\qquad \Delta H° = -151\ kJ\ mol^{-1}$$

$$NH_2COONH_4 \rightleftharpoons NH_2CONH_2 + H_2O \qquad\qquad \Delta H° = 32\ kJ\ mol^{-1}$$
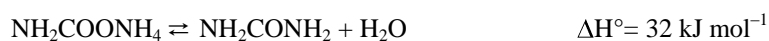
In the first reaction, carbon dioxide and ammonia are converted to ammonium carbamate; the reaction is fast and exothermic. In the second reaction, which is slow and endothermic, ammonium carbamate dehydrates to produce urea and water. Since more heat is produced in the first reaction than consumed in the second, the overall reaction is exothermic and no catalyst is required [52].
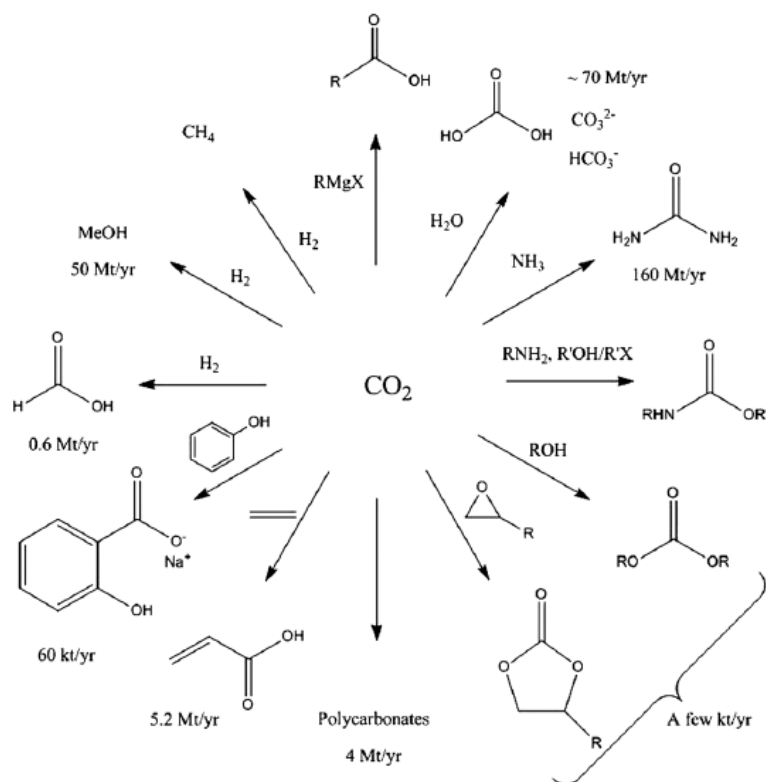
Figure 1.16. Chemical transformations of CO_2 into synthetic targets with large current or potential markets [50].

According to the International Fertiliser Association, current global production of urea is 159.4 Mt per year. Given that between 0.735 and 0.75 tonnes of CO_2 are consumed per tonne of urea, CO_2 consumption is around 119.6 Mt per year. Urea is used for soil and leaf fertilization (more than 90% of the total use); in the manufacture of urea–formaldehyde resins; in melamine production; as a nutrient for ruminants (cattle feed); as a reducing agent in SCR (Selective Catalyst Reduction) technology for NOx reduction in off-gases from combustion processes and in miscellaneous applications [52]. The climate change mitigation potential of ramping up urea production is limited: as shown in Table 1.1, the storage of CO_2 within urea is short, since the chemical breaks down upon application as fertiliser, releasing the CO_2 into the atmosphere.

1.6.4. CO_2-to-Fuels

The production of fuels from CO_2 is ostensibly an attractive goal, given that the global fuels market is roughly two orders of magnitude greater than that of chemicals. CO_2 is the lowest energy state of any binary neutral carbon species and the ultimate product of

energy-releasing hydrocarbon combustion and metabolic pathways. Therefore, a significant energy input is required to overcome the substantial thermodynamic and kinetic barriers of converting CO_2 into a useable fuel. In order to contribute to the efforts of climate change mitigation, the energy requirements must be supplied from non-fossil sources, i.e. RETs (Renewable Energy Targets) or nuclear. The idea is that the application of such technology may provide a way of storing excess electrical or intermittent electricity production (such as solar or eolic). When considering the energetics of CO_2 activation, only a very few synthetic fuel targets can possibly be considered viable, these targets include syngas, methane, methanol and formic acid [53]. However, the drawbacks of this approach are the low equilibrium yields and the very energy intensive process of H_2 production.

1.7.   References

[1] BP Energy Outlook 2035. BP p.l.c. London, United Kingdom. February 2015.
[2] International Energy Agency (IEA). World Energy Outlook 2012.
[3] International Energy Agency (IEA). World Energy Outlook Presentation. London, UK. 2013.
[4] International Energy Agency (IEA). Key World Energy Statistics 2014.
[5] Greenpeace. Energy [r]evolution - A Sustainable World Energy Outlook. Greenpeace. 2010.
[6] Intergovernmental Panel on Climate Change (IPCC). Renewable Energy Sources and Climate Change Mitigation. Cambridge University Press. Cambridge, United Kingdom and New York, NY, USA. 2011.
[7] K. Riahi. Chapter 17: Energy Pathways for Sustainable Development. In: Johansson TB, Nakicenovic N, Patwardhan A, Gomez-Echeverri L. (eds.). Global Energy Assessment: Toward a Sustainable Future. IIASA, Laxenburg, Austria and Cambridge University Press, Cambridge, United Kingdom and New York, NY, USA.
[8] United Nations Development Programme. World Energy Assessment: Overview 2004 Update. USA. 2004.
[9] Intergovernmental Panel on Climate Change (IPCC). Fifth Assessment Report (AR5). 2014.
[10] B. D. Santer, K. E. Taylor, T. M. L. Wigley, T. C. Johns, P. D. Jones, D. J. Karoly, J. F. B. Mitchell, A. H. Oort, J. E. Penner, V. Ramaswamy, M. D. Schwarzkopf, R. J. Stouffer, S. Tett. A search for human influences on the thermal structure of the atmosphere. Nature, 1996, 382, 39-46.
[11] G.C. Hegerl, H. von Storch, K. Hasselmann, B.D. Santer, U. Cubasch, P.D. Jones. Detecting Greenhouse-Gas-Induced Climate Change with an Optimal Fingerprint Method. J. Climate. 1996, 9, 2281–2306.
[12] V. Ramaswamy, M.D. Schwarzkopf, W.J. Randel, B.D. Santer, B.J. Soden, G.L. Stenchikov. Anthropogenic and Natural Influences in the Evolution of Lower Stratospheric Cooling. Science, 2006, 311, 1138-1141.
[13] B.D. Santer, M.F. Wehner, T.M.L. Wigley, R. Sausen, G.A. Meehl, K.E. Taylor, C. Ammann, J. Arblaster, W.M. Washington, J.S. Boyle, W. Brüggemann. Contributions of

Anthropogenic and Natural Forcing to Recent Tropopause Height Changes. Science, 2003, 301, 479-483.

[14] data from National Oceanic and Atmospheric Administration. http://www.noaa.gov/.

[15] data from Climatic Research Unit, University of East Anglia. http://www.cru.uea.ac.uk/.

[16] data from National Aeronautics and Space Administration (NASA). http://data.giss.nasa.gov/gistemp.

[17] T.C. Peterson, M.O. Baringer. State of the Climate in 2008. Special Supplement to the Bulletin of the American Meteorological Society, 2009,v. 90, no. 8, S17-S18.

[18] I. Allison, N.L. Bindoff, R.A. Bindschadler, P.M. Cox, N. de Noblet, M.H. England, J.E. Francis, N. Gruber, A.M. Haywood, D.J. Karoly, G. Kaser, C. Le Quéré, T.M. Lenton, M.E. Mann, B.I. McNeil, A.J. Pitman, S. Rahmstorf, E. Rignot, H.J. Schellnhuber, S.H. Schneider, S.C. Sherwood, R.C.J. Somerville, K. Steffen, E.J. Steig, M. Visbeck, A.J. Weave. The Copenhagen Diagnosis: Updating the World on the Latest Climate Science, UNSW Climate Change Research Center, Sydney, Australia, 2009.

[19] S. Levitus, J.I. Antonov, T.P. Boyer, R.A. Locarnini, H.E. Garcia, A.V. Mishonov. Global ocean heat content 1955–2008 in light of recently revealed instrumentation problems. Geophys. Res. Lett. 2009, 36, L07608.

[20] J.A. Church, N.J. White. A 20th century acceleration in global sea level rise. Geophys. Res. Lett. 2006, 33, L01602.

[21] L. Polyak, et.al., "History of Sea Ice in the Arctic," in Past Climate Variability and Change in the Arctic and at High Latitudes, U.S. Geological Survey, Climate Change Science Program Synthesis and Assessment Product 1.2, January 2009, chapter 7.

[22] data from National Snow and Ice Data Center. www.nsidc.org.

[23] United States Global Change Research Program, "Global Climate Change Impacts in the United States," Cambridge University Press, 2009.

[24] N. Oreskes. The Scientific Consensus on Climate Change. Science. 2004, 306, 1686.

[25] S. Arrhenius, Philos. Mag. 1896, 41, 237.

[26] National Research Council (NRC). Surface Temperature Reconstructions For the Last 2,000 Years. National Academy Press, Washington, DC. 2006.

[27] J. Cook, D. Nuccitelli, S.A. Green, M.Richardson, B. Winkler, R. Painting, R.Way, P.Jacobs, A.Skuce. Quantifying the consensus on anthropogenic global warming in the scientific literature. Environ. Res. Lett. 2013, 8, 024024 .

[28] W.R.L. Anderegg. Expert Credibility in Climate Change. Proceedings of the National Academy of Sciences. 2010, 107, No. 27, 12107-12109.

[29] P.T. Doran, M.K. Zimmerman. Examining the Scientific Consensus on Climate Change. Eos Transactions American Geophysical Union. 2009, Vol. 90 Issue 3, 22.

[30] N. Oreskes. Beyond the Ivory Tower: The Scientific Consensus on Climate Change. Science, 2004, Vol. 306, no. 5702, 1686..

[31] International Energy Agency (IEA). CO_2 Emissions From Fuel Combustion, 2014.

[32] M.Z. Jacobson. Correction to "Control of fossil-fuel particulate black carbon and organic matter, possibly the most effective method of slowing global warming. J. Geophys. Res. 2005, 110, D14105.

[33] WWF, Ecofys, Office of Metropolitan Architecture (OMA). The Energy Report. 100% Renewables by 2050. WWF. 2011. ISBN 978-2-9404-4326-0.

[34] J. Jared Ciferno, J. Litynski, L. Brickett, J. Murphy, R. Munson, C. Zaremsky, J. Marano, J. Strock. DOE/NETL Advanced Carbon Dioxide Capture R&D Program: Technology Update. May 2008.

[35] Intergovernmental Panel on Climate Change (IPCC). Special report on Carbon Dioxide Capture and Storage. Cambridge University Press. Cambridge, United Kingdom and New York, NY, USA. 2005. ISBN: 978-0-5218-6643-9.

[36] International Energy Agency (IEA). Energy Technology Perspectives 2010. Paris, France. 2010.

[37] European Commission. Energy Roadmap 2050. EC. 2012.

[38] International Energy Agency (IEA). Technology Roadmap. Carbon capture and storage. OECD/IEA, Paris. 2009

[39] C. Azar, K. Lindgren, E. Larson, K. Möllersten. Carbon Capture and Storage From Fossil Fuels and Biomass - Costs and Potential Role in Stabilizing the Atmosphere. Climatic Change, 2006, 74, 47-79.

[40] C. Azar, K. Lindgren, M. Obersteiner, K. Riahi, D.P. Van Vuuren, K.M.G.J. Den Elzen, K. Möllersten, E. Larson. The feasibility of low CO_2 concentration targets and the role of bio-energy with 290 carbon capture and storage (BECCS). Climatic Change, 2010, 100, 195-202.

[41] J. Koornneef, P. Van Breevoort, C. Hamelinck, C. Hendriks, M. Hoogwijk, K. Koop, M. Koper. Potential for Biomass and Carbon Dioxide. Capture and Storage. IEA GHG. July 2011. Report No.: 2011/06.

[42] Global CCS Institute. The global status of CCS: 2011. Global CCS Institute. 2011. ISBN: 978-0-9871-8630-0.

[43] E. Torralba-Calleja, J. Skinner, D. Gutiérrez-Tauste. CO_2 Capture in Ionic Liquids: A Review of Solubilities and Experimental Methods. Journal of Chemistry, 2013, Article ID 473584, 16 pages.

[44] X. Gui, Z. Tang, W. Fei. CO_2 capture with physical solvent dimethyl carbonate at high pressures. Journal of Chemical and Engineering Data, 2010, 55, no. 9, 3736–3741.

[45] A.L. Chaffee, G.P. Knowles, Z. Liang, J. Zhang, P. Xiao, P.A. Webley. CO_2 capture by adsorption: materials and process development. International Journal of Greenhouse Gas Control, 2007, 1, 11–18.

[46] C.A. Scholes, S.E. Kentish, G.W. Stevens. Carbon dioxide separation through polymeric membrane systems for flue gas applications. Recent Patents on Chemical Engineering, 2008, 1, 52–66.

[47] S. Burt, A. Baxte, L. Baxter. Cryogenic CO_2 Capture to Control Climate Change Emissions. Brigham Young University, Provo, Utah, USA, 84602 Sustainable Energy Solutions Orem, 84058, 2010.

[48] Organisation For Economic Co-Operation And Development (OECD), International Energy Agency (IEA). CO_2 Capture And Storage: A Key Carbon Abatement Option. 2008.

[49] G.T. Rochelle. Amine Scrubbing for CO_2 Capture. Science, 2009, 325, 1652–1654.

[50] M.E. Boot-Handford, J.C. Abanades, E.J. Anthony, M.J. Blunt, S. Brandani, N. Mac Dowell, J.R. Fernandez, M.C. Ferrari, R. Gross, J.P. Hallett, R.S. Haszeldine, P. Heptonstall, A. Lyngfelt, Z. Makuch, E. Mangano, R.T.J. Porter, M. Pourkashanian, G.T. Rochelle, N. Shah, J.G. Yao, P.S. Fennell. Carbon capture and storage update. Energy Environ. Sci., 2014, 7, 130–189.

[51] R.M. Cuéllar-Franca, A. Azapagic. Carbon capture, storage and utilisation technologies: A critical analysis and comparison of their life cycle environmental impacts. Journal of CO_2 Utilization, 2015, 9, 82–102.

[52] J.H. Meessen. Urea. Ullmann's Encyclopedia of Industrial Chemistry. 2010.

[53] N. MacDowell, N. Florin, A. Buchard, J. Hallett, A. Galindo, G. Jackson, C. S. Adjiman, C. K. Williams, N. Shah, P. Fennell. An overview of CO_2 capture technologies. Energy Environ. Sci., 2010, 3, 1645–1669.

24

2. CO$_2$ Capture by Chemical Absorption: State of Art

2.1. CO$_2$ Capture Process

A typical chemical absorption process consists of an absorber and a stripper in which the absorbent is thermally regenerated. Acid gas removal by absorption has been used to separate carbon dioxide and other acid gases from natural gas, hydrogen, and other gas streams since the 1930s [1,2]. The process covering this application, which is based on the temperature reversible reaction of CO$_2$ and other acid gases with aqueous solutions of amine based absorbents, was patented as early as 1930 by Bottoms [3] and shown in Figure 2.1.
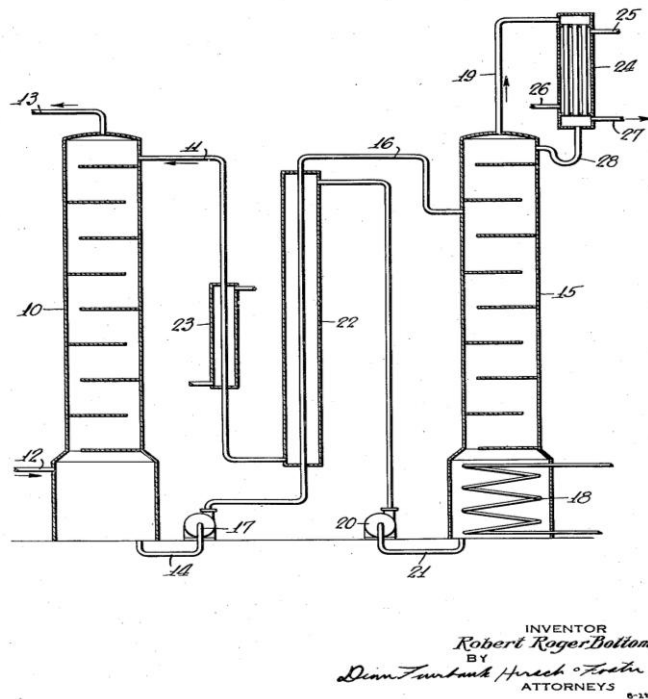
Figure 2.1. The acid gas removal process as invented by Bottoms in 1930 [3]. The left column is the absorber unit, the middle part shows pumps, a cooler, and a heat exchanger, and the right column is the desorber unit with an overhead water condenser.

The basic principles of this process are still very much like the ones used for acid gas removal today. The gas stream (CO$_2$ and H$_2$; CO$_2$ and CH$_4$; CO$_2$, O$_2$ and N$_2$, for example) flows into the absorber at the bottom of the column where it is contacted with the solvent at room temperatures. The solvent flows from the top in counter current

down the column where it gradually takes up more acid gas by a chemical reaction: the CO_2 rich absorbent leaves the bottom of the column. The treated gas leaves the top of the absorber to be used for the appropriate purposes (H_2 and CH_4) or released to the atmosphere (O_2 and N_2). The CO_2 rich solvent is heated in a heat exchanger before it is sent to the top of the desorber column where the absorbent is regenerated with steam at high temperatures (110 - 130°C). The acid gas is chemically released from the absorbent and flows up through the desorber column together with vaporized water. The vaporized water is condensed from the stripping gas in the overhead condenser, thus providing pure CO_2 which can be used or compressed and sequestered underground or under sea (oceans). The regenerated absorbent is directed back to the top of the absorber. This process has been used for many years for the removal of acid gases, mainly CO_2 and H_2S, from medium to high pressure gas streams to attain a desired gas composition of the treated stream.

With increased awareness of the consequences of CO_2 emissions to the atmosphere, the focus of removing CO_2 from exhausted gas streams has gained increased attention [4].

Today, the separation of CO_2 from gas mixtures using amine based solvents is a mature technology commercially applied to hydrogen production, biogas cleaning and natural gas sweetening. However, this technology has not yet demonstrated to be suitable for the application to CO_2 removing from large scale commercial power plants (up to 500 ton CO_2/h) due to the energy required by absorbent regeneration. The general chemical absorption process of CO_2 from flue gas is shown schematically in Figure 2.2. The flue gas is pumped through an absorption column where CO_2 reacts with the absorbent (about 30% by weight of aqueous amines) at temperatures between, typically, 40 to 60°C. The purified gas is recovered from the top of the absorber. The CO_2-rich solvent is sent to the top of the stripper column where heat is used to regenerate the solvent and to desorb CO_2 at a temperature between 100 and 140°C and pressure greater than 1 bar. This heat is usually generated in a reboiler by some steam extracted from the power plant cycle. The gas stream from the stripper is a CO_2/H_2O mixture. After the H_2O is recovered by a condenser, nearly pure CO_2 is pressurized to be sent to the sequestration site. The heat exchanger cools the regenerated solvent before being transferred to the absorber and simultaneously warms the CO_2 rich solvent to be regenerated.

The main advantage of the technology based on the chemical absorption of CO_2 by aqueous amines is its great efficiency: more than 90% of low pressure CO_2 can be captured because of the fast acid-base reaction which is right-hand shifted.
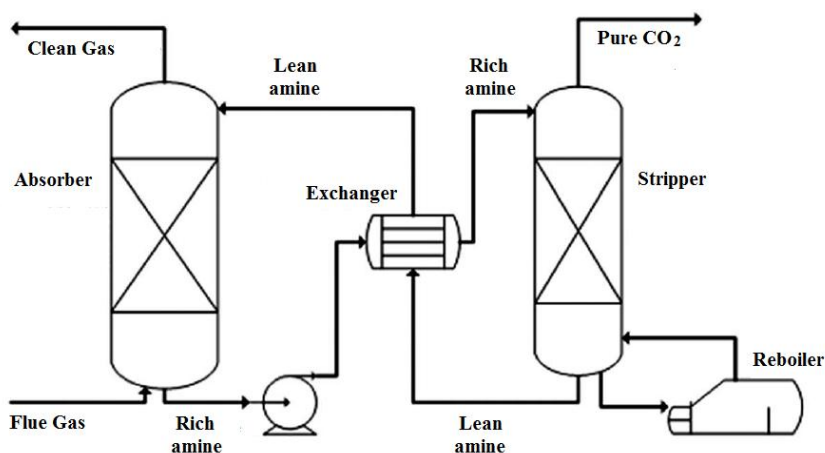
Figure 2.2. Schematic representation of a flue-gas CO_2 absorption process.

Additionally, this technology is suitable for retrofitting to the existing power plants and, in general, to stationary emission sources. However, this technology suffers several drawbacks and, and among these the most important is the high energy consumption for absorbent regeneration and CO_2 release. Other disadvantages are: (a) low CO_2 loading capacity; (b) large equipment size; (c) high equipment corrosion rate; (d) thermal and oxidative degradation of the absorbent, which requires a high absorbent makeup rate [2,5,6]. Furthermore, there is an increasing environmental concern regarding the use of some sorbents (in particular alkanolamines), due to the formation of very toxic degradation products, which can be released with the cleaned gas [7]. As the environmental impact of CO_2 capture is very important, the reduction in CO_2 emissions should not come at the expense of other environmental risks. In order to make more attractive the implementation of the CCS technology to large scale fossil fueled power plants, considerable research efforts are undertaken from engineering and chemical point of view, to make the process more economical efficient as well as environmental safe.

2.2. Features of the Ideal Sorbent

According to the US DOE (Department Of Energy) CO_2 capture goal, a 90% CO_2 capture efficiency with less than 35% increase of the electricity cost are required for CO_2 capture retrofitted power plants [8]. To achieve this objectives, the absorbent efficiency and its thermal and oxidative stability has to be increased, as well as energy costs of the absorbent regeneration should be decreased.

There are some essential factors directly related to the cost-efficiency and environmental impact of the capture process that need to be considered concerning the choice of the absorbents.

- The CO_2 absorption rate determines the height of the absorber tower; a fast rate of reaction reduced the tower height, lowering the capital investment cost.
- A high CO_2 solubility will reduce the amount of the solvent, thus reducing the heat necessary for absorbent regeneration, as well as the pump power.
- <u>A low heat of CO_2 absorption is important for lowering the energy requirements of the desorption step.</u>
- The solvent should have low vapor pressure, to avoid its loss during the process.
- Resistance to degradation is important in order to avoid the possible formation of toxic or corrosive degradation products.
- If a solvent is toxic or leads to toxic degradation products, its use is prohibited.
- Finally, the price of the solvent should be the lower possible.

The process of CO_2 chemical capture depends on three main features of the absorbent, namely the equilibrium constants of the reactions involved, the reaction rate and reaction enthalpy, often related to the equilibrium constant. High equilibrium constants and reaction enthalpy (in absolute value) will result in a high energy consumption for solvent regeneration, while low equilibrium constants or low reaction rate will result in reduced CO_2 absorption. Therefore it is not an easy issue to find the solvent with all of the features that will provide an optimum trade-off between uptake of CO_2 and energy consumption of the process [9].

2.3. Aqueous Alkanolamines

The structures of alkanolamines include primary, secondary, ternary amines containing at least one alcoholic function. Aqueous alkanolamines (in most absorbents 30% by weight) are widely used as absorbent for CO_2 capture due to the fast reaction between the amine function and CO_2 and to their solubility in water by virtue of the –OH group. The reactivity of amines with CO_2 follows the order primary, secondary and ternary amines. On the contrary, the CO_2 loading capacity (mol CO_2 absorbed/mol of amine) for aqueous tertiary amines is higher than those of primary and secondary amines.

Triethanolamine (TEA) was the first alkanolamine which became commercially available and was used by R.R. Bottoms in early acid gas treating plants [10]. Because of its low absorption efficiency and poor stability, TEA has been now scarcely used.

Primary and secondary alkanolamines quickly react with CO_2 to form carbamates; this reaction is usually described by the zwitterion mechanism. This two-step mechanism explains the reaction between CO_2 and the amine with the formation of a an intermediate zwitterion, and afterwards the deprotonation by a base, that leads to the carbamate formation [11-13]. AmH indicates primary or secondary alkanolamine, B is a base in the equations 1-4.

$$CO_2 + AmH \rightleftharpoons AmH^+COO^- \qquad (1)$$

$$AmH^+COO^- + B \rightarrow AmCOO^- + BH^+ \qquad (2)$$
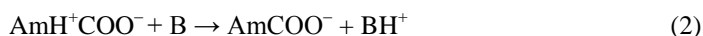
If the base B in the reaction described by equation (2) is the amine itself, the carbamate formation can be represented as follows:

$$AmH^+COO^- + AmH \rightarrow AmCOO^- + AmH_2^+ \qquad (3)$$

In this case, the overall reaction, which accounts for carbamate formation in solution, is given by the sum of reactions represented by equations (1) and (3):

$$CO_2 + 2\ AmH \rightleftharpoons AmCOO^- + AmH_2^+ \qquad (4)$$

If the heat of reaction (4) is high (in absolute value), because of the stability of carbamate, the energy costs of the solvent regeneration is high. Additionally, the CO_2 loading capacity of such alkanolamines is limited to 0.5 mol of CO_2 per mol of amine, as shown in equation (4).

By considering only the main ones, the following reactions may also take place simultaneously in an aqueous amine solution:

$$AmH + CO_2 + H_2O \rightleftharpoons AmH_2^+ + HCO_3^- \qquad (5)$$

$$AmCOO^- + CO_2 + 2\ H_2O \rightleftharpoons 2\ HCO_3^- + AmH_2^+ \qquad (6)$$
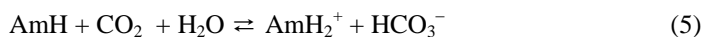
Tertiary alkanolamines do not have hydrogen atom attached to the nitrogen atom, as in the case of primary and secondary alkanolamines, thus the formation of carbamate cannot take place, resulting in a low reactivity with CO_2. Instead, tertiary amines act as a base in the reaction of CO_2 with water thus enhancing the formation of bicarbonate [11,14]. R_3N denotes a tertiary alkanolamine in equation (7).

$$R_3N + H_2O + CO_2 \rightarrow R_3N^+H + HCO_3^- \qquad (7)$$

The base-catalysis reaction could also be explained by a zwitterion-type mechanism [15]:

$$R_3N + CO_2 \rightarrow R_3N^+COO^- \qquad\qquad (8)$$

$$R_3N^+COO^- + H_2O \rightarrow R_3N^+H + HCO_3^- \qquad\qquad (9)$$
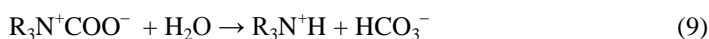
Equation (8) represents a reaction of the amine with CO_2 to form an unstable species. Equation (9) describes the homogeneous hydrolysis reaction in which water reacts with the zwitterion-type species to yield the bicarbonate. The reaction heat released in bicarbonate formation is lower than that of carbamate formation of most amines, thus reducing solvent regeneration costs. Moreover, tertiary amines have a high CO_2 loading capacity of 1 mol of CO_2 per mol of amine. The main disadvantage of the tertiary alkanolamines is their low reaction rate that results in low absorption efficiency.

Sterically hindered alkanolamines, such as 2-amino-2-methyl-1-propanol (AMP), has recently received considerable attention, as a class of amines with lower regeneration energy than those of conventional primary and secondary amines. These amines have one or more substituents attached to the α-carbon, and the steric hindrance near to the amine functionality greatly reduces the stability of the carbamate which cannot be formed in aqueous solution [16]. The reaction of CO_2 with aqueous hindered amines is similar to that of tertiary amines (eq. 7) and lead to the formation of bicarbonate (eq. 10):

$$CO_2 + AmH + H_2O \rightleftarrows HCO_3^- + AmH_2^+ \qquad (10)$$

The loading capacity is 1.0 mol of CO_2 per mol of amine, as high as that of ternary amine [11].

Many experimental studies describe the behavior of several aqueous alkanolamine as possible CO_2 absorbents: examples are 2-aminoethanol (monoethanolamine, MEA), 2,2'-iminodiethanol (diethanolamine, DEA), N-methyl-2-aminoethanol (methylethanolamine, MMEA), N-methyl-2,2'-iminodiethanol (methyldiethanolamine, MDEA), 2-amino-2-methyl-1-propanol (AMP), 2-(2-aminoethoxy)ethanol (diethylene glycol amine, DGA), 1-(2-hydroxypropylamino)propan-2-ol (diisopropanolamine, DIPA) and their blends that have been thoroughly studied in lab-scale experiments [17-22]. Aqueous MEA, in particular, have had industrial scale application to CO_2 capture from natural gas extraction, gas refinery and exhaust gases produced by fossil fuel fired power plant by virtue of its high rate of reaction and low cost [9, 23-27]. MEA however has several drawbacks too, including low CO_2 loading capacity (0.5 mol CO_2/mol amine), high

equipment corrosion rate, thermal and oxidative degradation which entails a high absorbent makeup rate, and, most important, high energy consumption for the absorbent regeneration due to the high stability of the carbamate derivative [27-30].

The tertiary amine MDEA has loading value approaches to 1.0 mol CO_2/mol amine as it does not form carbamates, but its absorption rate is very low as compared to primary and secondary amines [31]. A commercially attractive alternative solvent, the sterically hindered amine AMP, has good regeneration capability, degradation resistance, and higher absorption rate than MDEA but its reaction rate is lower than MEA at 40°C [32]. It is therefore usually used in a mixture with other solvents to enhance the absorption performance. The MEA/AMP blend showed greater removal efficiency than single AMP or MEA/MDEA [33]. Piperazine (PZ) is a cyclic diamine which has been used as the promoter for CO_2 capture with blended alkanolamines, such as MDEA/PZ or MEA/PZ, because of its rapid formation of carbamate with CO_2 [34]. PZ is also an effective resistant to oxygen degradation and thermal degradation to a temperature up to 150°C, but its solubility is limited. In summary, the blended absorbents gave better results as compared to a single solvent.

Alkanolamine degradation is a very relevant issue in chemical absorption processes because it causes economic, operational, and environmental problems. For the most commonly used absorbent, MEA, the degradation would cause the replacement of ~2.2 kg MEA every ton of captured CO_2, leading to an increase of operation cost [35].

Degradation can generally be classified into three types, thermal degradation, carbamate polymerization, and oxidative degradation. The degradation products of MEA are mainly formate, hydroxyethyl formamide, hydroxyethyl imidazole and oxalate. Carbamate polymerization requires the presence of amine at high temperatures so that it typically occurs in the stripper during the thermal regeneration [35,36]. In Figure 2.3 and 2.4 are reported some of the proposed thermal and oxidative degradation pathways for MEA [36].

The absorption/stripping technology based on aqueous solutions of alkanolamines is an energy intensive process and the overall cost of a CO_2 capture process is 52–77 US$/tonCO$_2$ [2]. The regeneration energy for CO_2 capture from a conventional coal-fired power plant lies from 3.24 to 4.2 GJ/tonCO$_2$. In this process, most energy consumption comes from the solvent regeneration step, accounting for about 60% of the required energy.
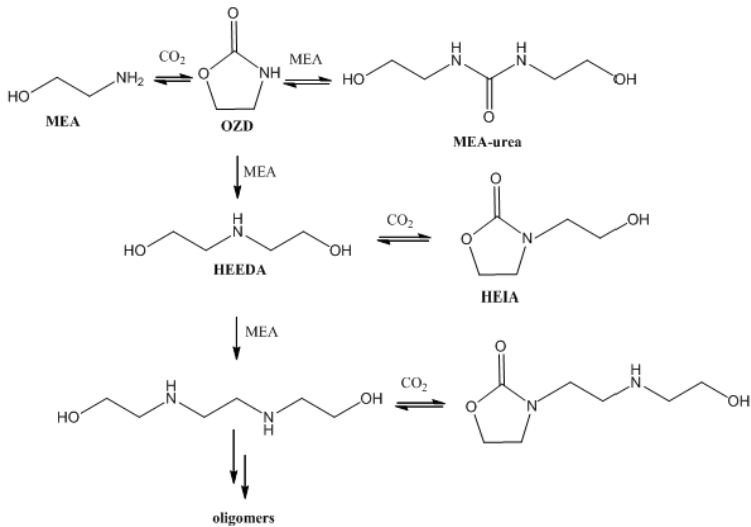
Figure 2.3. Proposed MEA thermal degradation pathways. OZD=Oxazolidinone; HEEDA=N-(2-Hydroxyethyl)ethylendiamine;HEIA=N-(2-hydroxyethyl)imidazolidinone.
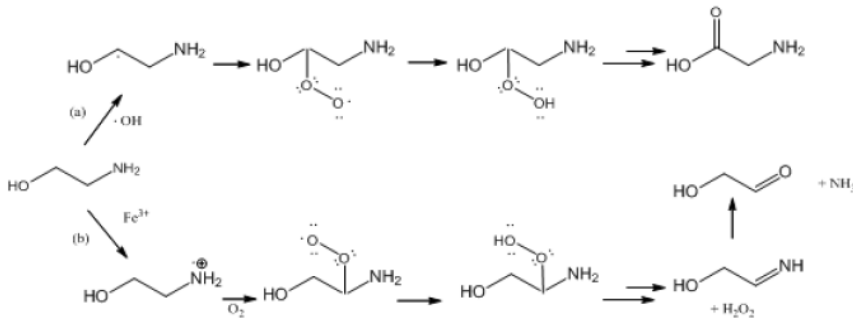
Figure 2.4. Proposed primary oxidation pathways for MEA.

2.4.   Sodium and Potassium Carbonates

The use of alkali (sodium and, mainly, potassium) metal carbonates, either as solids or in solution, for CO_2 capture has been studied for a long time and has been applied in more than 600 plants worldwide for carbon dioxide and hydrogen sulfide removal from streams, like ammonia synthesis gas, crude hydrogen, natural gas, and town gas [37-41]. The main advantages of carbonate solutions for CO_2 removal are the high loading (eq. 11), the more efficient and economical regeneration process compared to that of amines since the absorption can occur at high temperatures, the low solvent costs and the lack of toxicity and degradation problems [42,43].

32

The main reaction of CO_2 with the CO_3^{2-} solution is depicted in equation (11).

$$CO_2 + CO_3^{2-} + H_2O \rightleftharpoons 2\ HCO_3^- \qquad\qquad (11)$$

This reaction shows a favorable equilibrium (Keq $(20°C) = 8.6 \cdot 10^4$) which is substantially shifted toward the formation of bicarbonate when comparable amounts of CO_2 and CO_3^{2-} are reacted. However, the low rate of reaction and, consequently, the low mass transfer of CO_2 in the liquid phase, are the greatest weakness of this process when compared to processes with amines or NH_3 [42]. Additional drawbacks are due to steel corrosion problems (but carbonate is still less corrosive than the amines) and to the precipitation of the bicarbonate in the form of fouling and crystals accumulations. Several studies shows that high CO_2 capture rate generally requires large amounts of catalytic activators such as hindered amines (5–30% w/w) or arsenic(III) derivatives; moreover, corrosion and foam inhibitors are required [42,43]. Increasing the concentration of the absorbent (to 20–40% w/w) and/or raising the temperature close to the boiling point of the solution (>100°C) represent options to increase the absorption capability of the carbonate solution. The regeneration of carbonate and the desorption of CO_2 by heating large volumes of aqueous solutions is a still highly energy consuming step raising serious concerns to the use of this technology to CO_2 removal [42].

2.5.   Aqueous Ammonia

The ammonia scrubbing process, which consists in flowing gaseous CO_2 in an aqueous NH_3 solution, is another possibility for replacing the alkanolamines. Aqueous ammonia provides the advantage of high CO_2 loading capacity, high absorption efficiency with no absorbent degradation, low corrosion problems and therefore lower material costs. Another advantage is the potential low heat requirements as the heat of absorption of CO_2 in aqueous ammonia is lower than in aqueous MEA. However, this process suffers from serious energy penalties due to NH_3 loss avoidance in both absorption and regeneration steps and for the cost required by NH_3 separation from concentrated CO_2 that must be compressed and sequestered [5,44-46]. In order to reduce the NH_3 loss, in the so called "chilled ammonia process", absorption takes place at low temperature (2-10 °C) and the desorption is carried out at pressure greater 1 bar, but this technique is still economically unattractive.

Absorption and reaction kinetics occurring when CO_2 is absorbed into aqueous ammonia solutions are rather complex. The main reactions to be taken into account when CO_2 reacts with aqueous ammonia are:

$$NH_3 + CO_2 + H_2O \rightleftharpoons NH_4^+ + HCO_3^- \qquad (12)$$

$$NH_3 + HCO_3^- \rightleftharpoons NH_2CO_2^- + H_2O \qquad (13)$$

$$NH_3 + HCO_3^- \rightleftharpoons CO_3^{2-} + NH_4^+ \qquad (14)$$
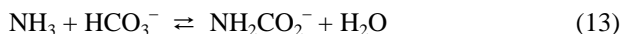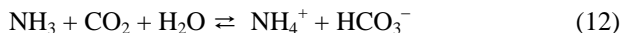
When the reaction occurs between comparable amounts of CO_2 and NH_3, the equilibrium (12) prevails and ammonium bicarbonate is the main species in solution. The same is even more true when an excess of CO_2 is loaded into the solution. In contrast, an excess of NH_3 with respect to the absorbed CO_2, increases the amount of ammonium carbamate and, to a lesser extent, of carbonate according to reactions (13) and (14), respectively. If an excess of NH_3 is maintained in the system, the overall reactions can be rewritten as in reactions (17) and (18) [46].

$$2\,NH_3 + CO_2 \rightleftharpoons NH_2CO_2^- + NH_4^+ \qquad (15)$$

$$2\,NH_3 + CO_2 + H_2O \rightleftharpoons CO_3^{2-} + 2\,NH_4^+ \qquad (16)$$
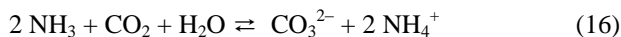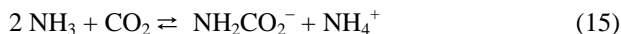
2.6.   Room Temperature Ionic Liquids

In order to avoid the disadvantages of aqueous amines, some research groups have recently proposed CO_2 absorbents based on room temperature ionic liquids. Ionic liquids (ILs) are composed by couples of anions and cations that are liquids even below 100 °C, unlike the common inorganic salts. The CO_2 capture by conventional ionic liquids is based on physical absorption, while functionalised (task-specific) ILs are usually designed to chemically react with CO_2 in the absorption process, increasing the overall absorption capacity. Ionic liquids have the advantage of very low vapor pressures, together with high thermal and chemical stability. In addition, these liquids are used without added water. In addition, the physical absorption mechanism requires lower energy demand in the solvent regeneration step [47]. Examples of these absorbents are "task-specific ionic liquids" (TSILs) [48,49], alkanol guanidines and amidines [50], tunable basic ionic liquids [51] and silylated amines [52]. Some of the most used anions and cations for ILs are reported in Figure 2.5 [53].
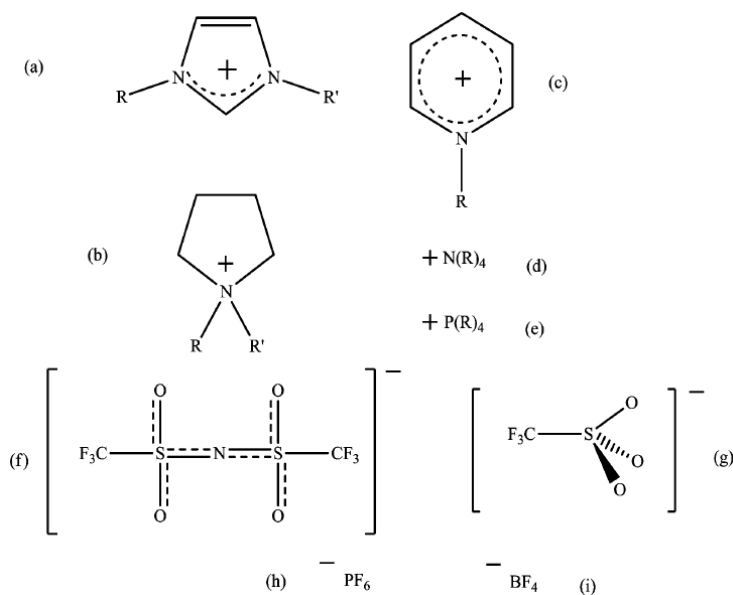
Figure 2.5. Selected IL cation and anion structures. (a) 1,3-dialkylimidazolium $[C_nC_mim]^+$; (b) N,N-dialkylpyrrolidinium $[C_nC_mpyrr]^+$; (c) alkylpyridinium $[C_npyr]^+$; (d) tetraalkylammonium $[C_wC_xC_yC_zN]^+$; (e) tetraalkylphosphonium $[C_wC_xC_yC_zP]^+$; (f) bis(trifluoromethylsulfonyl) imide $[NTf_2]^-$; (g) trifluoromethanesulfonate [OTf]; (h) hexafluorophosphate; (i) tetrafluoroborate [53].

However, the very high viscosity of the carbonated species, the pressure over 1 bar often required to attain a high CO_2 absorption capacity and the reduced pressure or N_2 flushing sometimes necessary for an efficient CO_2 desorption, prevent their application to the continuous absorption-desorption configuration of a commercial plant. Equimolar mixtures of alkanolamines and RTILs give solid compounds upon reaction with CO_2 and therefore are unsuited for the industrial application [54]. Moreover, the synthesis of these promising new solvents is complicated and it is by far more expensive than the commercially available traditional alkanolamines.

2.7. Conclusions

Owing to huge amount of the flue gases to be treated and the low CO_2 partial pressure in the flue gas from post-combustion power plants, wet chemical absorption is at the present the more suitable technology to achieve acceptable CO_2 capture yield. However, this technology is an energy intensive process in which more than 60% of total energy is consumed by CO_2 stripping and thermal regeneration of the carbonated absorbent. To have a large scale application of the chemical absorption, the research activities should

focus on the improvement of absorbent formulation aimed to obtain a sorbent featuring less corrosion problems, less viscosity, low vapor pressure, high reaction rate with CO_2, high CO_2 absorption capacity, and less regeneration energy: an absorbent that satisfies all the aforementioned requirements does not yet exist but this thesis report on the formulation of new absorbents and technique that have the potential of improve the performances of the so far reported solvents but avoiding their disadvantages.

2.8.   References

[1] A.L. Kohl, R.B. Nielsen. Gas Purification. Gulf Publishing Company, Houston, 5th edition, 1997.
[2] G.T. Rochelle. Amine Scrubbing for CO_2 Capture. Science, 2009, 325, 1652–1654.
[3] R.R. Bottoms. Process for Separating Acidic Gases. Girdler Corp., 1930. US Patent 1783901.
[4] Intergovernmental Panel on Climate Change (IPCC). Fifth Assessment Report (AR5). 2014.
[5] K.P. Resnik, J.T. Yeh, H.W. Pennline, Aqua ammonia process for simultaneous removal of CO_2, SO_2 and NOx. Int. J. Environ. Technol. Manage., 2004, 4, 89–104.
[6] R.S. Haszeldine. Carbon Capture and Storage: How Green Can Black Be? Science, 2009, 325, 1647–1651.
[7] B. Thitakamol, A. Veawab, A. Aroonwilas. Environmental impacts of absorption-based CO_2 capture unit for post-combustion treatment of flue gas from coal-fired power plant, International Journal of Greenhouse Gas Control., 2007, 1, 318-342.
[8] National Energy Technology Laboratory, U.S. Department of Energy (DOE/NETL). Carbon Dioxide Capture and Storage RD&D Roadmap. 2010
[9] Intergovernmental Panel on Climate Change (IPCC). Special report on Carbon Dioxide Capture and Storage. Cambridge University Press. Cambridge, United Kingdom and New York, NY, USA. 2005. ISBN: 978-0-5218-6643-9. [10] R.R. Bottoms. Organic Bases for Gas Purification. Ind. Eng. Chem., 1931, 23, 501-504.
[11] P.D. Vaidya, E.Y. Kenig. CO_2-Alkanolamine Reaction Kinetics: A Review of Recent Studies. Chem. Eng. Technol., 2007, 30, No. 11, 1467–1474.
[12] M.J. Caplow. Kinetics of carbamate formation and breakdown. J. Am. Chem. Soc., 1968, 90, 6795-6803.
[13] P.V. Danckwerts. The reaction of CO_2 with ethanolamines. Chem. Eng. Sci., 1979, 34, 443-446.
[14] T.L. Donaldson, Y.N. Nguyen. Carbon Dioxide Reaction Kinetics and Transport in Aqueous Amine Membranes. Ind. Eng. Chem. Fundam., 1980, 19, 260-266.
[15] W.-C. Yu, G. Astarita, D.W. Savage. Kinetics of carbon dioxide absorption in solutions of methyldiethanolamine. Chem. Eng. Sci., 1985, 40, 1585-1590.
[16] M.M. Sharma. Kinetics of reactions of carbonyl sulphide and carbon dioxide with amines and catalysis by Brönsted bases of the hydrolysis of COS. Trans. Faradey Soc. 1965, 61, 681-688.
[17] A.J. Teller, H.E. Ford. Packed column performance: CO_2-MEA. Ind. Eng. Chem., 1958, 50, 1201-1206.
[18] G. Astarita, D.W. Savage, A.Bisio. Gas treating with chemical solvents. John Wiley & Sons, New York. 1984.

[19] D. Bonenfant, M. Mimeault, R. Hausler. Determination of the structural features of distinct amines important for the absorption of CO_2 and regeneration in aqueous solution. Ind. Eng. Chem. Res., 2003, 42, 3179-3184.

[20] B.P. Mandal, A.K. Biswas, S.S. Bandyopadhyay. Selective absorption of H_2S from gas streams containing H_2S and CO_2 into aqueous solutions of N-methyldiethanolamine and 2-amino-2-methyl-1-propanol. Sep. Purif. Technol., 2004, 35, 191-202.

[21] W.C. Sun, C.B. Yong, M.H. Li. Kinetics of the absorption of carbon dioxide into mixed aqueous solutions of 2-amino-2-methyl-l-propanol and piperazine. Chem. Eng. Sci., 2005, 60, 503-516.

[22] W.J. Choi, K.C. Cho, S.S. Lee, J.G. Shim, H.R. Hwang, S.W. Park, K.J. Oh. Removal of carbon dioxide by absorption into blended amines: kinetics of absorption into aqueous AMP/HMDA, AMP/MDEA, and AMP/piperazine solutions. Green Chem., 2007, 9, 594-598.

[23] J.T. Yeh, H.W. Pennline, K.P. Resnik. Study of CO_2 absorption and desorption in a packed column. Energy Fuels, 2001, 15, 274-278.

[24] B.A. Oyenekan, G.T. Rochelle. Energy performance of stripper configurations for CO_2 capture by aqueous amines. Ind. Eng. Chem. Res., 2006, 45, 2457-2464.

[25] R. Idem, M. Wilson, P. Tontiwachwuthikul, A. Chakma, A. Veawab, A. Aroonwilas, D. Gelowitz. Pilot plant studies of the CO_2 capture performance of aqueous MEA and mixed MEA/MDEA solvents at the University of Regina CO_2 capture technology development plant and the Boundary Dam CO_2 capture demonstration plant. Ind. Eng. Chem. Res., 2006, 45, 2414-2420.

[26] A. Yamasaki. An overview of CO_2 mitigation options for global warming - emphasizing CO_2 sequestration options. Journal of Chemical Engineering of Japan, 2003, 36, 361-375.

[27] M.K. Mondal, H.K. Balsora, P.Varshney. Progress and trends in CO_2 capture/separation technologies: A review. Energy, 2012, 46, 431-441.

[28] J.K. Yeh, K.P. Resnik, K. Rygle, H.W. Pennline. Semi-batch absorption and regeneration studies for CO2 capture by aqueous ammonia. Fuel Processing Technology, 2005, 86, 1533-1546.

[29] B. Feng, M. Du, T.J. Dennis, K. Anthony, M.J. Perumal. Reduction of energy requirement of CO_2 desorption by adding acid into CO_2-loaded solvent. Energy and Fuels, 2010, 24, 213-219.

[30] H. Lepaumier, S. Martin, D. Picq, B. Delfort, P.L. Carrette. New amines for CO_2 capture III, effect of alkyl chain length between amine functions on polyamines degradation. Ind. Eng. Chem. Res., 2010, 49, 4553-4560.

[31] M.K. Mondal. Solubility of carbon dioxide in an aqueous blend of diethanolamine and piperazine. Journal of Chemical & Engineering Data 2009, 54, 2381-2385.

[32] R. Quadrelli, S. Peterson. The energy climate challenge: recent trends in CO_2 emission from fuel combustion. Energy Policy, 2007, 35, 5938-5952.

[33] B.P. Mandal, M. Guha, A.K. Biswas, S.S. Bandyopadhyay. Removal of carbon dioxide by absorption in mixed amines: modeling of absorption in aqueous MDEA/MEA and AMP/MEA solutions. Chemical Engineering Science, 2001, 56, 6217-6224.

[34] S.A. Freeman, R.D. Dugas, H.V. Wangener, G.T. Rochelle. Carbon Dioxide Capture with Concentrated, Aqueous Piperazine. Int. J. Greenhouse Gas Control, 2010, 4, 119–124.

[35] C.H. Yu, C.H. Huang, C.S. Tan. A Review of CO_2 Capture by Absorption and Adsorption. Aerosol and Air Quality Research, 2012, 12, 745–769.

[36] S.B. Fredriksen, K.-J. Jens. Oxidative degradation of aqueous amine solutions of MEA, AMP, MDEA, Pz: A review. Energy Procedia, 2013, 37, 1770 – 1777

[37] A. Kohl, R. Nielson. Gas Purification. Gulf Publishing Company, Houston, TX (1997).

[38] A. Pérez-Salado Kamps, E. Meyer, B. Rumpf, G. Maurer. Solubility of CO_2 in Aqueous Solutions of KCl and in Aqueous Solutions of K_2CO_3. J. Chem. Eng. Data, 2007, 52, 817-832.

[39] A. Corti. Thermoeconomic evaluation of CO_2 alkali absorption system applied to semi-closed gas turbine combined cycle. Energy 2004, 29, 415-426.

[40] H. Hayashi, J. Taniuchi, J. Furuyashiki, S. Sugiyama, S. Hirano, N. Shigemoto, T. Nonaka. Efficient Recovery of Carbon Dioxide from Flue Gases of Coal-Fired Power Plants by Cyclic Fixed-Bed Operations over K_2CO_3-on-Carbon. Ind. Eng. Chem. Res., 1998, 37, 185-191.

[41] G. Sartori, D.W Savage. Sterically hindered amines for CO_2 removal from gases. Ind. Eng. Chem. Fundam. 1983, 22, 239-249.

[42] F. Mani, M. Peruzzini, P. Stoppioni. Combined Process of CO_2 Capture by Potassium Carbonate and Production of Basic Zinc(II) Carbonates: CO_2 Release from Bicarbonate Solutions at Room Temperature and Pressure. Energy & Fuels, 2008, 22, 1714–1719.

[43] T.N.G. Borhani, A. Azarpour, V. Akbari, S.R.W. Alwi, Z.A. Manan. CO_2 capture with potassium carbonate solutions: A state-of-the-art review. International Journal of Greenhouse Gas Control, 2015, 41, 142–162.

[44] J.E. Pelke, P.J. Concannon, D.B. Manley, B.E. Poling. Product distributions in the carbon dioxide-ammonia-water system from liquid conductivity measurements. Ind. Eng. Chem. Res., 1992, 31, 2209–2215.

[45] V. Darde, K. Thomsen, W.J.M. van Well, E.H. Stenby. Chilled ammonia process for CO_2 capture. Int. J. Greenhouse Gas Control, 2010, 4, 131–136.

[46] F. Mani, M. Peruzzini, P. Stoppioni. CO_2 absorption by aqueous NH_3 solutions: speciation of ammonium carbamate, bicarbonate and carbonate by a ^{13}C NMR study. Green Chem., 2006, 8, 995–1000.

[47] M.J. Earle, K.R. Seddon. Ionic liquids. Green solvents for the future. Pure and Applied Chemistry, 2000, 72, 1391–1398.

[48] E.D. Bates, R.D. Mayton, I. Ntai, J.H.Jr. Davis. CO_2 capture by a task-specific ionic liquid. J. Am. Chem. Soc., 2002, 124, 926-927.

[49 L.M. Galán Sánchez, G.W. Meindersma, A.B. de Haan. Solvent properties of functionalized ionic liquids for CO_2 absorption. Chemical Engineering Research and Design, 2007, 85, 31-39.

[50] D.J. Heldebrant, P.K. Koech, M.T.C. Ang, C. Liang, J.E. Rainbolt, C.R. Yonker, P.G. Jessop. Reversible zwitterionic liquids, the reaction of alkanol guanidines, alkanol amidines, and diamines with CO_2. Green Chem., 2010, 12, 713-721.

[51] C. Wang, X. Luo, H. Luo, D. Jiang, H. Li, S. Dai. Tuning the Basicity of Ionic Liquids for Equimolar CO_2 Capture. Angew. Chem., Int. Ed., 2011, 50, 4918-4922.

[52] V. Blasucci, R. Hart, V. Llopis-Mestre, D.J. Hahne, M. Burlager, H. Huttenhower, B.J.R. Thio, P. Pollet, C.L. Liotta, C.A. Eckert. Single component, reversibile ionic liquids for energy applications. Fuel, 2010, 89, 1315-1319.

[53] M.E. Boot-Handford, J.C. Abanades, E.J. Anthony, M.J. Blunt, S. Brandani, N. Mac Dowell, J.R. Fernandez, M.C. Ferrari, R. Gross, J.P. Hallett, R.S. Haszeldine, P. Heptonstall, A. Lyngfelt, Z. Makuch, E. Mangano, R.T.J. Porter, M. Pourkashanian, G.T. Rochelle, N. Shah, J.G. Yao, P.S. Fennell. Carbon capture and storage update. Energy Environ. Sci., 2014, 7, 130–189.

[54] D. Camper, J.E. Bara, D.L. Gin, R.D. Noble. Room-temperature ionic liquid-amine solutions: tunable solvents for efficient and reversible capture of CO_2. Ind. Eng. Chem. Res., 2008, 47, 8496–8498.

3. The Formulation of New Liquid Sorbents and the Experimental Methodologies Used for their Test

3.1. Our Strategies for the Improvement of Amine-Based Absorbents

Despite the liquid absorbents for the chemical capture of CO_2 have found wide application in the field of gas purification (methane, hydrogen, ammonia), significant improvements are needed in order to apply this technology to the CO_2 capture from exhaust gases of large stationary plants (such as fossil fuel fired power plants). The ideal liquid for the chemical absorption of CO_2 should have these main features:

1) reversibility, *i.e.* capable to be regenerated for its reuse;
2) the carbonated species after CO_2 uptake must be soluble in the solvent used;
3) high capacity for CO_2 capture (ratio CO_2 / base close to 1);
4) high reaction rate combined with a low reaction enthalpy (in absolute value; less energy required for regeneration);
5) low volatility, thermal and oxidative stability.

The most studied liquids are aqueous solutions of alkanolamines, of alkali carbonates and ammonia, but none of these solutions has all the desirable features (see Sections 2.3-2.6).

With the aim of taking advantages of the high efficiency of conventional aqueous alkanolamines yet reducing their disadvantages, we have been pursuing a lab-scale research on alternative absorbent formulations aimed at reducing the energy of the absorbent regeneration and the amine degradation, yet maximising the CO_2 capture. The ultimate goal of all carbon capture and sequestration technologies should be to increase the net balance $CO_{2(captured)} - CO_{2(emitted)}$[2] that has to be taken into account for any reliable cost-to-benefit assessment in a large-scale application of the CO_2 capture technology.

In aqueous alkanolamines, CO_2 is captured in solution as HCO_3^- (only to a much lesser extent as CO_3^{2-}) and, for primary and secondary unhindered amines, also as thermally stable carbamate:

---

[2] $CO_{2(emitted)}$ represents the overall amount of CO_2 released in the atmosphere by burning fossil fuels to produce all forms of energy (electrical, thermal and mechanical) necessary to sustain the entire CO_2 removal cycle, from the production of the absorbing reagents to the final transport of CO_2 and its disposal.

$$AmH + CO_2 + H_2O \rightleftharpoons AmH_2^+ + HCO_3^- \qquad (1)$$

$$HCO_3^- + AmH \rightleftharpoons AmCO_2^- + H_2O \qquad (2)$$
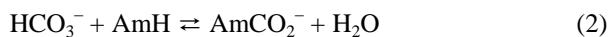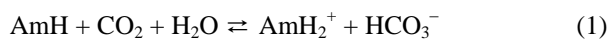
where AMH stands for the free amine; $AmCO_2^-$ and AmH_2^+ indicate the carbamate and the protonated amine, respectively. Tertiary amines are unable to form carbamate. ^{13}C NMR analysis has allowed to establish that the relative amount of the two species depends on both the amine concentration and CO_2/amine molar ratio [1-8]. By the consequence of both the reactions (1) and (2), the loading capacity of the primary and secondary alkanolamines is comprised between 0.6 and 0.8. The release of CO_2 from stable amine carbamates and from HCO_3^- requires high stripping temperatures, typically about 110–140 °C, pressure over 1 bar and, consequently, a huge amount of energy is consumed in the amine regeneration step. Moreover, a considerable amount of the energy required by the alkanolamine regeneration is consumed by water evaporation (high evaporation enthalpy, 2.26 kJ g^{-1}) and by its heating from the temperature of absorption (usually 30-40 °C) to desorption temperature (120-140 °C, high heat capacity of water, 4.18 kJ kg^{-1} $°C^{-1}$).

With the objective of reducing the energy required by the desorption process, we have devised the strategy to avoid water. The replacement of water by organic solvents, or the absence of any solvents at all, may redirect the reaction of amines with CO_2 towards less stable species which, consequently, require lower stripping temperatures at room pressure.

In this thesis, the study has been focused on amines which combine high reaction rate with CO_2 in a non-aqueous environment, with lower reaction enthalpy (in absolute value) and therefore these absorbents require lower regeneration temperatures compared to those of the aqueous solutions (75-95 °C at room pressure instead of 120-140 °C under pressure). Furthermore, the lower operating temperatures reduce the decomposition rate and the loss of the amines. As additional, not negligible benefit, the absence of water strongly reduces the equipment corrosion and avoids foaming problems.

A first study has been devoted to the replacement of water by organic solvents. The results obtained with solutions of alkanolamines in organic solvents are reported in Chapters 4 and 5.

Subsequently, the avoidance of any solvent has been considered. Therefore, our study has been focused on amines capable of absorbing CO_2 without any dilution, provided

they are liquid before and after the carbon dioxide uptake. The results obtained are reported in Chapter 6.

A last step of the study, still under development, concerns the use of a liquid biphasic system, a technique which combines the advantages of both organic solvents and solvent–free sorbents. A first series of experiments is reported in Chapter 7.

3.2.   How We Have Tested any New Sorbent

The amines that are identified as possible good absorbers are tested with a standard procedure which has been developed in order to evaluate their different CO_2 absorption capability and to compare their overall features.

The first step of our experimental protocol is the *batch experiment of CO_2 absorption*, to evaluate the maximum capacity of CO_2 absorption of the sorbent, the *loading capacity*. Afterward, the *batch experiment of CO_2 desorption* from the carbonated solution is carried out *,* to measure the amount of CO_2 released at high temperature and to evaluate the capability of absorbent regeneration.

If the batch experiments give satisfactory results, the sorbent is tested in the *continuous cycle of absorption and desorption*, aimed at verifying the ability of the sorbent to operate continuously in a mini pilot plant without losing efficiency over time.

The speciation of the carbonated species and of the unreacted amine recovered from each experiment has been obtained from ^{13}C NMR spectroscopy, in order to better understand the reactions involved.

3.2.1.   Batch Experiments of CO_2 Absorption

The absorber device, schematically shown in Figure 3.1, is a home-built glass cylinder with a diameter of 56 mm and a height of 300 mm, with a sintered glass diffuser. To enhance the rate of CO_2 capture by increasing the liquid-gas contact surface and extending the contact time between the gas and absorbent, the absorber was equipped with three polyethylene disks threaded on a 2 mm glass rod fitted within the liquid. A weighed amount of the amine solution is placed into the absorber device and it is saturated with pure CO_2 at the desired temperatures (20-40 °C); the absorption was stopped when no more CO_2 was absorbed. From the weight increase of the CO_2-saturated solution, it is possible to compute the amount of CO_2 capture and,

subsequently, the maximum amine loading capacity, defined as the ratio between the moles of CO_2 absorbed and of starting amine. The experiment temperature is constantly kept under control with a thermostatted water bath (Julabo model F33-MC refrigerated bath) regulated at the required absorption temperature. Pure CO_2 is continuously fed into the absorber through the sintered glass diffuser (16–40 mm pores) placed at the bottom of the absorbent solution. A cold condenser at 0°C avoided absorbent loss during the solvent carbonation.
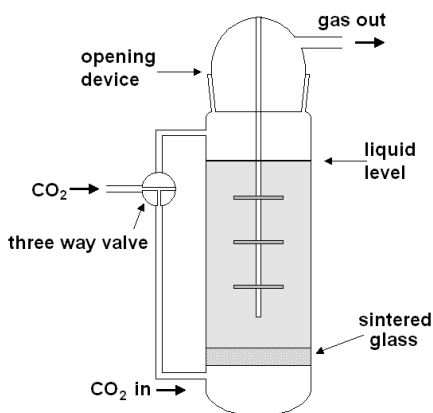
Figure 3.1. Simplified sketch of the CO_2 absorber used for the determination of amine loading.

3.2.2. Batch Experiments of CO_2 Desorption

In this test the CO_2-loaded solution obtained in the absorption experiment is heated to a preset temperature and the CO_2 released is measured, to assess the capability of the carbonated absorbent to be regenerated as a function of the temperature. The release of pure CO_2 during the desorption processes was measured using a gastight apparatus which comprises a conical flask containing half of the different solutions obtained during the absorption steps. In this way a duplicate measurement of the CO_2 release could be obtained for each solution. The conical flask was equipped with two condensers cooled to room temperature and connected to two 0.250 dm^3 gas burettes equipped with a pressure-equalising device. Both burettes and pressure-equalising devices were filled with CO_2 saturated water. Through three-way valves, one burette was filled with CO_2 while the other was emptied, thus allowing a continuous collection of gas. The gas pressures inside the burette and the external pressure continuously balanced each other. The total volume measurements were about ±0.005 dm^3 accurate.

3.2.3. Continuous Cycles of CO₂ Absorption-Desorption

This experiment is designed to simulate the behavior of the sorbent in a closed absorption/desorption system suitable to treat a continuous gas flow (Figure 3.2). In this way it is possible to determine the absorption efficiency of the sorbent and its thermal and oxidative degradation over time.
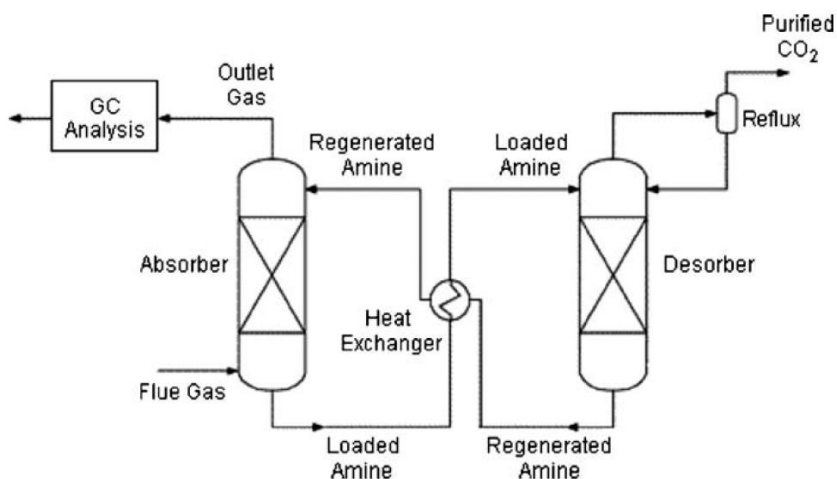
Figure 3.2. Simplified flow diagram of the absorber–stripper cyclic configuration.

The absorbent solution is put in our lab-scale pilot plant and continuously circulated between the columns of absorption and desorption, kept at different temperatures. The closed cycle absorption-desorption apparatus (Figure 3.3) consists of the absorber and the desorber units connected to each other by means of a double head peristaltic pump (Masterflex) allowing the solutions to circulate continuously in a closed loop between the absorber and the desorber at the desired flow rate. The absorber and desorber devices are two home-built glass cylinders with the internal diameter of 56 mm and height 400 mm, equipped with a jacket. The columns were packed with glass rings (diameter 5 mm). The temperature of both absorber (20-40 °C) and of desorber (75-95 °C) is maintained at the appropriate value by circulating a thermostatted liquid (Julabo model F33-MC bath) through the jackets.

The absorber was designed to operate in a counter current mode, namely the regenerated absorbent was introduced from the top of the packed column while the gas mixture was continuously injected at the bottom of the column below the packings. The carbonated absorbent exited at the bottom of the column. The desorber was equipped with a water cooled condenser to reflux the possible overhead vapour to the stripper. In some

experiments the carbonated amine solution exiting from the absorber was preheated by a cross heat exchanger with hot regenerated amine solution exiting from the desorber which is, in turn, cooled to room temperature before being recycled to the absorber.
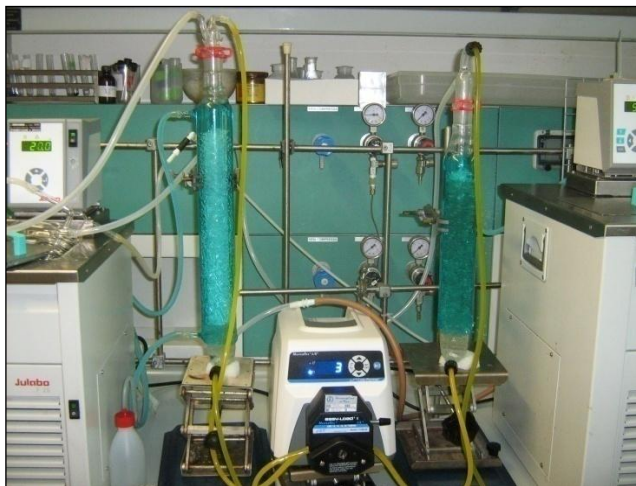
Figure 3.3. The lab-scale pilot plant used for continuous cycles of CO_2 absorption/desorption..

To mimic the composition of a flue gas of a power plants or the composition of a biogas, a gas mixture containing the desired percentage of CO_2 (12-40% v/v) in air is continuously fed into the absorber. Flow rates of air and CO_2 are measured with gas mass flow meters (Aalborg) equipped with gas controllers (Cole Parmer). The outlet gas from the absorber is in turn flowed through a condenser cooled at −5 °C, a concentrated H_2SO_4 solution and a gas purification tower filled with P_2O_5, before being analyzed by the gas chromatograph to evaluate the percentage of CO_2 captured and therefore the absorption efficiency. The inlet and outlet CO_2 concentrations in the flue gas mixture are measured with a Varian CP-4900 gas chromatograph calibrated with a 15% and 40% v/v CO_2/N_2 and a 100% CO_2 reference gas (Rivoira Spa). A complete cyclic experiment may last a few days and, for each desorption temperature, it is stopped when the reactions of CO_2 capture and amine regeneration reach a steady state. ^{13}C NMR spectroscopic analysis allows us to identify and evaluate the species that are formed during CO_2 capture. All of the experiments usually are repeated in duplicate or triplicate with good reproducibility of the results: the deviation from the average values is always in the range 1.5–3%.

3.3. ^{13}C NMR Spectroscopy

All the information about the identification and quantification of species in the different tested solutions were obtained through ^{13}C NMR spectroscopy.

The spectra of all the solutions were obtained at room temperature with a Bruker Avance III 400 spectrometer operating at 100.61271 MHz. Chemical shifts are to high frequency relative to tetramethylsilane as external standard at 0.00 ppm. CH$_3$CN was used as internal reference (CH$_3$, δ = 1.47). To provide enough signal for deuterium lock, D$_2$O (Aldrich) contained in a sealed glass capillary was introduced into the NMR tube containing the amine solution. To obtain quantitative ^{13}C NMR spectra, the pulse sequence with proton decoupling and NOE suppression was used to acquire the ^{13}C{^{1}H} with the following acquisition parameters: pulse angle, 90.0°; acquisition time, 1.36 s; delay time, 2–30 s; data points, 64 K; number of scans, 500–2000. The data were processed by using Bruker-Biospin Topspin software. Increasing the acquisition time and/or the relaxation delay time (up to 60 s) does not produce substantial changes in the relative peak areas of the CH$_2$ carbon atoms with the same number of protons [1,9].

The relative amounts of carbamate and of the rapidly equilibrating (free amine)/(protonated amine) have been estimated by peak integration for each CH$_2$ resonance by running ^{13}C NMR spectra of the solutions recovered from both absorber and desorber at successive steps of each experiment., as already reported in our previous works [5-7].

In order to quantify the relative amounts of carbamate and alkyl carbonate, we carefully integrated the carbon resonances of carbamate R-CO$_2^-$ and carbonate R'-OCO$_2^-$ falling in the range 164–159 ppm. The quaternary ^{13}C atoms of R-OCO$_2^-$ and of R'-CO$_2^-$ functionalities exhibit much longer relaxation times than -CH$_2$- groups, thus resulting in lower intensity resonances. Although some uncertainty in comparing the different integrals is unavoidable , nonetheless the method is certainly reliable and provides a first estimation of the concentration changes of the species originating from the adsorbed CO$_2$ in solution and of their dependence from the desorption temperature.

Normally, the integration of ^{13}C NMR resonances does not grant a reliable quantification of species with carbon atoms in different environments, because the spin–lattice T1 relaxation time strongly depends on the number of protons attached to the carbon atom [9]. In the species we have been dealing with, i.e. carbamate and the rapidly equilibrating (free amine)/(protonated amine), the ^{13}C atoms of the CH$_2$–CH$_2$ backbone have the same

number of directly attached hydrogens, and it is conceivable that they exhibit similar T1, as shown by the similar peak integrals occurred in each CH_2 resonance (estimated error < 2%). The feasibility of this procedure was tested by carrying out several ^{13}C NMR spectra on reference solutions and we found a quantitative relationship (estimated error <5%) between the relative peak areas of CH_2CH_2 carbon atoms and the known concentrations of each species. The quantification method is therefore, on an empirical level, quite reliable, consequently reflecting similarities of the relaxation rate for similar carbons in both carbamate and the rapidly equilibrating (free amine)/(protonated amine).

3.4.   References

[1] R.J. Hook. An investigation of some sterically hindered amines as potential carbon dioxide scrubbing compounds. Ind. Eng. Chem. Res., 1991, 36, 1779–1790.
[2] J. Oexmann, A. Kather. Minimising the regeneration heat duty of postcombustion CO_2 capture by wet chemical absorption: the misguided focus on low heat of absorption solvents. Int. J. Greenh. Gas Contr., 2010, 4, 36–43.
[3] S.J. Yoon, H. Lee. Substituent effect in amine–CO_2 interaction investigated by NMR and IR spectroscopies. Chem. Lett., 2003, 32, 344–345.
[4] J.Y. Park, S.J. Yoon, H. Lee. Effect of steric hindrance on carbon dioxide absorption into new amine solutions: thermodynamic and spectroscopic verification through solubility and NMR analysis. Environ. Sci. Technol., 2003, 37, 1670–1675.
[5] F. Barzagli, F. Mani, M. Peruzzini. A ^{13}C NMR study of the carbon dioxide absorption and desorption equilibria by aqueous 2-aminoethanol and N-methyl-substituted 2-aminoethanol. Energy Environ. Sci., 2009, 2, 322-330.
[6] F. Barzagli, F. Mani, M. Peruzzini. Continuous cycles of CO_2 absorption and amine regeneration with aqueous alkanolamines: a comparison of the efficiency between pure and blended DEA, MDEA and AMP solutions by ^{13}C NMR spectroscopy. Energy Environ. Sci., 2010, 3, 772-779.
[7] F. Barzagli, F. Mani, M. Peruzzini. A ^{13}C NMR investigation of CO_2 absorption and desorption in aqueous 2,2'-iminodiethanol and N-methyl-2,2'-iminodiethanol. Int. J. Greenh. Gas Contr. 2011, 5, 448-456.
[8] M. Ballard, M. Bown, S. James, Q. Yang. NMR studies of mixed amines. Energy Procedia, 2011, 4, 291–298.
[9] E. Breitmaier, W. Voelter. Carbon-13 NMR Spectroscopy, 3rd ed., 1990, VCH-Weinheim, Germany Breitmaier and Voelter.

4. CO$_2$ Absorption with Non-Aqueous Solvents Based on 2-amino-2-methyl-1-propanol (AMP)

4.1. Introduction

Replacing water with organic solvents may provide significant cost saving in the process of sorbent regeneration and concentrated CO$_2$ release. The potential advantages of this technology, in comparison to conventional aqueous solutions of identical alkanolamines, would include lower amine decomposition and evaporation as well as reduced equipment corrosion due to the reduced stripping temperature. Additionally, the lower heat capacity and evaporation enthalpy of the organic solvents compared to water should contribute to decrease the regeneration heat penalty (Table 4.1).
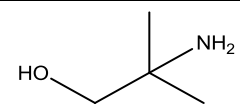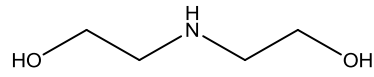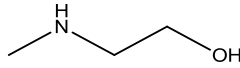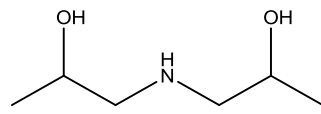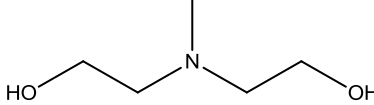
Table 4.1. Some properties of water and common organic solvents.

Solvent	Tb (°C)	Viscosity at 25°C (cP)	Heat Capacity at 25°C (J g^{-1} °C^{-1})	Heat of vaporization at Tb (kJ g^{-1})
Water	100	1.001	4.18	2.26
Ethanol	78.4	1.074	2.44	0.84
1-Propanol	97	1.938	2.39	0.69
Ethylene glycol	197.6	16.9	2.41	0.81
Diethylene glycol monomethyl ether	194	3.5	2.26	0.39

The study here reported was aimed at investigating the CO$_2$ capture properties of sorbents formed by single 2-amino-2-methyl-1-propanol (AMP), or its blends with diethanolamine (DEA, 2,2-iminodiethanol), methylethanolamine (MMEA, N-methyl-2-aminoethanol), methyldiethanolamine (MDEA, N-methyl-2,2-iminodiethanol), diisopropanolamine (DIPA, bis(2-hydroxypropyl)amine) dissolved in different alcohol mixtures (ethylene glycol/methanol; ethylene glycol/ethanol; ethylene glycol/1-propanol; 1,2-propandiol/ethanol) or in single 1-propanol and diethylene glycol monomethyl ether (DEGMME). The selected amines are reported in Table 4.2.

AMP based solvents have been selected as suitable candidates to test the efficiency of this technique, because of their relatively low regeneration energy and high thermal stability [1,2]. AMP indeed cannot form carbamate in water solution due to steric hindrance at the amine functionality [3].

Table 4.2. Abbreviation, name and formula of the tested amines.

AMP	2-amino-2-methyl-1-propanol	
DEA	diethanolamine	
MMEA	methylethanolamine	
DIPA	diisopropanolamine	
MDEA	methyldiethanolamine	

Finally, AMP blended with different amines has been tested as the performances of the amine blends are generally superior over their single components, due to the faster CO_2 absorption of the ancillary amines [4,5].

The choice of the alcohols to be mixed with amines was dictated by four main considerations: (a) low cost, (b) high boiling temperature, (c) solubility of the compounds formed by CO_2 uptake and (d) avoidance of foaming problems and immiscible liquid phases. Concerning point (c), ethylene glycol (hereafter indicated as EG) was found necessary to avoid the formation of precipitates during CO_2 absorption. Unfortunately, pure EG is unsuitable for CO_2 capture in spite of its high boiling temperature and low cost, due to its high absolute viscosity (μ = 16.9 cP at 25 °C) that reduces the mass transfer, therefore lowering the absorption efficiency. Consequently, most experiments were carried out with mixtures of EG with alcohols to reduce the viscosity of the solvent yet maintaining a boiling temperature up to 150 °C.

Systematic experimental investigations of amine–CO_2 reactions in organic solvents are still scarce, unlike in aqueous solutions, and have been limited to kinetic and solubility studies of MEA, DEA, MDEA in a variety of organic solvents [6,7].

4.2.   General Experimental Information

All used chemicals were of analytical grade. The alkanolamines (>98%) and the alcohols (>99%) were purchased from Sigma–Aldrich and were used as received without further purification.

The saturation of each amine solution with pure CO_2 was carried out at thermostatted 20 °C as described in Section 3.2.1. From the weight increase of the CO_2 saturated solution, we computed the maximum amine loading capacity. The absorption experiments were carried out in a continuous cycle with CO_2 capture and simultaneous amine regeneration, with a technique and apparatus previously described in Section 3.2.3. To mimic the flue gas, a gas mixture containing 12% (v/v) CO_2 in air was passed through a humidifier before being continuously fed into the bottom of the absorber with a flow rate of 14.0 $dm^3 h^{-1}$ (CO_2, 0.0689 mol h^{-1} at 24 °C). The inlet and outlet CO_2 concentrations in the flue gas mixture were measured with a Varian CP-4900 gas chromatograph. The stripped CO_2 was not recovered. Quantitative measurements carried out with a condenser cooled to -5 °C and properly designed to collect the condensed vapor, are indicative of no alcohol loss. A complete cyclic experiment lasted 24-36 h and, for each desorption temperature tested, it was stopped when the reactions of CO_2 capture and amine regeneration were equilibrated to each other.

The viscosity of the tested solutions was measured at 27 °C with a Gilmont "Falling Ball Type" Viscometer by using 0.005 dm^3, approximately, of the appropriate amine. The viscometer tube was immersed in a constant temperature bath with a transparent window to observe the fiduciary lines. The proper ball was selected and dropped into the tube using the ball release device. The time of descent between the two sets of fiduciary lines was measured with a stop-watch. The reproducibility of the measurements was in the range 0.2– 1.0% depending upon the time of descent.

The speciation of the carbon-containing species in the CO_2 saturated solutions, in the starting solutions (50% CO_2 saturation), in the carbonated (absorber) and regenerated (desorber) solutions at increasing temperatures (65–80°C) was analyzed by running ^{13}C NMR spectra of the solutions at successive steps of each experiment as described in Section 3.3.

4.2.1. AMP-Amine Blends Experiments

The starting solutions of blended amines were at overall concentrations 2.0 mol dm^{-3}. AMP/amine molar ratios were 1/1 but AMP/DEA was 2/1 in DEGMME. Mixed solvents were 1/1 on volume scale, except the 1/2 volume ratio of EG/1-propanol. Both the absorber and the desorber were charged with the same volume (0.300 dm^3) of the appropriate solution that was previously 50% saturated with CO_2. To prepare these solutions, 0.300 dm^3 of the appropriate amine solution were pre-saturated with pure CO_2 and then mixed with the required volume of the same free amine solution to obtain an overall 0.600 dm^3 solution.

Absolute viscosity values (at 27 °C) of the starting solutions have been reported in Section 4.3. The reference value at 25 °C of aqueous AMP/DEA is 1.78 cP.

The saturation with 12% CO_2 of 0.300 dm^3 of 2.0 mol dm^{-3} AMP/DEA in 1-propanol for 40 min causes the slow formation of a voluminous white precipitate which was separated by filtration, washed in turn with the same solvent, a mixture of the solvent with diethyl ether (1/1, v/v) and diethyl ether alone, before being dried at room temperature with a dry N_2 stream. The mass of the solid was 64% with respect to the mass of the starting AMP. In an analogous CO_2 saturation experiment, the precipitate was not separated from the solution and the slurry was decomposed at increasing temperatures between 50 and 65 °C, at room pressure, until the release of CO_2 ended and the solid phase disappeared. The volume of the overall desorbed CO_2 was measured at room temperature and pressure using the previously described gastight apparatus [8]. In the CO_2 absorption experiments yielding solid precipitates, ^{13}C NMR spectra of the solutions were carried out either before or after precipitation of the solid compounds. The ^{13}C NMR spectrum of the solid was also recorded. Cross polarization magic angle spinning (CP-MAS) ^{13}C NMR spectra were recorded at room temperature on a Bruker Avance DRX-400 spectrometer equipped with a 4 mm BB CP-MAS probe at a working frequency of 100.62 MHz. The spectra were recorded using a cross polarization pulse sequence under magic angle spinning at a spinning rate of 10.0 kHz.

4.2.2. Single AMP Experiments

The CO_2 capture by single AMP solutions was carried out with two different procedures aimed at increasing the efficiency of CO_2 release. The AMP concentrations were 2.0-3.0 mol dm^{-3}. Mixed solvents were EG/ethanol 1/1 and 1/2 and EG/1-propanol 1/3 (volume

scale). In the experiments the entire apparatus was charged with 0.300 dm^3 of AMP/alcohols that had been previously 50% saturated with CO_2.

In one type of experiments two desorbers operating in sequence were used: the summed height of the glass rings contained into the two columns is the same to that in the single desorber used in most experiments. In another type of experiments an original cyclohexane aided desorption device was used. To this purpose, liquid cyclohexane was continuously fed by a peristaltic pump from the reservoir into the bottom of the desorber solution set to a temperature higher than the boiling point of cyclohexane-alcohol azeotrope. The gaseous cyclohexane blowing along the desorber greatly accelerate the CO_2 desorption. An overhead condenser, cooled by cold water, at the top of the desorber condensed gaseous cyclohexane-alcohol azeotrope in the reservoir whereas CO_2 exited from the top of the condenser.

4.3.   AMP-Amine Blends: Results

In this series of experiments we employed AMP blended with DEA, MDEA, MMEA and DIPA. As a solvent, we used 1:1 (v/v) mixtures of EG with either methanol or ethanol and, for comparison purposes, we also used amine solutions in pure 1-propanol and diethylene glycol monomethyl ether (DEGMME). In order to verify how the absorption efficiency depends on the desorber temperature and to find the best compromise between regeneration temperature and CO_2 absorption efficiency, the experiments were carried out at increasing desorber temperature (65, 70, 75 and 80°C). Each experiment was stopped when the reactions of CO_2 capture and amine regeneration reached the steady state and the absorption efficiency did not change with time.

A summary of the operating conditions is reported in Table 4.3, while the results of some representative experiments are reported in Table 4.4.

As expected, increasing the desorber temperature increases the CO_2 release and the amine regeneration and, consequently, the CO_2 absorption efficiency. Taking into account both the loading capacity, 43.4 wt% (the maximum loading capacity, CO_2/amine molar ratio, is 0.81) and the lowest desorption temperature required to attain an absorption efficiency greater than 90%, the blended AMP–MMEA solution in EG–methanol mixture (Table 4.4, entry 6) showed the best performances.

Table 4.3. Operating conditions employed in the absorption-desorption AMP-blended experiments.

Absorption solution	0.300 dm^3 50% carbonated solution
Desorption solution	0.300 dm^3 50% carbonated solution
Absorption temperature	20 °C
Desorption temperature / pressure	65-70-75-80 °C / 1 bar
Amine concentration	2.00 mol dm^{-3}; 16.8-22.6 wt%
Liquid flow rate	0.600 dm^3 h^{-1}
Gas flow rate	14 dm^3 h^{-1}

Table 4.4. CO$_2$ loading capacity at 20 °C and absorption efficiency by the different amines at increasing desorption temperatures. The overall amine concentration is 2.0 mol dm^{-3}.

Entry	Amine	Solvent[a]	Amine conc. (wt%)	Viscosity at 27°C (cP)	Loading capacity[b] (molar ratio)	Loading capacity[c] (wt%)	Average absorpt. efficiency[d] and desorpt. temp. (°C)			
							65	70	75	80
1	AMP/DEA	1,2-PD[e]/ethanol	20.6	8.65	0.65	29.4	75.7	84.7	91.8	93.8
2	AMP/DEA	EG[f]/methanol	19.3	4.28	0.77	34.9	73.5	84.9	92.4	
3	AMP/DEA	1-Propanol[g]	22.1	3.40	0.65	29.4		81.7	87.9	92.9
4	AMP/DEA[h]	DEGMME[i]	18.3	5.76	0.70	31.7	73.1	77.4	89.5	91.6
5	AMP/MDEA	EG/methanol	20.7	3.33	0.70	28.7		81.3	88.5	93.5
6	AMP/MMEA	EG/methanol	16.9	3.73	0.81	43.4	76.7	79.0	91.3	95.9
7	AMP/MMEA	EG/ethanol	16.8	5.51	0.76	40.7		62.5	86.4	92.6
8	AMP/DIPA	EG/ethanol	22.6	8.05	0.69	27.3		73.8	87.2	93.1

[a] Solvent mixtures are 1:1 in volume, unless otherwise stated. [b] Molar ratio between absorbed CO$_2$ and starting amine; absorption carried out with pure CO$_2$. [c] Percent ratio between the masses of absorbed CO$_2$ and starting amine. [d] Percent ratio between absorbed and flowed CO$_2$; absorption carried out with 12% (v/v) CO$_2$ in air; the deviation from the average values was always in the range 1.5–3%. [e] 1,2-Propanediol. [f] Ethylene glycol. [g] A small amount of solid formed during absorption. [h] AMP/DEA = 2:1 on molar basis. [i] Diethylene glycol monomethyl ether.

A comparison of the absorption efficiency (greater than 90%) of AMP–DEA and AMP–MDEA in organic solvents (Table 4.4) with aqueous DEA (69.1%), MDEA (69.0%), AMP–DEA (77.1%) and AMP–MDEA (78.8%) [1] under similar conditions (amine concentration, absorption temperature), clearly shows that amine regeneration is easier in non-aqueous solvents, despite the higher desorption temperature of the aqueous amine solutions (90 °C) with respect to organic solvents (80 °C).

In the absence of water, CO$_2$ reacts with both primary and secondary amines forming unstable carbamic acids (AmH denotes either primary or secondary amine):

$$AmH + CO_2 \rightleftarrows AmCO_2H \qquad (1)$$

Once formed, the carbamic acid may react with an excess of amine:

$$AmCO_2H + AmH \rightleftarrows AmCO_2^- + AmH_2^+ \qquad (2)$$

Although tertiary amines such MDEA cannot react with CO_2 in anhydrous conditions, they can still enter in the CO_2 capture process when mixed with primary or secondary amines when they behave as bases for the carbamic acid deprotonation (reaction 2). Additionally, the alcohol itself could take part in the CO_2 uptake in the presence of a base (*i.e.* the amine) forming an alkyl carbonate (R denotes an alkyl group):

$$AmH + CO_2 + ROH \rightleftarrows AmH_2^+ + ROCO_2^- \qquad (3)$$

Reaction (3) has been reported to occur with saturated alcohols in the presence of alkylbromide and Cs_2CO_3, dibutyltin(IV)oxide and of both amidine and guanidine [9,10]. It also occurs with unsaturated alcohols in the presence of tert-butyl ipoiodide [11]. However, the fast CO_2 alkylation in very mild condition (20 °C and $P(CO_2) = 0.12$ bar) promoted by a common amine is noteworthy. The stoichiometric loading capacity is 1, according to reaction (3), and 0.5 according to reactions (1) and (2). In our experiments, the measured loading capacity was in the range 0.65–0.81 (Table 4.4) thus indicating that reaction (3) was competing with reactions (1) and (2) in the absorption step. In the CO_2 saturated solutions, the alkyl carbonates may overcome the formation of amine carbamate (see, for example Figure 4.1 and Table 4.5, entry 1: DEA carbamate 31% and summed alkyl carbonates 69%). One should notice that the amine carbamate cannot react with CO_2 in the absence of water and, consequently, cannot increase its 0.5 loading capacity, according to the stoichiometry of reactions (1) and (2).

To collect further confirmatory evidence for this hypothesis, we analyzed the CO_2 loaded solutions by ^{13}C NMR spectroscopy, as already reported for aqueous solutions [1,8]. The peak assignment was done according to literature data [12-15]. Besides the most intense signals due to the carbon atoms of the alcohols and of both protonated and free amines that are fast exchanging on the NMR time scale, a couple of resonances at about 67.0 and 60.9 ppm can be assigned to the carbon atoms of the monoalkyl carbonate derivative of ethylene glycol ($HO\text{-}CH_2\text{-}CH_2\text{-}OCO_2^-$). Furthermore, a resonance at 159.2 ppm identifies the alkyl carbonate quaternary carbon ($R\text{-}OCO_2^-$). Additionally, ^{13}C resonances ascribable to the monoalkyl carbonates derivatives of methanol (160.1, 52.6 ppm), ethanol (159.5, 61.0, 14.7 ppm) or 1-propanol (159.4, 67.1, 22.9, 10.4 ppm), respectively, were observed. Finally, the resonances of the carbamate derivative of DEA (164.24, 61.75, 51.06 ppm), MMEA (164.02, 60.53, 51.07, 35.15 ppm) and DIPA (164.88, 67.90, 54.70, 20.74 ppm) were found in the spectra. On the contrary, the AMP carbamate could not be detected. The ^{13}C resonance assignments for the AMP–DEA–EG–CH_3OH are reported in Table 4.5.

Table 4.5. ^{13}C NMR resonances (ppm, carbon atoms in italics) of AMP–DEA–EG–methanol solution in the CO_2 saturated solution (entry 1), in the starting solution (50% CO_2 saturated) for cyclic experiments (entry 2), in both the absorber (entry 3) and desorber solutions (entry 4) at the end of each experiment (desorption at 75 °C). Percentages of DEA carbamate with respect to the total carbonated species are reported in parentheses.

Entry	carbon atoms	AMP/ AMPH$^+$	DEA/ DEAH$^+$	DEACO$_2^-$	EG	EGCO$_3^-$	MeOH	MeCO$_3^-$
1	R-CO_2^-			164.30				
	R-CO_3^-					159.45^a		160.10
	CH_2OH	67.31	57.54	61.73 (31)	63.32	67.10		
	-CH_2-O-					61.03		
	-C-NH$_2$	54.99						
	-C-NH		49.76	51.03				
	-CH_3	22.12					49.16	52.65
2	R-CO_2^-			164.40				
	R-CO_3^-			159.31		159.48^a		160.13
	CH_2OH	68.67	59.61	61.88(76)	63.34	67.12		
	-CH_2-O-					61.08		
	-C-NH$_2$	53.65						
	-C-NH		50.68	51.15				
	-CH_3	23.28					49.17	52.65
3	R-CO_2^-			164.43				
	R-CO_3^-					159.42^a		160.06
	-CH_2OH	68.59	59.54	61.79(80)	63.28	67.08		
	-CH_2-O-					61.01		
	-C-NH$_2$	53.63						
	-C-NH		50.60	51.07				
	-CH_3	23.25					49.15	52.64
4	R-CO_2^-			164.45				
	R-CO_3^-					159.43^a		160.07
	-CH_2OH	69.28	59.93	61.82(93)	63.31	67.09		
	-CH_2-O-					61.03		
	-CNH-		50.79	51.11				
	-C-NH$_2$	52.95						
	-CH_3	23.82			17.87	14.81		

^{a} The summed percentage of both carbonates is the difference with respect to DEA carbamate percentage.

A possible mechanism accounting for the formation of monoalkyl carbonate (reaction 3) is shown in Scheme 4.1 A and B. The reaction was initiated by the nucleophilic attack of the AMP amine lone pair to the CO_2 carbon followed by amine deprotonation, resulting in the formation of both AMP carbamate and protonated AMP (Scheme 4.1 A). Subsequently, the unstable AMP carbamate intermediate may undergo the nucleophilic attack at the carbonyl atom by the oxygen of alcohol, which gives back the amine while forming the monoalkyl carbonate (Scheme 4.1 B). An indirect support for the above mechanism is given by the complete conversion of the solid AMP carbamate to alkyl

carbonate upon dissolution in alcohols (see later). The above mechanism suggests that the direct nucleophilic attack of the ROH oxygen atom to the CO_2 carbon is disfavored by a greater activation energy.
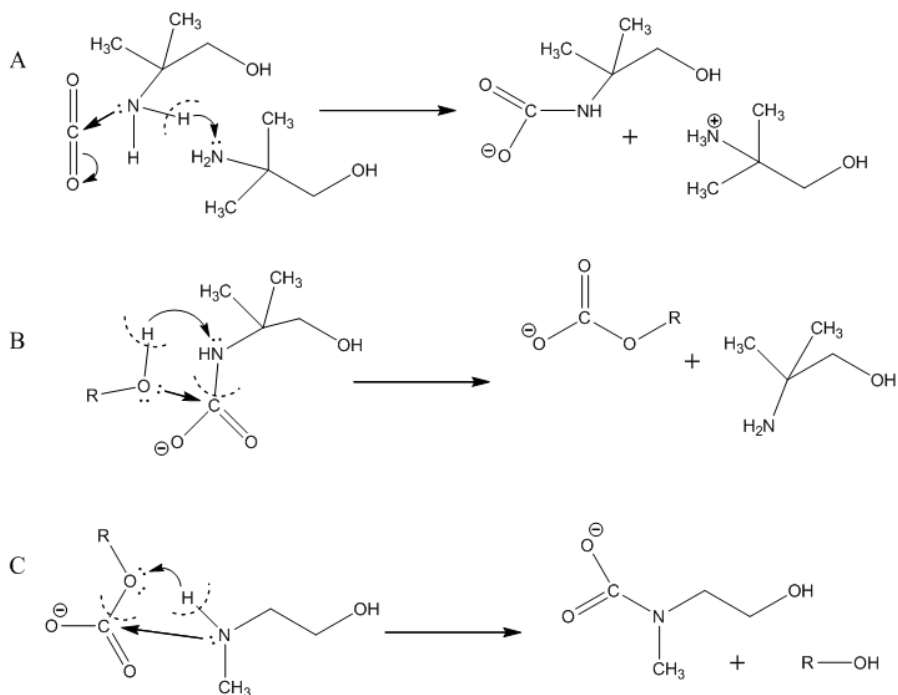
Scheme 4.1.

Interestingly, the addition of free amine to each solution just containing the prevalence of monoalkyl carbonates, results in the formation of greater amounts of the amine carbamates (amine = DEA, MMEA, DIPA; see Table 4.5, entry 2; see also Figure 4.1) and causes a decrease of the amount of $R\text{-}OCO_2^-$ [R = CH_3, C_2H_5, C_3H_7, $(CH_2)_2OH$], with the exception of MDEA, unable to produce a carbamate derivative.

A possible pathway for the alkyl carbonate transformation to amine carbamate is depicted in the Scheme 4.1 C. The conversion of alkyl carbonate to carbamate caused by an excess of free amine is just the reverse of the conversion of carbamate to alkyl carbonate in the CO_2 saturated solutions (Scheme 4.1 B) where most of the free amine has been consumed. The relative amount of the secondary amine (DEA, MMEA, DIPA) carbamate, in turn, increases with the desorption temperature and, on going from absorption to desorption, at any step of desorption temperature, contrary to alkyl carbonates (Figure 4.1). These features indicate that the thermal decomposition of alkyl

carbonates (inverse of reaction (3)) occurs at a greater extent compared to that of amine carbamate (AmH stands for DEA, MMEA, DIPA):

$$AmCO_2^- + AmH_2^+ \rightleftarrows 2AmH + CO_2 \qquad (4)$$

Finally, we can notice that CO_2 is captured by AMP–MDEA–EG–methanol solution as alkyl carbonates, being both AMP and MDEA unable to produce amine carbamate, at least in solution.
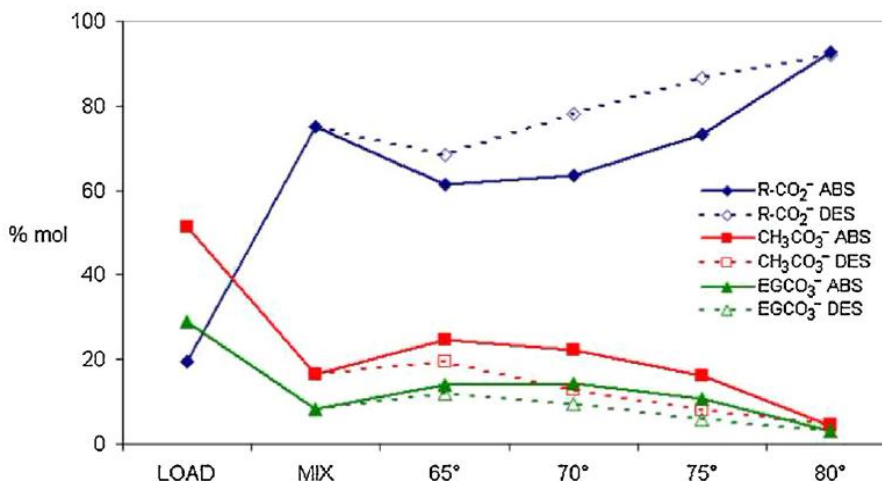
Figure 4.1. CO_2 absorption in the AMP–MMEA–EG–CH$_3$OH system: change of the relative amounts (% on molar scale) of MMEA carbamate and of R-OCO$_2^-$ [R = CH$_3$, (CH$_2$)$_2$OH] as a function of the desorption temperature and CO$_2$/amine ratio. LOAD stands for the CO$_2$ fully saturated solution and MIX for the CO$_2$ 50% saturated starting solution. In the inset, ABS and DES stand for absorption and desorption solutions, respectively.

The solid compound which separated out from AMP–DEA–1-propanol–CO_2 system (Table 4.4, entry 3) was identified as the AMP carbamate, [(AMPH)(AMPCO$_2$)], from its ^{13}C solid state NMR spectrum (Figure 4.2). The nature of the compound was then confirmed by single crystal X-ray structure determination which was also independently published [16]. Surprisingly, the CO_2-saturated solutions, either during the precipitation and after the separation of the precipitate by filtration, do not contain detectable amounts of the AMP carbamate, as inferred from the ^{13}C NMR spectra that display only resonances ascribable to the DEA carbamate and 1-propanol carbonate, besides those of the amines and the unreacted alcohol. The proposed mechanism for the carbamate formation is reported in Scheme 1A. A perusal of these results indicate that: (i) the AMP carbamate is less soluble than either DEA carbamate and 1-propanol carbonate; (ii) the

lattice energy due to the ionic interactions stabilizes [(AMPH)(AMPCO$_2$)] in the solid state in spite of its instability in solution.

The solid state stabilization of AMP carbamate due to the lattice energy, is further supported by its instability in solvents like methanol, ethanol and ethylene glycol where it instantaneously converts to the monoalkyl carbonate (reaction 5), while HCO$_3^-$ is produced in water solution:

$$AMPCO_2^- + CH_3CH_2OH \rightleftharpoons AMP + CH_3CH_2\text{-}OCO_2^- \tag{5}$$
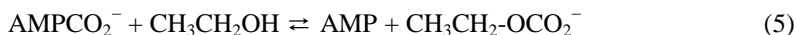
The proposed conversion mechanism of AMPCO$_2^-$ to alkyl carbonate is described by Scheme 4.1B. Reaction (5) can be substantially shifted forward or backward by adding an excess of alcohol or of free amine, respectively. Additionally, when solid AMP carbamate is dissolved in either primary or secondary amines (MEA, MMEA, DEA) which give stable carbamates, ^{13}C NMR spectroscopy indicates that AMP–CO$_2^-$ is completely converted to free AMP, whereas AMPH$^+$ is neutralized by the excess of the added amine:

$$AMPH^+ + AMPCO_2^- + 2AmH \rightarrow AmH_2^+ + AmCO_2^- + 2AMP \tag{6}$$

Where AmH stand for MEA, DEA and MMEA.
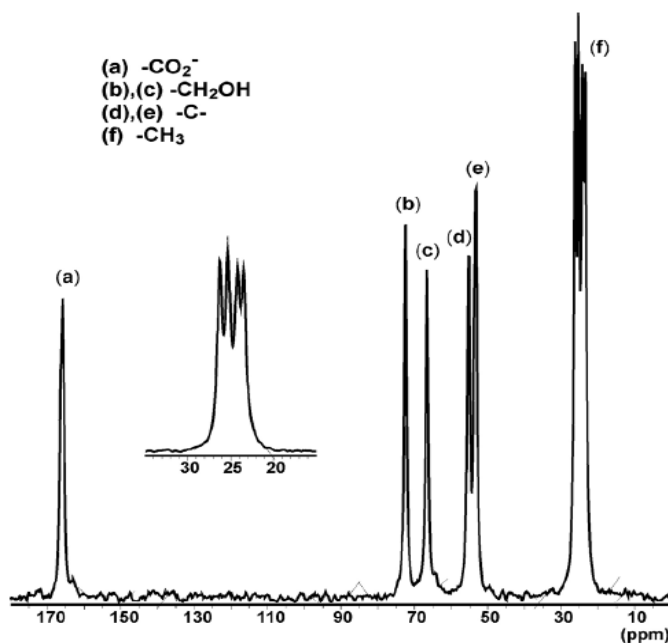
Figure 4.2. Solid state ^{13}C CP-MAS NMR spectrum of [(AMPH)(AMPCO$_2$)] (100.62 MHz). The inset expands the signal due to the CH$_3$ groups (f). The inequivalence of the two methyl groups in each AMP residue results in four chemical shifts.

The slurry formed in the AMP–DEA–1-propanol–CO_2 system has been decomposed at increasing temperatures between 50 and 65 °C and at room pressure until no more CO_2 was released and the solid phase disappeared. The average efficiency of CO_2 desorption, measured as the percent ratio between the desorbed CO_2 and that absorbed in the saturation step, is 94% and corresponds to the regeneration efficiency. The overall performance of this slurry appears superior to any of the solutions without precipitates, reported in Table 4.4, as a high amine regeneration efficiency is obtained at lower desorption temperature. However, a more detailed comparison between the two types of experiments cannot be carried out due to the different procedures employed.

4.4. Single AMP: Results

The experiments were carried out with single AMP and 1:1 to 1:3 (v:v) mixtures of EG with either ethanol or 1-propanol in a continuous cycle of CO_2 capture and solvent regeneration. A summary of the operating conditions is reported in Table 4.6.

Table 4.6. Operating conditions employed in the absorption-desorption single AMP experiments.

Solution volume	0.300 dm^3 50% carbonated solution
Absorption temperature	20-40 °C
Desorption temperature/pressure	80-90 °C/1 bar
Amine concentration	2.00 – 3.00 mol dm^{-3}
Liquid flow rate	0.150 – 0.600 dm^3 h^{-1}
Gas flow rate	14 dm^3 h^{-1}
Gas mixture	12% (v/v) CO_2 in air

In the absence of water, CO_2 may react with the amine AMP as previously described in Section 4.3 by the reactions (1), (2) and (3).

The measured loading capacity of AMP/EG/EtOH = 0.92, and of AMP/EG/PrOH = 0.87, indicates that the reaction (3) overcomes reactions (1) and (2) in the CO_2 saturated solutions, as expected. To gain evidence for this hypothesis, we analysed the CO_2 loaded solutions by means of ^{13}C NMR spectroscopy (Table 4.7). Besides the most intense signal due to the carbon backbones of ethylene glycol, ethanol and 1-propanol, additional resonances are easily assigned to both protonated and free AMP that are fast exchanging on the NMR time scale via proton scrambling and to the monoalkyl carbonate derivative of the three alcohols.

Table 4.7. ^{13}C NMR resonances (δ, ppm) of AMP/EG/EtOH solution in the CO_2 saturated solution (entry 1), in the starting solution (50% CO_2 saturated) for cyclic experiments (entry 2), in both the absorber (entry 3) and desorber solutions (entry 4) at the end of the experiment (desorption at 80 °C). Percentages of AMP carbamate with respect to summed $R\text{-}CO_3^-$ are reported in parentheses.

Entry	carbon atoms	AMP/ AMPH$^+$	AMP-CO$_2^-$	EG	EG-CO$_3^-$	EtOH	EtCO$_3^-$
1	R-CO$_2^-$						
	R-CO$_3^-$				159.26		159.45
	-CH$_2$OH	67.49		63.23	67.01	57.20	
	-CH$_2$-O-				60.95		61.03
	-C-NH$_2$	54.77					
	-CH$_3$	22.45				17.81	14.76
2	R-CO$_2^-$		164.23 (17)				
	R-CO$_3^-$				159.31		159.45
	-CH$_2$OH	69.30	71.73	63.25	67.06	57.21	
	-CH$_2$-O-				61.00		61.05
	-C-NH$_2$	52.96	52.96				
	-CH$_3$	24.04	20.98			17.86	14.80
3	R-CO$_2^-$		164.23 (24)				
	R-CO$_3^-$				159.30		159.49
	-CH$_2$OH	70.23	71.71	63.22	67.06	57.19	
	-CH$_2$-O-				60.90		61.04
	-C-NH$_2$	51.97	52.95				
	-CH$_3$	24.83	21.52			17.86	14.80
4	R-CO$_2^-$		164.25 (27)				
	R-CO$_3^-$				159.32		159.50
	-CH$_2$OH	70.63	71.74	63.23	67.07	57.20	61.04
	-CH$_2$-O-				60.27		
	-C-NH$_2$	51.59	52.97				
	-CH$_3$	25.17	21.79			17.87	14.81

No resonance has been found at about $\delta = 164$ ppm, that should identify the carbamate carboxyl of AMP (AMP–CO$_2^-$). The ^{13}C NMR spectrum of CO_2 saturated AMP–EG–EtOH solution is reported in Figure 4.3.

The starting solutions employed in the continuous absorption-desorption experiments, are prepared by mixing 0.150 dm^3 of the aforementioned CO_2 saturated solutions with the equimolar amount of free AMP in the same solvent mixture (0.150 dm^3). Interestingly, the addition of free amine to each solution just containing the monoalkyl carbonates results in the formation of appreciable amounts of the carbamate derivative of AMP (Table 4.6, entry 2) and in a decrease of the amount of R-OCO$_2^-$ [R=C$_2$H$_5$, C$_3$H$_7$, (CH$_2$)$_2$OH]. In reaction (7) AmH denotes AMP

$$AmH + R\text{-}OCO_2^- \rightleftarrows Am\text{-}CO_2^- + R\text{-}OH \qquad (7)$$
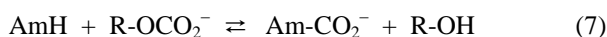
The CO_2 absorption efficiency has been measured in different operational conditions, namely at different absorption and desorption temperatures, amine concentration and liquid flow rate. The results are reported in Table 4.8 and indicate that a number of AMP/alcohol absorbents gave CO_2 absorption efficiency over 90%. As expected, increasing the desorber temperature (Table 4.8, entries 4, 5 and 15,16) causes a substantial increase of absorbent regeneration and, consequently, of the CO_2 absorption efficiency. Increasing the amine concentration (Table 4.8, entries 1,6 and 10,13) and decreasing the absorber temperature (Table 4.8, entries 2,4; 7, 9 and 13,15) gave the same results. A comparison of the absorption efficiency at different liquid flow rate, indicates that the best performances were attained with a rate of 0.300 dm^3 h^{-1} (Table 4.8, entries 1-3; 6-8 and 12-14), the other operational conditions being the same. The intermediate 0.300 dm^3 h^{-1} liquid flow rate represents the best compromise between two opposite effects, namely the more residence time of the liquid in both absorber and desorber (lower liquid flow rate) that favours both absorption and desorption and the greater amount of regenerated absorbent transferred to the absorber that favours the absorption (higher liquid flow rate).
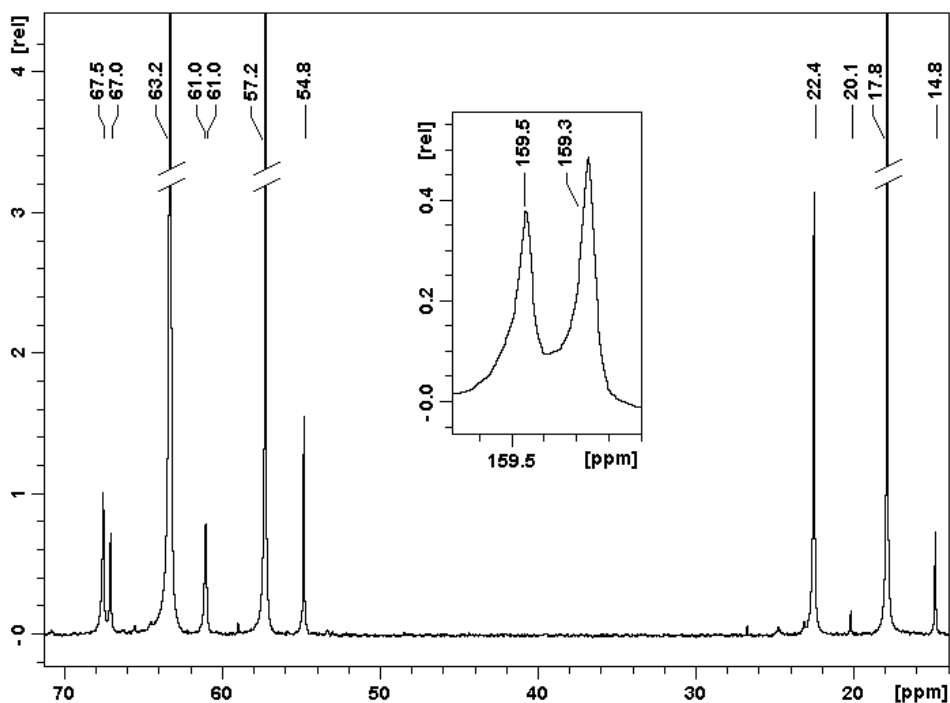
Figure 4.3. ^{13}C NMR spectrum of AMP–EG–EtOH solution saturated by CO_2. The inset rises the signal due to carboxyl groups. The chemical shift assignment is reported in Table 4.7, entry 1.

Table 4.8. CO$_2$ absorption efficiency by the AMP-alcohol absorbents at different operational conditions.

Entry	Solvent (v/v ratio)	Amine conc. (mol dm^{-3})	T$_{abs}$-T$_{des}$ (°C)	Liquid flow (dm^3 h^{-1})	Gas/liquid flow ratio	Absorption efficiency (%)
1	EG/EtOH (1/2)	2.00	20-80	0.600	20.4	88.6
2	EG/EtOH (1/2)	2.00	20-80	0.300	40.8	92.4
3	EG/EtOH (1/2)	2.00	20-80	0.150	81.6	77.7
4	EG/EtOH (1/2)	2.00	30-80	0.300	40.8	78.4
5	EG/EtOH (1/2)	2.00	30-90	0.300	40.8	92.3
6	EG/EtOH (1/2)	3.00	20-80	0.600	20.4	90.5
7	EG/EtOH (1/2)	3.00	20-80	0.300	40.8	94.3
8	EG/EtOH (1/2)	3.00	20-80	0.150	81.6	88.3
9	EG/EtOH (1/2)	3.00	30-80	0.300	40.8	83.5
10	EG/PrOH (1/3)	2.50	20-80	0.300	40.8	89.0
11	EG/PrOH (1/3)	2.50	30-90	0.300	40.8	91.7
12	EG/PrOH (1/3)	3.00	20-80	0.600	20.4	84.6
13	EG/PrOH (1/3)	3.00	20-80	0.300	40.8	92.3
14	EG/PrOH (1/3)	3.00	20-80	0.150	81.6	78.6
15	EG/PrOH (1/3)	3.00	30-80	0.300	40.8	80.6
16	EG/PrOH (1/3)	3.00	30-90	0.300	40.8	91.5

The CO$_2$ absorption efficiency of the AMP/EG/PrOH absorbent as a function of some operational conditions is summarised in Figure 4.4.
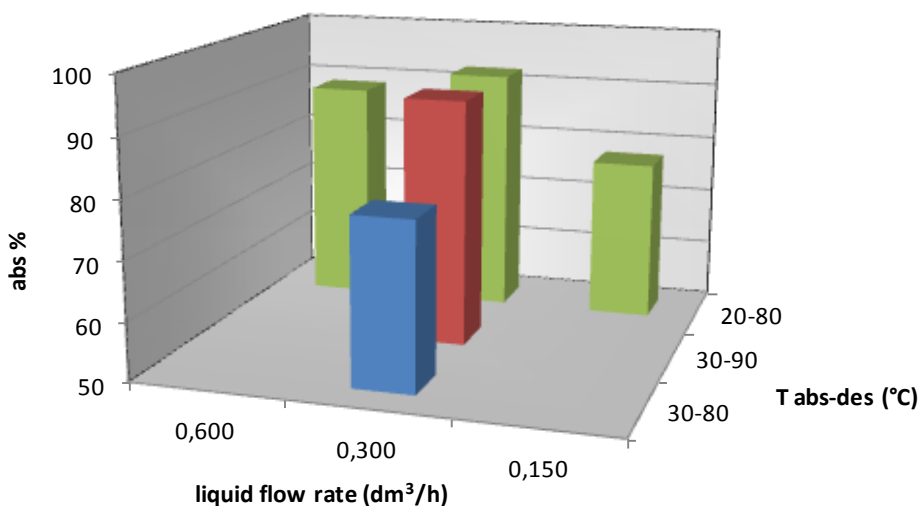
Figure 4.4. Absorption efficiency of AMP/EG/PrOH absorbent as a function of solution flow rate, and absorption/desorption temperature.

Most of the CO_2 is captured in solution as monoglycol and monoethyl carbonate (Figure 4.5). However, the amount of $AMP-CO_2^-$ relative to that of alkyl carbonate increases as the desorption temperature increases and from absorption to desorption at any desorption temperature. These features indicate that the thermal decomposition of alkyl carbonates (inverse of reaction 3) occurs at a greater extent compared to that of AMP carbamate (reaction 4).
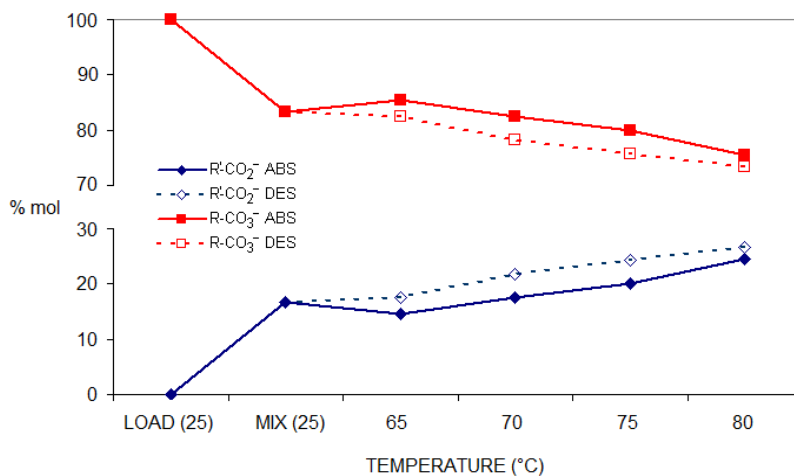
Figure 4.5. CO_2 absorption in the AMP/EG/EtOH system: change of the relative amounts (% on molar scale) of AMP carbamate (R'-CO_2^-) and of the summed R-OCO_2^- [R= C_2H_5, $(CH_2)_2OH$] as a function of the desorption temperature. LOAD stands for the CO_2 fully saturated solution and MIX for the CO_2 50% saturated starting solution. ABS and DES stand for absorption and desorption, respectively, solutions.

In order to quantify the relative amounts of carbamate and alkyl carbonates, we used the integration of the carboxyl resonances of carbamate R–CO_2^- and carbonate R'–OCO_2^- in the range δ = 164–159 ppm. Even if the results we obtained may be considered as semi-quantitative (5% deviation), they should be nonetheless sufficient to summarize the variation of the CO_2 containing species in solution as a function of the CO_2–AMP ratio and of the employed temperatures.

Aimed at increasing the rate of CO_2 release in the desorption step and, consequently, at enhancing the overall absorption efficiency, we have devised two different desorption strategies, namely two desorber columns or a transport gas. The results are reported in Table 4.9. As expected, two desorbers increase significantly the absorption efficiency (Table 4.9, entries 1 and 2) in comparison with that achieved by one absorber (Table 4.8, entries 10, 11). Even at lower liquid flow rate (Table 4.9, entries 3, 4), the absorption efficiency is still above 90 %.

Table 4.9. CO$_2$ absorption efficiency of the AMP–alcohol solutions at different desorption setup and operational conditions.

Entry	Solvent (v/v ratio)	Amine conc. (mol dm^{-3})	Tabs-Tdes (°C)	Liquid Flow (dm^3 h^{-1})	Gas/liquid flow ratio	Absorption efficiency (%)
1	EG/PrOH (1/3)	2.50	20-80	0.300	40.8	91.1[a]
2	EG/PrOH (1/3)	2.50	30-90	0.300	40.8	93.5[a]
3	EG/PrOH (1/3)	2.50	20-90	0.200	61.2	93.4[a]
4	EG/PrOH (1/3)	2.50	30-90	0.200	61.2	91.3[a]
5	EG/EtOH (1/1)	2.00	30-80	0.600	20.4	98.4[b]
6	EG/EtOH (1/1)	2.00	40-80	0.600	20.4	91.8[b]

[a] two desorber columns; [b] cyclohexane added as transport gas.

A gas stream injected into the bottom of the desorber greatly increases the liquid turbulence therefore accelerating the CO$_2$ release. Obviously, the use of N$_2$ or another inert gas would be a nonsense and it should be mandatory to use a transport gas easily separable from the CO$_2$ exited from the desorber. To this purpose we used cyclohexane (Tb = 80.7 °C) that was continuously fed into the desorber at the bottom of the solution. Cyclohexane forms a low boiling azeotrope with ethanol (Tb = 64.9 °C) that turned to gas once in contact with the desorber solution at 80 °C. An overhead condenser cooled by water recovered liquid cyclohexane for its reuse whereas CO$_2$ exited from the top of the condenser. This simple device greatly increases the absorption efficiency from 88.6% (Table 4.8, entry 1) to 98.4 % (Table 4.9, entry 5), in spite of the higher absorption temperature (30 °C) and higher viscosity (EG/EtOH, 1/1) of the latter experiment. It is noteworthy the 91.8 % efficiency of the 40-80 °C experiment (Table 4.9, entry 6). As a final consideration, the water-free technology has been found to be tolerant towards moisture. Moreover, the addition of 5% of water (v/v) to two AMP/EG/PrOH solutions (Table 4.8, entries 10, 11) does not affect the results.

4.5.   Conclusions

CO$_2$ is reversibly captured by non aqueous alkanolamines as either monoalkyl carbonate (R-OCO$_2^-$) and amine carbamate. Due to the lower stability of monoalkyl carbonates with respect to HCO$_3^-$ and to the carbamates which are formed in the aqueous solutions, stripping temperatures of 75–90°C at room pressure are sufficient to attain absorption efficiencies greater than 90%. The CO$_2$ desorption at 80 °C can be greatly accelerated

by means of a transporting gas (gaseous cyclohexane) that allows an absorption efficiency up to 98%. The relatively low amine concentration (17–22 wt%) and the lower stripping temperatures, as compared with the aqueous alkanolamines, should also have beneficial effects by reducing the amine loss by evaporation, their thermal and oxidative degradation and, additionally, the equipment corrosion rate It is generally accepted that about half of the total energy of the CCS process is due to the sorbent regeneration [16,17]. The lower heat capacity of alcohols and the reduced evaporation of the absorbents combined with the lower stripping temperature, all together should co-operate to reduce the energy demand of sorbent regeneration. Additionally, the higher CO_2 loading in the organic sorbents results in a lower circulation rate and lower sensible heat loss. We could admittedly conclude that a major drawback of the amine-alcohol absorbent technique here described could be the cost of alcohols. Presumably, the greater capital cost due to alcohols, that are completely recycled, could be compensated by the lower amine concentration (about 20 wt%) and by the reduced evaporation/thermal degradation, due to the lower operating temperatures.

4.6.   References

[1] F. Barzagli, F. Mani, M. Peruzzini. Continuous cycles of CO_2 absorption and amine regeneration with aqueous alkanolamines: a comparison of the efficiency between pure and blended DEA, MDEA and AMP solutions by ^{13}C NMR spectroscopy. Energy Environ. Sci., 2010, 3, 772-779.
[2] S.A. Freeman, J. Davis, G.T. Rochelle. Degradation of aqueous piperazine in carbon dioxide capture. Int. J. Greenh. Gas Control, 2010, 4, 756-761.
[3] G. Sartori, D.W Savage. Sterically hindered amines for CO_2 removal from gases. Ind. Eng. Chem. Fundam. 1983, 22, 239-249.
[4] B.P. Mandal, A.K. Biswas, S.S. Bandyopadhyay. Absorption of carbon dioxide into aqueous blends of 2-amino-2-methyl-1-propanol and diethanolamine. Chem. Eng. Sci., 2003, 58, 4137–4144.
[5] W.-C. Sun, C.-B. Yong, M.-H. Li. Kinetics of the absorption of carbon dioxide into mixed aqueous solutions of 2-amino-2-methyl-l-propanol and piperazine. Chem. Eng. Sci., 2005, 60, 503–516.
[6] H.J. Xu, C.F. Zhang, Z.S. Zheng. Solubility of hydrogen sulfide and carbon dioxide in a solution of methyldiethanolamine mixed with ethylene glycol. Ind. Eng. Chem. Res., 2002, 41, 6175-6180.
[7] S.W. Park, J.W. Lee, B.S. Choi, J.W. Lee. Kinetics of absorption of carbon dioxide in monoethanolamine solution of polar organic solvents. J. Ind. Eng. Chem, 2005, 11, 202–209.
[8] F. Barzagli, F. Mani, M. Peruzzini. A ^{13}C NMR study of the carbon dioxide absorption and desorption equilibria by aqueous 2-aminoethanol and N-methyl-substituted 2-aminoethanol. Energy Environ. Sci., 2009, 2, 322-330.

[9] S.I. Kim, F. Chu, E.E. Dueno, K.W. Jung. Alkyl carbonates: efficient three component coupling of aliphatic alcohols, CO2, and alkyl halides in the presence of Cs_2CO_3. J. Org. Chem. 1999, 64, 4578-4579.

[10] G. Jimil, P. Yogesh, P.S. Muthukumaru, M. Pradip. Methanol assisted selective formation of 1,2-glycerol carbonate from glycerol and carbon dioxide using Bu_2SnO as a catalyst. J. Mol. Cat. 2009, A. 304, 1-7.

[11] S. Minakata, I. Sasaki, T. Ide. Atmospheric CO_2 fixation by unsaturated alcohols using t-BuOI under neutral conditions. Angew. Chem. Int. Ed., 2010, 49, 1309-1311.

[12] J.Y. Park, S.J. Yoon, H. Lee. Effect of steric hindrance on carbon dioxide absorption into new amine solutions: thermodynamic and spectroscopic verification through solubility and NMR analysis. Environ. Sci. Technol., 2003, 37, 1670–1675.

[13] D. Stueber, D. Patterson, C.L. Mayne, A.M. Orendt, D.M. Grant, R.W. Parry. Carbonates, thiocarbonates and the corresponding monoalkyl derivatives, 1. Their preparation and isotropic ^{13}C NMR chemical shifts. Inorg. Chem.,2001, 40, 1902–1911.

[14] S. Ma'mun, J.P. Jakobsen, F. Svendsen, O. Juliussen. Experimental and modeling study of the solubility of carbon dioxide in aqueous 30% mass 2-((2-aminoethyl)amino)ethanol solution. Ind. Eng. Chem. Res. 2006, 45, 2505-2512.

[15] R.J. Hook. An investigation of some sterically hindered amines as potential carbon dioxide scrubbing compounds. Ind. Eng. Chem. Res., 1991, 36, 1779–1790.

[16] E. Jo, Y.H. Jhon, S.B. Choi, J.-H. Shim, J.H. Lee, K.-R. Jang, J. Kim. Crystal structure and electronic properties of 2-amino-2-methyl-1-propanol (AMP) carbamate. Chem.l Comm.,2010, 46, 9158–9160.

[17] A.B. Rao, E.S. Rubin. Identifying Cost-Effective CO_2 Control Levels for Amine-Based CO_2 Capture Systems. Ind. Eng. Chem. Res., 2006, 45, 2421-2429.

5. Carbon Dioxide Removal for Biogas Upgrading
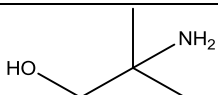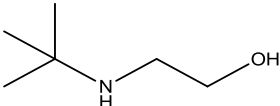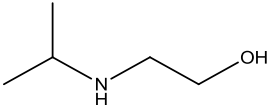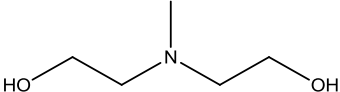
5.1. Introduction

We used the non aqueous absorbents also for the processes of biogas cleaning and upgrading. Methane production from municipal biomass waste is a topic of increasing interest as an environmentally benign and available energy option. Besides CH_4, biogas from landfill wastes contains approximately 15-50% of CO_2, small amounts of H_2S and N_2 and trace amounts of other compounds. Biogas cleaning and upgrading to natural gas quality is the prerequisite for most of its use: afterwards it can be mixed with natural gas and injected into existing gas grid or used in power plants or as transportation fuel.

The cleaning of the biogas requires H_2S, water and trace compounds removal. In particular, H_2S must be removed due to its harmfulness and corrosive nature in the presence of water. In order to raise its energy content, it is mandatory to upgrade the biogas by means of CO_2 removal. The most common techniques for CO_2 removal are the high pressure water scrubbing, pressure and thermal swing absorption, physical and chemical capture by organic solvents or amines, membrane or cryogenic separation [1-10]. More recently, metal-organic frameworks (MOF) are emerging as promising alternatives for CO_2 separation [11]. All of these techniques display both advantages and disadvantages and their cost to benefit assessment helps to choice the technique for the implementation in a large scale plant.

The experimental study here reported relates to an efficient method for the selective separation of CO_2 and H_2S from a simulated biogas containing either 15% or 40% of CO_2 in air and, in some experiments, 50 ppm of H_2S. It was mandatory to perform the absorption experiments with the CO_2/air mixture instead of CO_2/methane, as the use of methane is not allowed in our laboratories because of safety rules. However, air and methane display the same features in the absorption experiments because of the methane inertness towards amines. The absorbents were either single or blended amines (1:1, on molar scale), overall 3.0 mol dm^{-3}, dissolved in a 1:1 (volume scale) mixture of ethylene glycol (EG) and 1-propanol (PrOH) or in single diethylene glycol monomethyl ether (DEGMME). The selected amines are reported in Table 5.1.

Table 5.1. Abbreviation, name and formula of the tested amines.

AMP	2-amino-2-methyl-1-propanol	
TBMEA	2-(*tert*-butylamino)ethanol	
IPMEA	2-(isopropylamino)ethanol	
MDEA	methyldiethanolamine	

Two sets of experiments have been designed:

1) CO_2 absorption and, separately, thermal amine regeneration aimed at selecting the most efficient absorbents;

2) continuous cycles of CO_2 absorption-desorption carried out in packed columns with the purpose of verify the efficiency of CO_2 and H_2S capture. The carbonated species in solution were qualitatively and quantitatively analyzed by ^{13}C NMR spectroscopy (as described in Section 3.3), and were found to be originated from the amine and alcohol carbonatation.

5.2.   General Experimental Information

The starting amine solutions were fixed at overall 3.00 mol dm^{-3}; amine blends were 1:1 molar ratio. Mixed EG/PrOH was 1:1 (v/v). Gas mixtures of 15% and 40% CO_2 in air were used to simulate the biogas. In some experiments the gas mixture contains 50 ppm H_2S.

The CO_2 absorption in the batch experiments was measured with a gastight apparatus which comprises a 2.0 dm^3 flask (actual volume 2.20 dm^3) equipped with a digital pressure gauge, magnetic stirrer and a pressure-equalizing dropping funnel containing 40.0 cm^3 of the appropriate ammine (0.12 mol) solution (Figure 5.1). After the air was removed with a vacuum pump, the flask was filled with the appropriate CO_2 mixture at room pressure. This operation was repeated five times before the final one. After the amine solution was quickly introduced from the funnel into the flask, the stirring was

started and the pressure decrease shown by the pressure gauge allowed us to measure the CO_2 absorption as a function of time. The experiment was stopped when the pressure did not change with time (20-45 min). The thermal release of pure CO_2 was accomplished with two 100 cm^3 gas burettes (Volac) as already described in Section 3.2.2. The desorption rate at 90 °C rapidly decreased with time and a steady state was reached within 60 min.
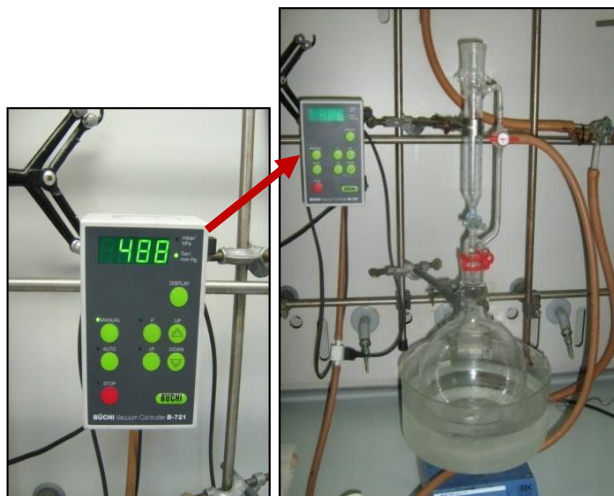
Figure 5.1. Apparatus for the CO_2 absorption used in the batch experiments.

The apparatus and the operational procedures used for continuous absorption-desorption cycles have been already described in Section 3.2.3. The solutions circulate continuously between the absorber and the desorber at the flow rate of 0.330, 0.650 and 0.950 dm^3 h^{-1}. The gas mixture was continuously fed into the bottom of the column with a flow rate of 12.0 dm^3 h^{-1} (15% CO_2, 0.0750 mol h^{-1}; 40% CO_2, 0.200 mol h^{-1} at 24 °C). The equipment was charged with 0.400-0.450 dm^3 of amine-alcohol solution that had been previously 50% saturated with CO_2 (see Section 4.2). A complete cyclic experiment lasted 24-36 h and it was stopped when the efficiency of CO_2 capture remained constant with time.

In the experiments aimed at separating H_2S from CO_2, a gas (15% or 40% CO_2 in air) stream containing 50 ppm H_2S was employed. Another set of H_2S capture experiments were carried out with the AMP/IPMEA/DEGMME solution charged with 5,0 g of $Na_2S \cdot 9H_2O$ (0.021 mol) dissolved in the minimum amount of water. The selective removal of H_2S was accomplished subsequently to the CO_2-H_2S stripping by flowing the gas mixture through a H_2O_2 aqueous solution either 0.10 or 0.65 mol dm^{-3}. The

68

precipitation of $CaSO_4$ was accomplished in a separate vessel with the stoichiometric amount of CaO. The unreacted H_2O_2 solution was recycled to the H_2S absorber. To check the efficiency of H_2S removal, the CO_2 stream exited from the H_2S absorber was bubbled through an aqueous solution of Cu(II). No CuS precipitation was detected in all of the experiments.

The ^{13}C NMR spectra of the solutions were obtained as already described in Section 3.3.

5.3.   Batch Experiments of CO_2 Absorption and Desorption

The choice of the AMP based organic absorbents for CO_2 capture was based on the considerations and results obtained in our experiments described in Chapter 4. To the purpose of lowering the high absolute viscosity ($\mu = 16.9$ cP at 25 °C) of pure EG that would reduce the CO_2 absorption efficiency, and would be an hindrance to the absorbent flow, a 1:1 (v/v) mixtures of EG with 1-propanol ($\mu = 1.07$ cP at 25 °C) was used and a boiling temperature up to 150 °C was still attained. The amine solutions in pure 2-(2-methoxyethoxy)ethanol (diethylene glycol monomethyl ether, DEGMME) were used for comparison purposes.

The percentage of CO_2 absorbed by single or 1:1 (molar scale) amine blends, overall 3.0 mol dm^{-3}, in EG/PrOH 1:1 (v/v) or DEGMME is summarized in Figures 5.2 and 5.3 as a function of the absorption time. Overall, the percentage (in other words, the absorption efficiency) decreases in the order:

- AMP > IPMEA > TBMEA > MDEA
- AMP/IPMEA ≥ AMP/TBMEA > AMP/MDEA
- amine blends > single amines (with the exception of AMP)
- EG/PrOH > DEGMME
- CO_2 15% > CO_2 40%

As far as the single amines are concerned, the absorption efficiency decreases with increasing steric hindrance at amine function. The absorption efficiency is comprised between 13% (MDEA-DEGMME and 40% CO_2) and 100% (several amines, EG/PrOH and CO_2 15%). The greater amine efficiency with 15% CO_2 compared to 40% CO_2 is due to the greater amine/CO_2 ratio. For the same experimental conditions, the mixture EG/PrOH has an appreciable advantage over DEGMME because of its greater reactivity

towards CO_2. In particular, the MDEA efficiency increases from 13% in DEGMME to 52% in EG/PrOH (CO_2, 15%).
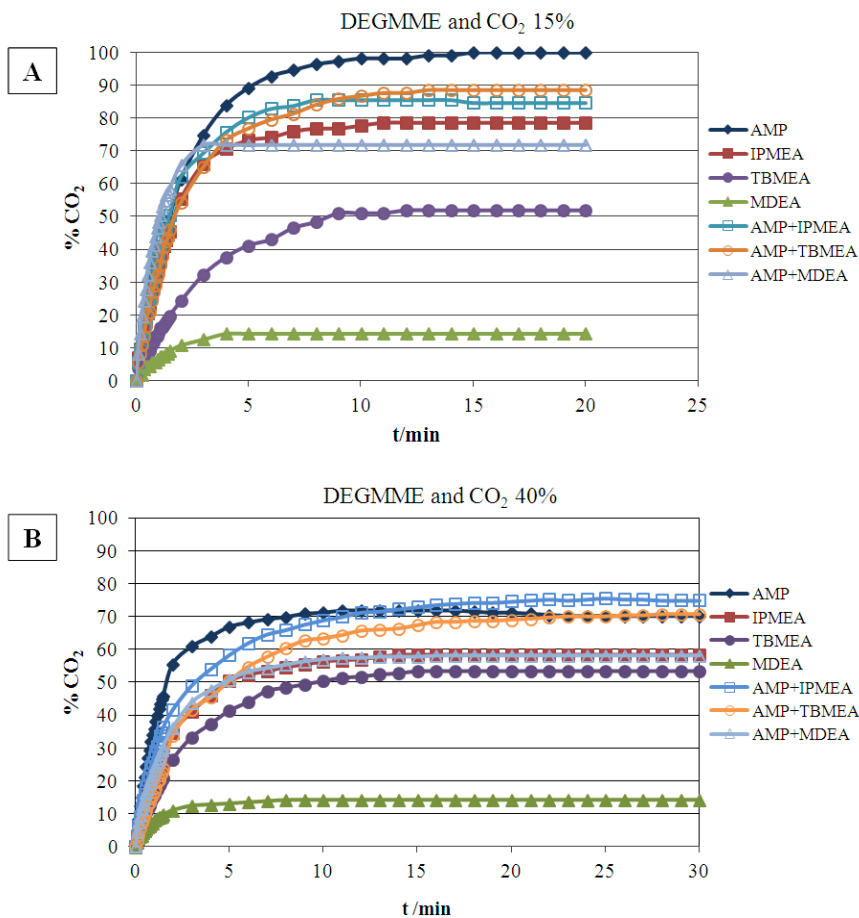
*Figure 5.2. Variation of the CO_2 (15%, **A** and 40%, **B**) absorption efficiency of the different amines in DEGMME solutions as a function of time.*

The tertiary amine MDEA is unable to react with CO_2 in the absence of water and DEGMME is poorly reactive towards CO_2, contrary to EG and PrOH that form alkyl carbonates. The single amines AMP and IPMEA and the mixed AMP/IPMEA display a greater initial reaction rate irrespective of the solvent employed and the CO_2 percentage. The amine regeneration occurred in a conical flask heated at 90 °C and the CO_2 release was measured with two 100 cm^3 gas burettes filled with CO_2 saturated water. The CO_2 desorption required a maximum of 60 min. The Figures 5.4 and 5.5 summarize the average values of three measurements of CO_2 absorption and desorption efficiency (the

latter is the percentage of the desorbed CO_2 with respect to that absorbed), after the steady state was reached, according to the different amines and experimental conditions.
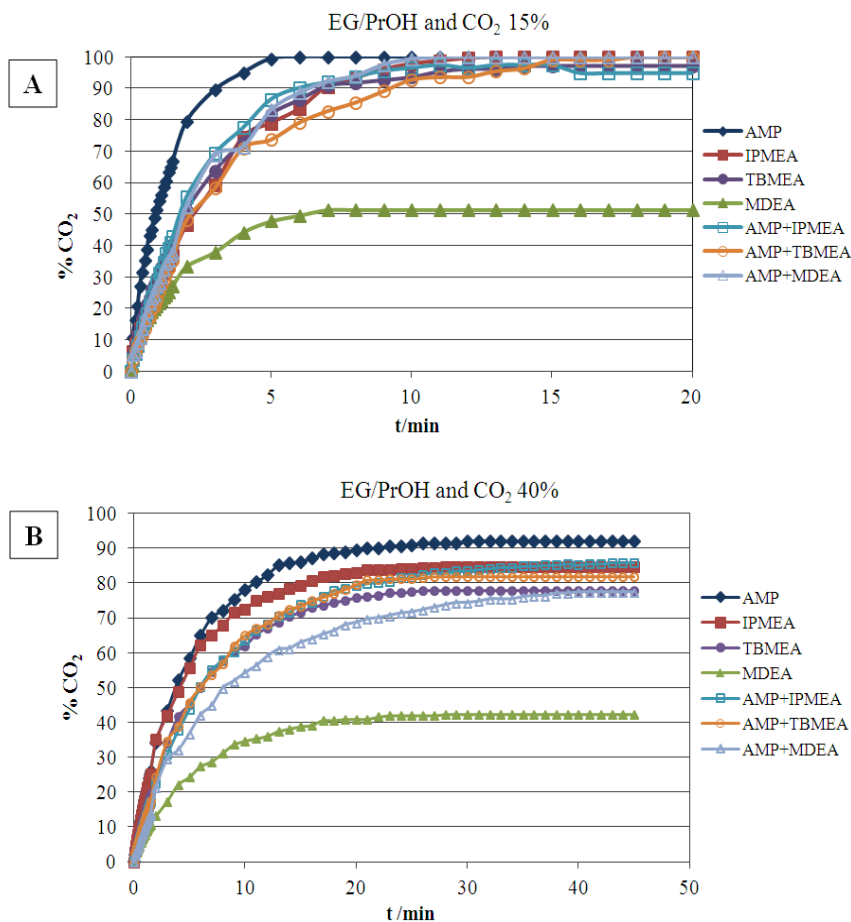
*Figure 5.3. Variation of the CO_2 (15%, **A** and 40%, **B**) absorption efficiency of the different amines in EG/PrOH solutions as a function of time.*

In general, the desorption and the absorption efficiency displays an opposite trend: this feature is particularly evident for MDEA.

Analogous experiments carried out for comparison purposes with the amines MEA, DEA, MMEA, gave high absorption efficiency (over 95%) but were discarded for cyclic experiments because of the low desorption efficiency (15-30% at 90 °C).

The chemistry of CO_2 absorption in non-aqueous sorbents has been previously described in the Section 4.3, as well as the speciation of the carbonated solutions on the basis of the ^{13}C NMR analysis. As an example, the ^{13}C NMR spectrum of carbonated IPMEA (40% CO_2) in EG/PrOH is reported in Figure 5.6.
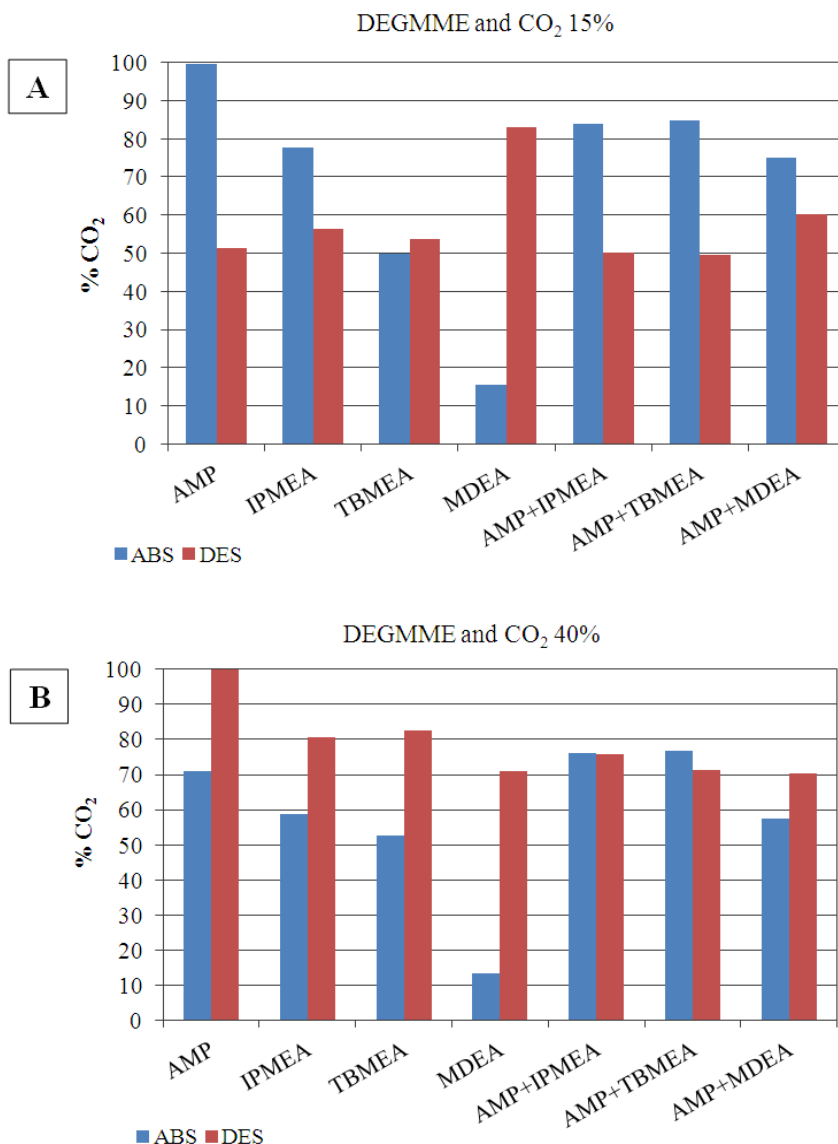
Figure 5.4. The CO_2 desorption efficiency of the different amines carbonated by 15%, A, and 40% CO_2, B, in DEGMME. The desorption efficiency is compared with the average absorption efficiency in the same solutions.

The sterically hindered amines AMP, TBMEA, IPMEA in EG/PrOH give less stable carbamates and promote the formation of alkyl carbonates of EG and PrOH. Therefore, these absorbents may be efficient in both absorption and desorption steps. The CO_2 capture either as alkyl (EG, PrOH, DEGMME) carbonate or amine (AMP, IPMEA, TBMEA) carbamate, is the result of the competition between the relative stability of the alkyl carbonates and amine carbamates and of the CO_2/amine ratio.

72
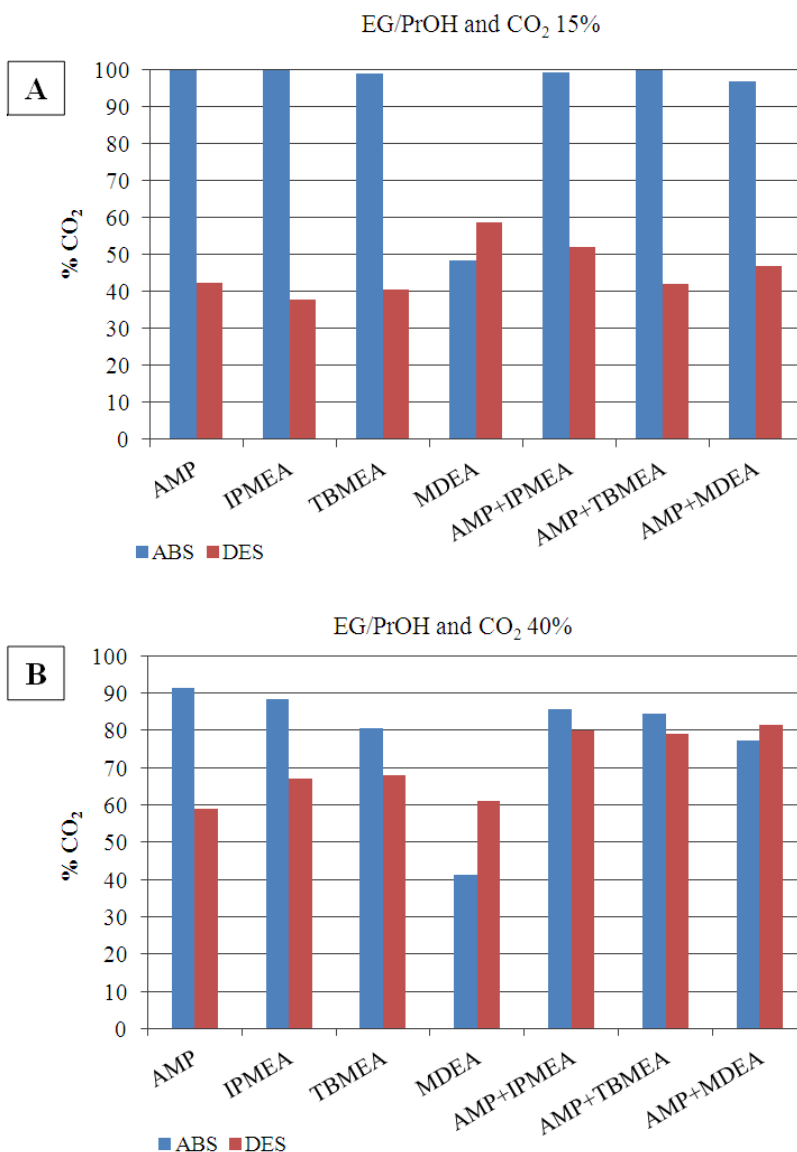
Figure 5.5. The CO$_2$ desorption efficiency of the different amines carbonated by 15%, A, and 40% CO$_2$, B, in EG/PrOH. The desorption efficiency is compared with the average absorption efficiency in the same solutions.

The IPMEA carbamate is the prevailing species in the IPMEA and AMP/IPMEA solutions carbonated by 15% CO$_2$ (70-75% in AMP/IPMEA; AMP-CO$_2^-$, < 3%) with respect to the alcohol carbonates. On the contrary, the summed carbonates of EG and PrOH prevail (60 %) over the IPMEA carbamate in the solutions saturated with 40% CO$_2$ (Figure 5.6). In general, the –CO$_3^-$ signal of EG carbonate is more intense than that of PrOH carbonate. The carbonate derivative of DEGMME could not be detected in the

^{13}C NMR spectra. In summary, the alkyl carbonate stability decreases in the order EG > PrOH > DEGMME and carbamate stability decreases in the order IPMEA > AMP > TBMEA. The tertiary amine MDEA is unable to form the corresponding carbamate and, consequently, MDEA-DEGMME is the least efficient absorbent: the small absorption capacity (13-16%) measured is, presumably, due to a physical absorption. The 40% CO_2 absorption by AMP, IPMEA and TBMEA and by their blends in DEGMME, gave rise to the amine carbamates $[Am\text{-}CO_2^-][AmH_2^+]$ in the solid state (AmH denotes the amine). The lattice energy due to the ionic interactions stabilizes the carbamates of AMP and TBMEA in spite of their relative instability in solution.
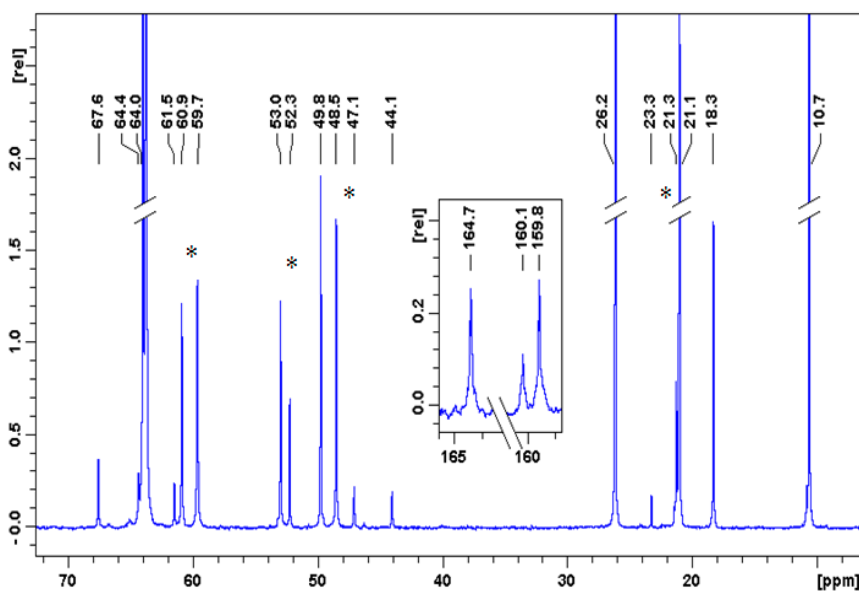
Figure 5.6. The ^{13}C NMR spectrum of IPMEA-EG/PrOH carbonated by 40% CO_2. The inset reports the chemical shifts of carbonyl atoms of IPMEA carbamate (δ=164.7 ppm) and alcohol carbonates δ=160.1-159.8 ppm). The asterisk denotes the chemical shifts of carbon backbones of IPMEA carbamate and of both free IPMEA and protonated IPMEA fast exchanging in the NMR scale.

5.4. Continuous Cycles of CO_2 Absorption-Desorption and of H_2S Capture

The CO_2 absorption efficiency was measured in continuous cycles of CO_2 capture and solvent regeneration carried out, separately, in two glass columns packed with glass rings as described in Section 3.2.3. Each complete experiment lasted 24-36 h before the

74

0reactions of CO_2 capture and amine regeneration reached a steady state. Based on the batch results reported in section 5.3.1, the amines AMP, AMP/IPMEA and AMP/TBMEA in EG/PrOH 1/1 (v/v) were employed in the continuous cycles experiments. A summary of the operating conditions is reported in Table 5.2 whereas the results of the cyclic experiments are reported in Table 5.3.

Table 5.2. Operating conditions employed in the continuous absorption-desorption experiments

Solution volume	0.400, 0.450 dm^3 50 % carbonated solution
Absorption temperature	20 °C
Desorption temperature/pressure	90, 95 °C/1 bar
Overall amine concentration	3.00 mol dm^{-3} (single or 1/1 molar ratio)
Liquid flow rate	0.330, 0.650, 0.950 dm^3 h^{-1}
Gas flow rate	12.2 dm^3 h^{-1}
Gas mixture	15% and 40% (v/v) CO_2 in air

Table 5.3. CO_2 absorption efficiency of amines in EG/PrOH in the continuous absorption-regeneration cycles as a function of the operational parameters

Amine	Liquid flow rate (dm^3/h)	T_{absorb} (°C)	T_{desorb} (°C)	Efficiency %
CO_2 40%v				
AMP	0,33	20	95	95,0
	0,65	20	90	93,5[a]
	0,65	20	95	96,5[a]
	0,95	20	95	92,0[a]
AMP-IPMEA	0,33	20	90	89,1
	0,65	20	90	92,1
	0,65	20	95	94,0
	0,65	20	95	94,7[a]
	0,95	20	90	89,4
AMP-TBMEA	0,65	20	95	95,7[a]
CO_2 15%v				
AMP	0,33	20	90	91,3
	0,33	20	95	93,3
	0,33	20	95	95,4[a]
AMP-IPMEA	0,33	20	90	88,9
	0,33	20	95	91,3
	0,33	20	90	89,4[a]
	0,65	20	95	86,7
AMP-TBMEA	0,33	20	95	91,0[a]
	0,65	20	95	93,3[a]

[a] Volume of the absorbent 0,450 dm^3; in all of the other experiments is 0,400 dm^3.

As expected, the absorption efficiency increases with desorption temperature and with the increased volume of amine solution. The dependence on the liquid flux deserves a comment. The lower flux, 0.330 dm^3 h^{-1}, increases the residence time of the liquid into both absorber and desorber, thereby enhancing both the absorption and desorption reactions. The higher flux, 0.950 dm^3 h^{-1} makes a greater amount of the sorbent to come from the desorber to the absorber, and *vice versa*.The higher absorption efficiency was the result of the best compromise between the two opposite features that allowed to transfer the greatest amount of both loaded and regenerated absorbent between the desorber and the absorber. Anyway, an absorption efficiency up to 95-96% with 40% CO_2 and 91-95% with 15% CO_2 was obtained by adopting the best operational conditions. The absorption efficiency of 40% CO_2 higher than that of 15% is most likely due to the increased CO_2 partial pressure which enhances the reaction rate.

The selective capture of H_2S and its conversion into a harmless compound was performed with aqueous H_2O_2 in two absorption-desorption cycles of AMP/IPMEA/DEGMME solution (0.400 dm^3, 3.00 mol dm^{-3}) sequentially to the CO_2 and H_2S stripping. In one experiment, a gas mixture of 15% CO_2 in air also containing 50 ppm of H_2S was used.

The oxidation reaction was

$$H_2S + H_2O_2 \rightarrow S + 2H_2O \qquad\qquad (1)$$

In order to verify whether this system successfully works with a greater amount of sulfide as well, the absorbent solution was charged with 5,0 g of $Na_2S \cdot 9H_2O$ (0,021 mol) dissolved in the minimum amount of water. With H_2O_2 0,65 mol dm^{-3} and a molar ratio $H_2O_2/H_2S = 3/1$ the oxidation reactions was :

$$H_2S + 4H_2O_2 \rightarrow SO_4^{2-} + 2H^+ + 4H_2O \qquad\qquad (2)$$
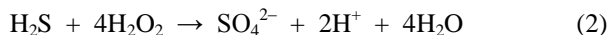
SO_4^{2-} was separated from the solution with the stoichiometric amount of CaO that neutralized the acidity of the reaction (2)

$$SO_4^{2-} + 2H^+ + CaO \rightarrow CaSO_4 + H_2O \qquad\qquad (3)$$

The oxidation reactions (1) and (2) were complete and no detectable amount of H_2S exited from the system (see experimental).

5.5. Conclusions

The results of the experimental study here reported indicate that AMP, AMP/IPMEA and AMP/TBMEA in EG/PrOH 1/1 (v/v) are the most suited absorbent for biogas

upgrading and absorption efficiencies up to 96% are attained with stripping temperatures of 90-95 °C at room pressure. The efficiency of these non-aqueous absorbents are due either to the fast reactions with CO_2 at room temperature and to the fast CO_2 release because of the lower stability of both monoalkyl carbonates and of amine carbamates with respect to HCO_3^- and to stable amine carbamates that are formed in aqueous solutions.

In two continuous absorption-desorption experiments H_2S was selectively oxidised with aqueous H_2O_2 and separated from CO_2 by either harmless elemental sulfur or $CaSO_4$ with the addition of CaO. The selective capture of H_2S here reported is more simple and efficient than the traditional capture protocols based on Fe(II) precipitation, oxidation with Fe(III) complexes, activated carbon, and so on.

5.6. References

[1] S. Heyne, S. Harvey. Impact of choice of CO_2 separation technology on thermo-economic performance of Bio-SNG production processes. Int. J. Energy Res., 2014, 38, 299-318.

[2] E.I. Privalova, P. Mäki-Arvela, K. Eränen, A.K. Avetisov,J.P. Mikkola, D.Y. Murzin. Amine Solutions for Biogas Upgrading: Ideal versus Non-Ideal Absorption Isotherms. Chem. Eng. Technol. 2013, 36, 740-748.

[3] M.E. Lopez, E.R. Rene, M.C. Veiga, K. Kennes, in Environmental Chemistry for a Sustainable World. E. Lichtfouse, J. Schwarzbauer, D. Robert Ed. Vol.2 pag. 347-378. Springer, Dordrecht, 2012.

[4] Q. Xue, X. Liu. Mixed-amine Modified SBA-15 as Novel Adsorbent of CO_2 Separation for Biogas Upgrading. Separ. Sci. Technol. 2011, 46, 679-686.

[5] M. Götz, W. Koppel, R. Reinert, F. Graf. Potential to Optimize Scrubbers for Biogas Cleaning. Part 1 – Physical Scrubbers. Chemie Ing. Technik, 2011, 83, 858-866.

[6] F.V.S. Lopes, C.A. Grande, A.E. Rodrigues. Activated carbon for hydrogen purification by pressure swing adsorption: Multicomponent breakthrough curves and PSA performance. Chem. Eng. Sci., 2011, 66, 303-317.

[7] A.L. Chaffee, G.P. Knowles, Z. Liang, J. Zhang, P. Xiao, P.A. Webley. CO_2 capture by adsorption: Materials and process development. Int. J. Green. Gas Control, 2007, 1, 11-18.

[8] H. Yang, Z. Xu, M. Fan, R. Gupta, R.B. Slimane, A.E. Bland. Progress in carbon dioxide separation and capture: a review. J. Environ. Sci., 2008, 20, 14-27.

[9] S. Sridhar, B. Smitha, T.M. Aminabhavi. Separation of carbon dioxide from natural gas mixtures through polymeric membranes-a review. Sep. Purif. Rev., 2007, 36, 113-174.

[10] R.W. Bucklin, R.L. Schendel. Comparison of Fluor solvent and Selexol processes. Energy Progr. 1984, 4, 137-142.

[11] S. Chaemchuen, N.A. Kabir, K. Zhou, F. Verpoort. Metal–organic frameworks for upgrading biogas via CO_2 adsorption to biogas green energy. Chem. Soc. Rev., 2013, 42, 9304-9332.

6. CO$_2$ Absorption with Solvent-Free Secondary Amines

6.1.   Introduction

Even if the replacement of water by organic solvents (Chapters 4 and 5) may reduce the costs of the stripping process, a lot of energy is wasted by the organic solvent heating from the absorption to the desorption temperatures. Moreover, the solvent, either water or alcohols account for about 70% of the absorbent and therefore requires very large equipments. The avoidance of any solvent, should be a decisive improvement towards the ideal absorbent.

In recent years, some single-component specific organic liquids have been designed and investigated for CO$_2$ capture as alternative to aqueous amines by virtue of their high thermal stability and negligible vapour pressure [1]. These absorbents include "task-specific ionic liquids" (TSILs) [2,3], alkanol guanidines and amidines [4], tunable basic ionic liquids prepared by neutralizing weak proton donors with phosphonium hydroxide[5,6] and silylated amines [7,8]. However, none of the previous ionic liquid-based absorbents were tested in a continuous absorption-regeneration cycling configuration because of the very high viscosity of the carbonated species or the formation of solid carbamates. Moreover, the procedures often required to attain a high CO$_2$ capacity (CO$_2$ pressure over 1 bar) [9,10] or an efficient absorbent regeneration (reduced pressure or N$_2$ flushing) cannot be applied to a commercial large scale plant. Additionally, some ionic liquid-based absorbents have high hydrophilic character and are readily decomposed by moisture. As a final consideration, the cost of the reagents and of the multistep synthetic procedures make all of these absorbents much more expensive than the commercially available conventional organic absorbents.

In the continuous efforts to improve the absorbents for CO$_2$ capture, we have formulated a class of single-component switchable absorbents that do not require dilution with a solvent because they are liquid both before and after the CO$_2$ uptake and have the potential of taking advantages from both aqueous amines and ionic liquids but avoiding their major disadvantages. These solvent-free reversible absorbents are the commercially available and inexpensive secondary amines dipropylamine (DPRA), N-ethylbutylamine (EBUA), dibutylamine (DBUA), dipentylamine (DPEA), dihexylamine (DHEA) and

dioctylamine (DOCA). Because of their high volatility, secondary amines with lower molecular weight were not taken into consideration.

Because of their low vapour pressure and high boiling temperature, the neat alkanolamines 2-(isopropylamino)ethanol (IPMEA), 2-(methylamino)ethanol (MMEA), 2-(ethylamino)ethanol (EMEA), 2-(benzylamino)ethanol (BZMEA) and 2-(butylamino)ethanol (BUMEA) would give additional advantages and should also enable us to have a more appropriate comparison with the features of the aqueous alkanolamines which represent a well established technology for CO_2 capture.

It is the first experimental study on the application of solvent-free organic absorbents to the CO_2 separation from other gases carried out in continuous cycles of absorption-desorption.

6.2. General Experimental Information

All reagents were reagent grade (95-98 %) except 2-(isopropylamino)ethanol that contains 30 wt % of the tertiary amine N-isopropyl-2,2'-iminodiethanol. The batch experiments designed to measure the CO_2 loading and the thermal release of CO_2 were carried out with the technique and the apparatus described in Sections 3.2.1 and 3.2.2. The absorber was charged with 0.100 dm^3 of the amine and the temperature of the reaction was constantly kept under control. The carbonated amines were checked by ^{13}C NMR spectroscopic measurements.

The CO_2 uptake as a function of the reaction time (only for alkanolamines) was measured with a gastight apparatus described in Section 5.2 (Figure 5.1). The experiment was stopped when the pressure did not change with time (40-90 min).

The continuous cycle experiments of CO_2 absorption-desorption were carried out as previously described in Section 3.2.3. The entire apparatus was charged with 0.250 dm^3 (in a few experiments the volumes were 0.150 dm^3 or 0.350 dm^3) of the appropriate amine that had been previously 50% saturated with CO_2. The solutions circulate continuously between the absorber and the desorber at the rates in the range 0.060 and 0.300 dm^3 h^{-1}. To mimic the flue gas, we used 15% or 40% (v/v) CO_2 in air (overall pressure of the gas mixture set at 1.0 bar) which was water saturated before being injected into the absorber at a flow rate of 12.0 dm^3 h^{-1} and 29.0 dm^3 h^{-1} (15% CO_2, 0.0743 and, respectively, 0.180 mol h^{-1} at 22 °C; 40% CO_2 12.0 dm^3 h^{-1}, 0.198 mol h^{-1}).

A complete cyclic experiment lasted 24-36 h and, for each desorption temperature tested. The viscosity, of both the free and carbonated amines (the latter were measured at the end of each cyclic experiments) was measured at 25 °C, 40 °C and 50°C with a Gilmont "Falling Ball Type" Viscometer by using 0.005 dm^3, approximately, of the appropriate amine. The viscometer tube was immersed in a constant temperature bath with a transparent window to observe the fiduciary lines. The proper ball was selected and dropped into the tube using the ball release device. The time of descent between the two sets of fiduciary lines was measured with a stop-watch. The reproducibility of the measurements was in the range 0.2– 1.0% depending upon the time of descent.

The vapour pressure measurements were performed with a home-made gastight apparatus which comprises a 0.100 dm^3 flask equipped with a digital pressure gauge. The flask was filled with 0.020 dm^3 of the amine at room temperature and pressure, afterwards the air was removed with a vacuum pump and the flask thermostatted at 80 °C. The pressure increase measured by the pressure gauge enabled us to estimate the pressure vapor as a function of temperature. The experiment was stopped when the pressure did not change with time (20 min).

The CO_2 uptake under 20 bar pressure was performed in a Parr 0.100 dm^3 stainless steel pressure vessel, with a thermocouple, a pressure gauge and a device to inject CO_2 at the appropriate pressure. 0.050 mol (5.07-12.07 g) of each amine and a stir bar contained in a glass container were charged into the vessel. After the air was removed from the reactor with a vacuum pump, the system was immersed in a thermostatted bath and pressurized with CO_2 to constant 20 bar for 60 min under magnetic stirring. The amount of CO_2 absorbed was determined at the end of each experiment by gravimetry.

The FTIR spectra were performed with a Perkin-Elmer FT-IR Spectrometer, using two KBr windows and recorded in the range 4400-400 cm^{-1}.

The ^{13}C NMR spectra of the liquid mixtures were obtained at room temperature as previously described in Section 3.3.

6.2.1. Comparison of the Sensible Heat of 30% MEA and Neat BUMEA

For the comparison, we used the results obtained in the cyclic experiments carried out with two absorber configuration and 93.5 % efficiency of both absorbents. The flux of 0.100 dm^3 h^{-1} of aqueous 30 wt % MEA ($d_{(50 °C)}$ = 1.07 kg dm^{-3}) corresponds to 0.0749 kg of water and 0.0321 kg of MEA [heat capacity 4.18 kJ kg^{-1} °C^{-1} and 2.6 kJ kg^{-1} °C^{-1},
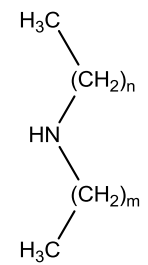
respectively [11] to be heated from 50 °C (absorber) to 105 °C (desorber). Meanwhile 0.168 mol h^{-1} of CO_2 was captured from the gas mixture (flux rate 29.0 dm^3 h^{-1} at 22 °C, 15.0 v/v % CO_2 and 93.5 % of absorption efficiency). From these figures, 129 kJ/mol CO_2 were required to heat aqueous MEA. The same calculus for neat BUMEA and 0.120 dm^3 h^{-1} ($d_{(50 °C)}$ = 0.904 kg dm^{-3}; heat capacity 2.47 kJ kg^{-1} °C^{-1} [12]) gave 75 kJ/molCO_2.

6.3.   Secondary Amines: Results

6.3.1.   Batch Experiments of CO_2 Uptake and Release

The neat secondary amines reported in Table 6.1 react with CO_2 at room temperature and pressure to give liquid carbonated species in the absence of any solvent.

Table 6.1. Abbreviation, name and formula of the tested amines.

DPRA	dipropylamine	n = m = 2	H$_3$C
EBUA	N-ethylbutylamine	n = 1 m = 3	(CH$_2$)$_n$
DBUA	dibutylamine	n = m = 3	
DPEA	dipentylamine	n = m = 4	HN
DHEA	dihexylamine	n = m = 5	(CH$_2$)$_m$
DOCA	dioctylamine	n = m = 7	H$_3$C

On standing at room temperature, CO_2-saturated dioctylamine gave a gel-like product that reverted to the liquid state at 35-40 °C. Some experimental data are reported in Table 6.2.

The loading capacity (mol CO_2/mol amine) of the different amines, except DOCA, obtained by gravimetric measurements, was found in the range 0.63-0.65 (average values 15.2-28.3% by weight, depending on the molar mass of each amine; Table 6.2), greater than the theoretical 0.5 value that should be expected in the absence of any aqueous or non-aqueous solvent (the secondary amine is denoted as AmH in the equation).

$$CO_2 + 2AmH \rightleftarrows AmH_2^+ + AmCO_2^- \qquad (1)$$

On the basis of the ^{13}C NMR and FTIR analyses (see later), the 0.13-0.15 additional uptake of CO_2 per mole amine could not be ascribed to physical adsorption and was due to the contribution of the unexpected carbamic acid formation with a stoichiometric loading 1, according to the reaction (2)

$$CO_2 + AmH \rightleftarrows AmCO_2H \qquad (2)$$

Table 6.2. Some properties of the neat and CO$_2$ loaded amines.

amine	Viscosity (cP)		Loading [a]		Acid/salt molar scale [f]
	Neat amine [b]	Loaded amine [c]	Gravim.[d]	NMR [e]	
DPRA	0.56	18.00	0.65	0.64	0.70
EBUA	0.58	16.96	0.63	0.65	0.65
DBUA	0.85	20.27	0.63	0.62	0.63
DPEA	1.19	20.04	0.65	0.68	1.00
DHEA	2.08	26.09	0.64	0.62	0.63
DOCA	3.82	30.92	0.59 [g]		

[a] mol CO_2/mol amine. [b] Viscosity of neat amines at 24 °C. [c] Viscosity of CO_2 loaded amines at 40 °C. [d] From gravimetric measurements. [e] From ^{13}C NMR analysis. [f] minimum value (see text) of $AmCO_2H/[AmCO_2^-][AmH_2^+]$. [g] At 40 °C.

To gain evidence for this assumption, the fully carbonated amines were analyzed by means of ^{13}C NMR spectroscopy that allowed us to identify and quantify the species in equilibrium at the end of the CO_2 uptake. The ^{13}C NMR spectra are simple displaying at least one couple of resonances in the range 48.96-10.84 ppm (DPRA), 46.59-10.89 ppm (EBUA), 47.31-13.59 ppm (DBUA), 55.06-10.76 ppm (DPEA), 47-64-13.68 ppm (DHEA) and 47.97-13.73 ppm (DOCA) ascribed to the $-CH_2-$ and $-CH_3$ carbon atoms of amine backbones. The more intense signals were attributed to the carbon atoms of protonated, $AmCO_2H$, and not protonated, $AmCO_2^-$, that are fast exchanging on the NMR time scale. The less intense signals are ascribed to the same carbon atoms of the summed protonated AmH_2^+ and possible unreacted amines. To complete the ^{13}C NMR picture, the low-intensity resonances at 160.70-160.43 ppm were assigned to the fast exchanging $-CO_2^-/-CO_2H$ pairs. Interestingly, these low intensity resonances were progressively downfield shifted with decreasing the percentage of the carbamic acid compared to the carbamate salt. As an example, the spectra of the CO_2 saturated and CO_2 desorbed dibutylamine are reported in Figure 6.1.

Remarkably, the loading capacities obtained by ^{13}C NMR analysis are very close to those measured by gravimetric experiments. As an example we can take into account the ^{13}C NMR spectrum of the CO_2 saturated dibutylamine that is reported in Figure 6.1 A. The careful integration of the $-CH_2-$ signals of the respective species, gave 62% (average, on molar scale; 46.22 and 30.96 ppm) of the summed $AmCO_2H$ and $AmCO_2^-$ and 38% of the AmH_2^+ and possible unreacted AmH (47.31 and 28.25 ppm). As the CO_2 loading is the ratio between the percentage of the carbonated species and the overall amine, the 0.62 loading obtained by the NMR analysis is in good agreement with 0.63 evaluated from gravimetric measurements (Table 6.2).
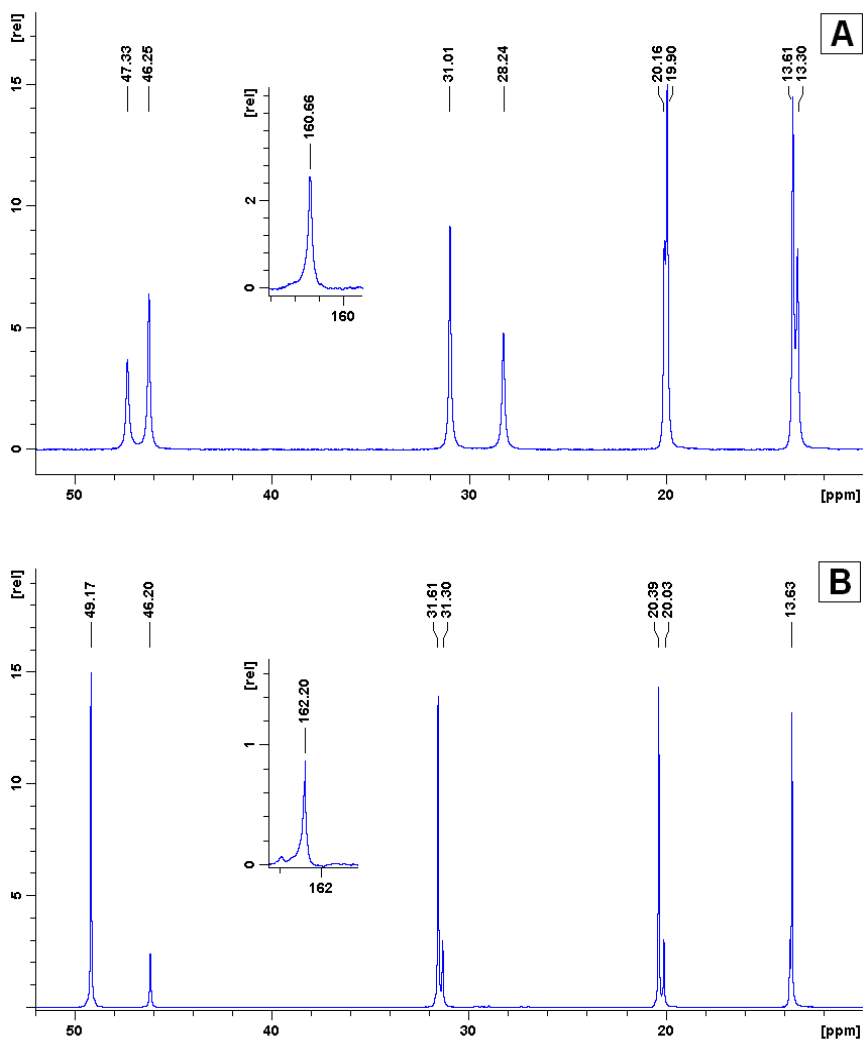
Figure 6.1. ^{13}C NMR spectrum of the CO_2 loaded DBUA (A) and of the same system desorbed at 80 °C (B). The signals at 46.25 and 31.01 ppm (A) and 46.20 and 31.30 ppm (B) are due to the –CH_2– carbon atoms of the summed carbamate and carbamic acid. The signals at 47.33 and 28.24 ppm (A) and 49.17 and 31.61 ppm (B) are due to the same carbon atoms of the protonated DBUA. The inset reports the raised signal of the carbon atom of the carbonyl groups.

The relative contribution of the reactions (1) and (2) to the overall CO_2 loading reported in Table 6.2 as acid/salt molar ratio, has been tentatively computed as follows. By assuming a negligible amount, if any, of the unreacted amine upon the CO_2 saturation and considering that the percentage of $AmCO_2^-$ and of the protonated amine, AmH_2^+, must be the same, the percentage of the salt $[AmCO_2^-][AmH_2^+]$ is 38% and the difference between 62% and 38% represents the percentage of the carbamic acid. From a chemical point of view, the presence of residual unreacted amine can be hardly

reconciled with the formation of the carbamic acid and with the excess of CO_2. Notwithstanding, it must be pointed out that any supposed amount of unreacted amine after the CO_2 saturation, results in a corresponding decrease of both the protonated amine and the carbamate and, consequently, in an increase of the carbamic acid in such a way that the overall percentage, 62%, of carbamate and carbonic acid must be retained. As a consequence the CO_2 loading does not change and the carbamic acid/carbamate salt molar ratios reported in Table 6.2 are the lowest limiting values. It is clear that the chemical capture of CO_2 as the sole carbamate salt should have given the same integrated signals ascribed to $AmCO_2^-$ and AmH_2^+, contrary to the result of the ^{13}C NMR analysis. Based on these results, the 0.13-0.15 additional CO_2 uptake cannot be due to physical adsorption, at least entirely. For a further confirmatory evidence, we carried out FTIR spectra of the CO_2 loaded amines. The FTIR spectra of DPRA before and after CO_2 uptake are reported in Figure 6.2.
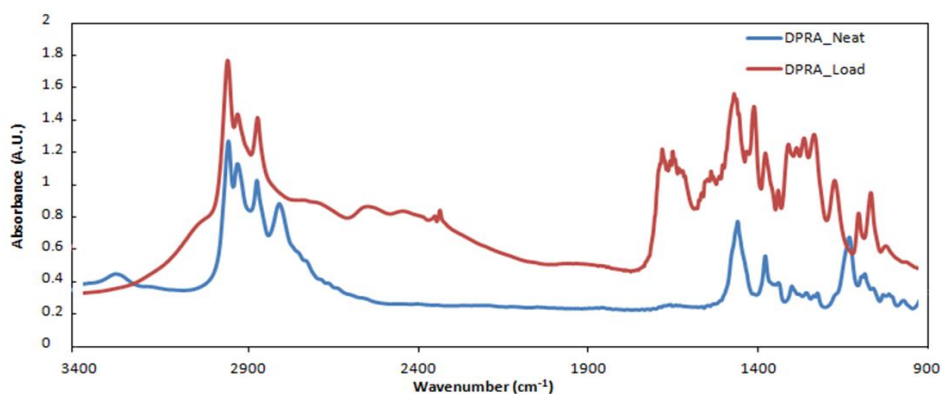
Figure 6.2. FTIR spectrum of neat and CO_2 loaded dipropylamine.

The remarkable broadening of the absorption in the range 2600−3100 cm^{-1} of CO_2 loaded amine was due to the O-H stretching of the carbamic acid whereas the absorption at 1684 cm^{-1} was ascribed to the carbonyl stretching of the carbamic acid in agreement with the literature assignments [13,14]. The absorption at 1552 cm^{-1}, assigned to the asymmetric CO_2^- stretching of the carbamate anion and the absorption at 2558 cm^{-1} due to the NH_2^+ moiety confirmed the presence of the amine carbamate salt. A small amount of physically absorbed CO_2 could be indicated by the low intensity of the asymmetric stretching of CO_2 at 2330 cm^{-1}. The unique example so far reported of a carbamic acid-carbamate salt equilibria is the reaction of CO_2 with some 3-(aminopropyl) trialkylsilylanes [13].

84

The CO_2 loading of DOCA is 0.59 and the carbonated species is the sole amine carbamate because of the 1/1 molar ratio $[AmCO_2^-]/[AmH_2^+]$ displayed by the ^{13}C NMR spectrum. The additional 0.09 mol of CO_2 uptake was likewise due to physical absorption.

The CO_2 release was accomplished at 80 °C with stirring for 60 min at room pressure and is comprised between 95% (DPEA) and 75% (DPRA). Increasing either desorption temperature or time, forces more CO_2 to be released. The volumetric measurements of CO_2 release was confirmed by the ^{13}C NMR analysis. The ^{13}C NMR spectrum of the CO_2 desorbed DBUA is reported in Figure 6.1 B. A near complete CO_2 desorption was accomplished at 60 °C under N_2 flushing through the liquid for 120 min.

In order to verify if the absorbents are capable of additional CO_2 uptake, some loading experiments were performed in a 0.100 dm^3 Parr pressure vessel at room temperature under 20 bar of CO_2 and magnetic stirring. The loading capacities evaluated by gravimetric measurements are comprised between 0.77 (DBUA) and 0.83 (DPRA), with an appreciable increase with respect to the room pressure loading. The ^{13}C NMR spectra did not account for the 0.14-0.18 additional uptake of CO_2, with respect to 1.0 bar capture, that was likewise mostly due to physical absorption. As a matter of fact, some CO_2 was instantly released by the loaded absorbents after the pressure vessel was opened and the room pressure was restored.

The viscosity of the absorbent is a hindrance to the diffusion rate of the gas into the liquid and will cause a reduced mass transfer and, consequently, a reaction rate reduction. The viscosity of the amines we have measured at 24 °C increases from 0.56 cP (DPRA) to 3.82 cP (DOCA) on increasing the alkyl chain length that enhances the weak intermolecular interactions. Upon CO_2 uptake, the viscosity of the carbonated absorbents was comprised between 16.9 cP of EBUA and 30.9 cP of DOCA at 40 °C (Table 6.2). Even though these viscosity values are relatively high, they are well below those reported for the traditional CO_2 saturated ionic liquids. Furthermore, it is expected a further decrease of the viscosity by decreasing the partial pressure of CO_2, by using a gas mixture instead of pure CO_2. On the basis of these considerations, our amines could be suitable absorbents for an efficient CO_2 capture from a simulated flue gas in an absorption-desorption cycle operating in continuous.

6.3.2. Continuous Cycles of CO$_2$ Absorption-Desorption

In order to check whether the solvent-free amines were capable of successfully working in a continuous absorption-desorption cycle, we designed bench-scale experiments as previously described in Section 3.2.3. In these experiments, the absorbents were continuously circulating in a closed cycle between the absorber (set at 40-45 °C) and the desorber (set at 70-85 °C). The lean and rich absorbents circulated at the same rate of 0.300 dm^3 h^{-1}. The gas mixture of 15% and 40% (v/v) CO$_2$ in air (overall gas pressure set at 1.0 bar) was continuously feeding into the base of the absorber where comes in contact with the liquid getting down off the top. The percentages of CO$_2$ were selected to address the CO$_2$ content of the post combustion gas mixture and of the natural gas (15%), as well as of the biogas mixture from biomass (40%). The rate of 15% CO$_2$ flowing gas was 12.0 and 29.0 dm^3 h^{-1} The entire apparatus was charged with 0.250 dm^3 of each amine, previously 50% saturated with CO$_2$. Each experiment lasted 24-36 h and it was stopped when the reactions of CO$_2$ capture and of amine regeneration reached a steady state. The working conditions are summarized in Table 6.3.

Table 6.3. Operating conditions employed in the continuous absorption desorption experiments.

Amine volume	0.250 dm^3
Absorption temperature	40, 45 °C
Desorption temperature / pressure	70, 75, 80, 85 °C / 1 bar
Liquid flow rate	0.300 dm^3 h^{-1}
Gas flow rate	12.0, 29.0 dm^3 h^{-1}
Gas mixture	15%, 40% (v/v) CO$_2$ in air
Pressure of gas mixture	1.0 bar

In order to find the best compromise between the highest absorption and lowest desorption temperatures that achieve the target removal efficiency of 90%, most of the absorption experiments were carried out at 40, 45 °C and the desorption at 75, 80 °C. The desorption temperature of the lower boiling DPRA and EBUA was limited to 75 °C. The results of the experiments with the different amines and the different operational conditions are reported in Table 6.4.

As expected, increasing the desorption temperature enhances the CO$_2$ release which causes an increasing of the absorption efficiency (percentage of CO$_2$ absorbed/CO$_2$ flowed). The same result was obtained by decreasing the absorption temperature that increases the solubility of CO$_2$ and favours the exothermic acid-base reaction. Even if the greater viscosity at lower temperatures would reduce the mass transfer between the gas and the liquid phase, the thermodynamic constraints overcome the kinetic ones.

Table 6.4. Absorption efficiency of the secondary amines.

amine	Teb (°C)	Vp[a] (bar)	Mol[b] amine	Absorption Efficiency (%)[c] at different ABS-DES temperature and different CO₂ percentage														
				40-70 °C			40-75 °C			40-80 °C			45-80 °C			40-85 °C		
				15%[d]	15%[a]	40%[d]	15%[d]	15%[a]	40%[d]	15%[d]	15%[a]	40%[d]	15%[d]	15%[a]	40%[d]	15%[d]	15%[a]	40%[d]
DPRA	107	0.328	1.82	87.5	75.0	94.3	95.5	92.1	98.5									
EBUA	111	0.293	1.83	82.3	67.4	93.1	92.6	86.6	97.7									
DBUA	159	0.085	1.48			88.0	85.5	78.2	96.3	94.5	92.3	97.6	90.2	88.0	97.1			
DPEA	202	0.040	1.22			88.0	82.6	68.5	93.7	91.1	85.3	96.6	85.3	72.4	95.0			
DHEA	236	0.038	1.07				85.9	57.8	77.1	92.4	85.2	97.2	89.1	73.2	93.0			
DOCA	297	0.034	0.83				77.7	52.0	54.6	88.7	66.0	75.6	84.0	53.3	58.6	93.1	75.9	96.7

[a] Vapour pressure of neat amines at 80°C. [b] Amount of amine in 0.250 dm³. [c] Per cent ratio between absorbed and flowed CO₂; the deviation from the average values was always in the range 1.5–3%. [d] Gas flow rate = 12 dm³ h⁻¹. [e] Gas flow rate = 29 dm³ h⁻¹.

The viscosity of the absorbents circulating between the absorber and the desorber is relatively low: below 5 cP at 24 °C, with the exception of dioctylamine whose 12 cP value was obtained by using a 40% CO_2 gas mixture. Overall, the absorption efficiency under identical working conditions and amine volumes decreases in the order DPRA > ETBUA > DBUA > DHEA ~ DPEA > DOCA, roughly according to the decreasing amine moles. Even if DPRA and EBUA were found to display the greatest absorption efficiency at 40-75 °C, nonetheless their relatively low boiling temperature and high vapour pressure (Table 6.4) make these amines more prone to evaporation, in spite of the relatively low desorption temperature. Consequently, they are unsuited for a commercial large-scale application. The evaporation of DPEA, DHEA and DOCA is highly reduced by their high boiling temperatures and low vapour pressure, even under the maximum desorption temperature at 80-85 °C. It is noteworthy that the vapour pressures of DPEA, DHEA and DOCA ($0.020 \cdot 10^{-2}$ – $0.001 \cdot 10^{-2}$ bar at 20 °C) are lower than those of MEA ($0.036 \cdot 10^{-2}$ bar at 20 °C), the reference solvent of any CO_2 capture process, and of water ($2.34 \cdot 10^{-2}$ bar at 20 °C).

The feature of DOCA that required 85 °C desorption to attain an efficiency greater than 90 % is easily explained by the lowest amount of amine (less than half DPRA, on molar basis) in the same 0.250 dm^3 volume.

It is likely that the higher absorption efficiency on going from 15% to 40% CO_2 (Table 6.4) was due to the increased reaction rate because of the greater CO_2 partial pressure. On changing the flue gas rate of 15% CO_2, the lower gas flux, 12.0 $dm^3\ h^{-1}$, increases the residence time of the gas within the absorber, thereby enhancing the rate of absorption reactions and, consequently, the absorption efficiency. Anyway, an absorption efficiency greater than 90% could be obtained by adopting a number of different operational conditions and amines.

The distribution of the carbonated amines recovered from absorber and desorber was analyzed by ^{13}C NMR spectroscopy at the end of any experiment, when the stationary conditions were reached. The CO_2 containing species is the carbamate salt (reaction 1) dissolved in the excess of free amine that prevents the formation of the carbamic acid. The percentage of carbamate salt ranges between 30-40% in the absorber and 10-25% in the desorber.

For comparison purposes, we carried out experiments of CO_2 capture by 30 wt % aqueous MEA under the same working conditions of neat amines: the absorption efficiency was not greater than 69 % with absorption-desorption temperatures at 30-90

°C. It may be of interest to notice that 0.250 dm^3 of either 30 % MEA or neat DPEA contain approximately the same moles of amine but DPEA displays a 91% efficiency at 40-80 °C. The thermal stability of the high boiling DBUA, DPEA, DHEA and DOCA was measured by heating at 100 °C for 30-40 days the CO_2 loaded amines recovered at the end of the cyclic experiments. The ^{13}C NMR spectra of DHEA and DOCA did not reveal degradation products within the liquids whereas 2-3 % of unidentified by-products were detected by the ^{13}C NMR spectra of DBUA and DPEA.

6.4. Secondary Alkanolamines: Results

6.4.1. Batch Experiments of CO_2 Uptake

The neat secondary alkanolamines reported in Table 6.5 react with CO_2 to give carbonated species in the liquid phase notwithstanding the absence of any dilution with an added solvent. The acid-base reactions are thermally reversible thus allowing to recover the free amines and pure CO_2. Some properties of the alkanolamines we used are reported in Table 6.6.

To measure the experimental loading capacity of the different amines, pure CO_2 was flowed through 0.100 dm^3 of each neat amine maintained at 40 °C until no more CO_2 was absorbed.

Table 6.5. Abbreviation, name and formula of the tested alkanolamines.

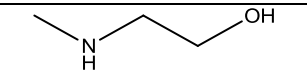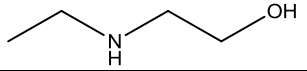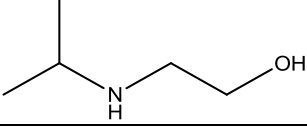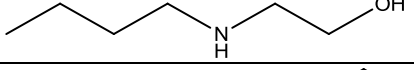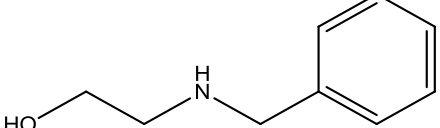|		
MMEA	2-(methylamino) ethanol	
EMEA	2-(ethylamino) ethanol	
IPMEA	2-(isopropylamino) ethanol	
BUMEA	2-(butylamino) ethanol	
BZMEA	2-(benzylamino) ethanol	

Table 6.6. Some properties of the alkanolamines used for CO_2 capture.

amine	molar mass (g mol^{-1})	T_b (°C)	density at 20°C (kg dm^{-3})	viscosity at 50°C (cP)	loading at 40°C
MMEA	75.11	158	0.940	4.39	0.52
EMEA	89.14	170	0.914	4.55	0.50
IPMEA	103.17	182	0.897	9.49	0.49
BUMEA	117.19	199	0.891	5.63	0.50
BZMEA	151.21	156	1.063	15.54	0.48

The loading capacity measured by gravimetry (see experimental) of the different amines is quite similar to each other and ranges between 0.48 of BZMEA and 0.52 of MMEA (Table 6.6), near to the expected theoretical value in the absence of any aqueous or non-aqueous solvent (reaction 1).

The formation of the ionic couple upon the CO_2 uptake was confirmed by the analysis of the ^{13}C NMR spectra which allowed us to identify and quantify the carbonated species. The ^{13}C NMR resonances (δ, ppm) of the carbon atoms of the carbamate and protonated amines (in parentheses) saturated by CO_2 were: MMEA, 163.55, 60.32, 50.93, 34.80; (56.74, 50.93, 32.54); EMEA, 163.21, 61.88, 48.68, 42.15, 13.42; (57.26, 49,21, 42.15, 11.17); IPMEA, 162.33, 63.22, 51.43, 43.51, 20.00 (58.38, 48.82, 46.02, 20.67); BZMEA, 164.17, 139.71, 128.87, 127.69, 126.44, 61.78, 51.38, 49.23 (135.63, 128.37, 128.11. 126.90, 58.67, 51.81, 49.52); BUMEA, 163.55, 62.37, 49.39, 47.83, 30.64, 19.57, 13.42 (57.69, 49.93, 47,51, 28.53, 19.57, 13.12).

The ^{13}C spectra display couples of resonances in the range 60.32 and 32.54 ppm (MMEA), 61.88 and 11.17 ppm (EMEA), 63.22 and 20.00 ppm (IPMEA), 139.71 and 49.2 ppm (BZMEA), 61.20 and 13.12 ppm (BUMEA) assigned to the CH, CH$_2$ and CH$_3$ carbon atoms of the amine carbamates and of the fast exchanging protonated amines and free amines. The low-intensity resonances in the range 164.17-162.23 ppm were ascribed to the carbonyl group of the carbamate. As an example of the ^{13}C NMR spectra of the ionic couples carbamate-protonated amine, the spectrum of BUMEA carbonated by 40% CO_2 is reported in Figure 6.3.

The CO_2 (15 % v/v in air) uptake by the different alkanolamines as a function of time was compared with that of aqueous 30% wt MEA in experiments carried out in a 2.0 dm^3 flask (Section 6.2) containing the same amount (about 0.12 mol) of the different amines which were in a large excess with respect to the fixed amount of CO_2 charged in the flask (0.0137-0.0141 mol).
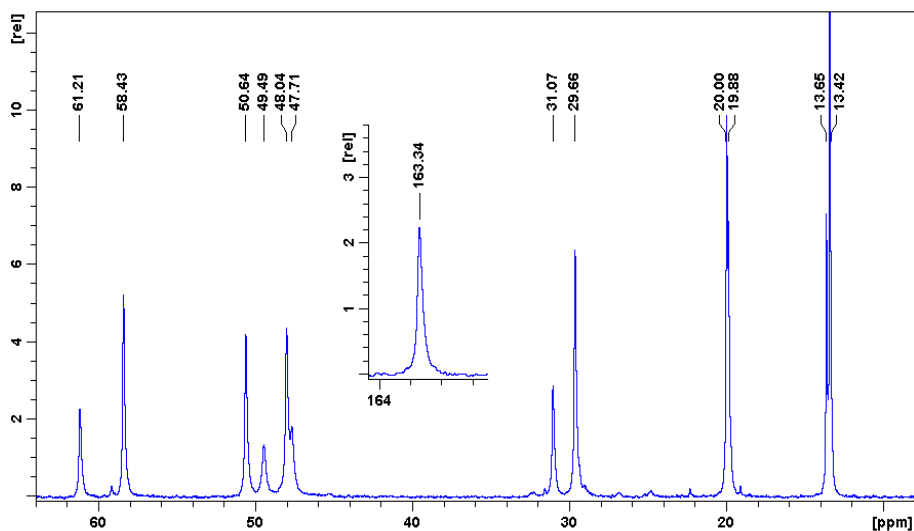
Figure 6.3. ^{13}C NMR spectrum of BUMEA carbonated by 40% CO_2 in the absorption cycle carried out at 50 °C. The signals (δ, ppm) at 61.21, 49.49, 47.71, 31.07, 19.88 are due to the $-CH_2-$ and 13.65 to the $-CH_3$ carbon atoms of the amine carbamate. The signal (δ, ppm) at 58.43, 50.64, 48.04, 29.66, 20.00 and 13.42 are due to the same carbon atoms of the summed protonated and free amine. The inset reports the raised signal (163.34 ppm) of the carbon atom of the carbonyl group.

The results obtained are reported in Table 6.7. After 90 min, no more CO_2 was absorbed and the experiment was stopped. The percentage of CO_2 absorbed with respect to that contained in the flask is reported as a function of time in Figure 6.4. At the end of the absorption experiment, the neat alkanolamines absorbed over 90 % of the CO_2 contained in the flask with the exception of IPMEA (77.3 %; Table 6.7). It is worth considering that the CO_2 absorption capacity of aqueous MEA was lower, 82 %, notwithstanding aqueous MEA is recognised as a very efficient absorbent.

Table 6.7. Some data of the batch experiments of CO_2 (15% in air) uptake by neat alkanolamines and 30% aqueous MEA as a function of time.

Amine	vol [a] (dm^3)	mol amine	T (°C) [b]	P (bar) [c]	mol CO_2	abs % [d]
MMEA	0.0096	0.1201	21	1.0145	0.0141	92.0
EMEA	0.0117	0.1200	24	1.0013	0.0137	92.4
IPMEA	0.0197	0.1199	22	1.0146	0.0140	77.3
BUMEA	0.0158	0.1201	22	1.0173	0.0140	92.0
BZMEA	0.0171	0.1202	21	1.0159	0.0140	91.3
MEA 30%	0.0245	0.1200	25	1.0067	0.0137	82.2

[a] volume of the neat alkanolamines and of aqueous MEA; [b] temperature of the gas mixture in the flask; [c] starting pressure of the gas; [d] overall percentage of CO_2 uptake at the end of the experiment.

As far as the rate of CO_2 uptake is concerned, MMEA, EMEA, BUMEA and aqueous MEA displayed a quite similar behaviour and less than 5 minutes were required to reach the respective equilibrium, whereas the reaction rates of both BZMEA and IPMEA were considerably lower. Presumably, the steric hindrance of the *i*-propyl group at the amine function (IPMEA) disfavours the insertion of CO_2 and makes the carbamate derivative less stable, thus disfavouring both the reaction rate and equilibrium. Moreover, the high viscosity of the neat IPMEA (Table 6.6) is a hurdle to the mass transfer between the gas and the liquid. The relatively low reaction rate of BZMEA, in spite of its high uptake efficiency at equilibrium, could be explained by its greatest viscosity (15.54 cP at 50 °C). On the contrary, the low viscosity of the aqueous MEA explains its high reaction rate, but its fairly less CO_2 removal efficiency was difficult to explain, unless it was due to the combined effects of the water dilution and of the low pressure of the residual CO_2 which adversely affected the acid-base equilibrium.
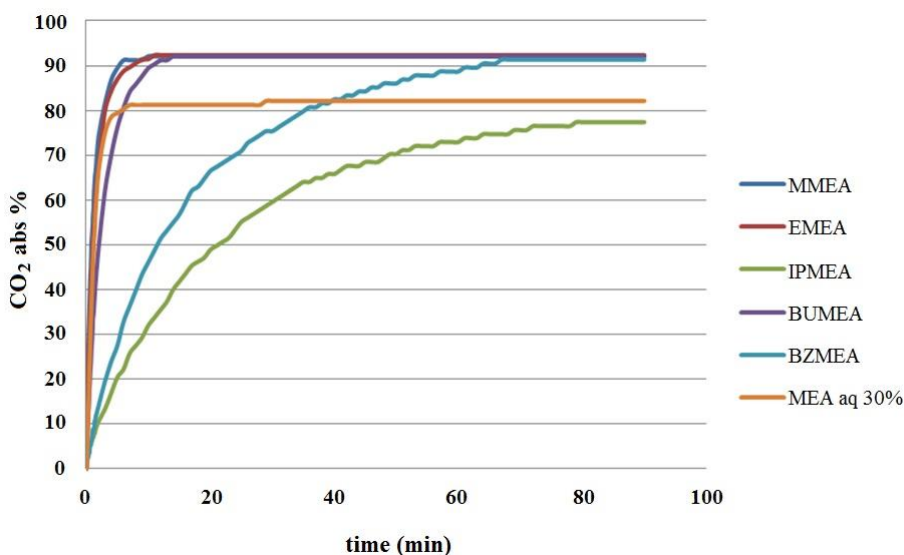
Figure 6.4. Variation with time of the CO_2 (15% in air) uptake by the different neat alkanolamines and of 30% aqueous MEA.

6.4.2. Continuous Cycles of CO_2 Absorption-Desorption

In most experiments, the CO_2 loaded and regenerated absorbents (overall, 0.250 dm^3) were continuously circulated between the absorber (set at 50-60 °C) and the desorber (set at 100-120 °C) at the flow rate of 0.300 dm^3 h^{-1}. The gas mixtures which simulate the flue gas contain either 15 % or 40 % (v/v) CO_2 in air and accounts for average CO_2 content of post combustion gas streams (15 %) and of biogas from biomass waste (40

%). The flow rate of 15 % CO_2 gas mixture was 12.0 and 29.0 $dm^3 h^{-1}$ (0.0743 mol h^{-1} and, respectively, 0,180 mol h^{-1} of CO_2 at 22 °C). The rate of 40% gas mixture was 12.0 $dm^3 h^{-1}$ (the CO_2 content is 0.198 mol h^{-1} at 22 °C). For comparison purposes, analogous experiments were carried out with 30 wt % aqueous MEA, the reference absorbent of any CO_2 capture technology. Each complete experiment lasted 24-36 h and was stopped when the process reached a steady state and the CO_2 capture efficiency did not change with time. A summary of the experimental setup is reported in Table 6.8.

Table 6.8. Operational conditions employed in most of the experiments of CO_2 capture carried out in the continuous cycles of absorption-desorption.

Amine volume	0.150, 0.250, 0.350 dm^3
Absorption temperature	40, 50, 60 °C
Desorption temperature/pressure	100, 110, 120 °C/1 bar
Liquid flow rate	from 0.060 to 0.300 $dm^3 h^{-1}$
Gas flow rate	12.0, 29.0 $dm^3 h^{-1}$
Gas mixture	15%, 40% (v/v) CO_2 in air
Pressure of the gas mixture	1.0 bar

The choice of the relatively high absorption temperature (50-60 °C) was dictated by the viscosity of the carbonated absorbents at room temperature that reduces the rate of CO_2 uptake, even if a high absorption temperature was a detriment to the equilibrium of the exothermic reaction. Additional advantages of the absorption temperature at 50-60 °C would be the less cooling of the exhaust gas from power plants and the lower difference between the absorber and the desorber temperatures. The results of the experiments carried out with the different amines and operating conditions are reported in Table 6.9: several combinations of amines and experimental conditions gave efficiency over 90 %. As a general remark, the absorption efficiency of the different amines increased with increasing the desorption temperature and decreasing the absorption temperature.

In spite of the enhanced viscosity, the absorber temperature reduction from 60 °C to 50 °C had a beneficial effect on the exothermic reaction as well as on the CO_2 solubility, and the absorption efficiency of all amines increased. On the other hand, the reduced reaction rate on going from 60°C to 50°C should be negligible by virtue of the fast reactivity of most of the amines even at room temperature (Figure 6.4). Due to the high viscosity of MMEA (168 cP, Table 6.9), no cyclic experiment could be done at temperatures below 60 °C. The greater volume of IPMEA (0.350 dm^3, 2.13 mol of pure amine, Table 6.9) takes into account the 70% content of the pure ammine in the commercial product.

Table 6.9. Absorption efficiency of the alkanolamines as a function of the different absorption/desorption temperatures, absorbent volume, CO_2 percentage and liquid and gas flow rate.

Amine	V^a dm³	mol[b]	viscosity[c] (cP, 50°C)	T^d, 40-100			T^d, 50-100			T^d, 50-110			T^d, 60-110			T^d, 60-120		
				15%[e]	15%[f]	40%[e]	15%[e]	15%[f]	40%[e]	15%[e]	15%[f]	40%[e]	15%[e]	15%[f]	40%[e]	15%[e]	15%[f]	40%[e]
MMEA	0.250	3.13	168.43										95.2	77.7	97.7			
EMEA	0.250	2.56	51.58				94.8	75.4	97.3	98.1	95.4	99.4	96.0	90.8	98.9			
	0.150	1.54											93.1	78.1	96.2			
IPMEA	0.350	2.13	15.85	82.1	59.7	88.0	74.1			79.8	<50	84.2						
	0.250	1.90					95.6	77.0	97.0	97.8	95.6	99.1	92.6	86.2	97.4	97.0	93.1	99.0
BUMEA	0.250[g]	1.90	21.25				91.2	52.0	65.6	96.6	76.3	73.5	85.8	43.0	62.3	91.9	53.6	73.2
	0.150	1.14					94.1	72.0	91.9	97.0	90.4	99.0	92.8	77.0	96.7	96.8	90.7	98.9
BZMEA	0.250	1.76	56.24				84.6	48.6	86.3	95.4	74.3	97.3	89.2	56.9	92.6			

[a] volume of the absorbent; [b] amount in mol of the absorbent; [c] viscosity of the carbonated absorbent measured at 50 °C; [d] absorption and desorption temperatures; [e] flow rate of the gas mixture: 12.0 dm³ h⁻¹; [f] flow rate of the gas mixture: 29.0 dm³ h⁻¹; [g] flow rate of the absorbent: 0.100 dm³ h⁻¹.

The lowest efficiency of IPMEA was presumably the result of its low reaction rate, as shown by batch experiments (Figure 6.4), that did not allow the acid-base reaction to reach the equilibrium in the continuous cycles of absorption-desorption.

The comparison of the amine performances measured in the cycles carried at 60-110 °C with different gas flow (12.0 and 29.0 dm^3 h^{-1}) and CO_2 percentage (15% and 40%), indicates that the efficiency decrease in the order EMEA > BUMEA > MMEA > BZMEA.

Considering the amount of the amines contained in the fixed volume of 0.250 dm^3 that decreases in the order MMEA (3.13 mol) > EMEA (2.56 mol) > BUMEA (1.90 mol) > BZMEA (1.76) and the viscosity of the carbonated absorbents (measured at 50 °C) that decreases in the order MMEA >> BZMEA > EMEA > BUMEA, the higher efficiency of both EMEA and BUMEA was likewise due to their lower viscosity, rather than to the amount of amine.

As a matter of fact, the reduction of the volume of EMEA and BUMEA from 0.250 to 0.150 dm^3 (15 % and 40 % CO_2, 12 dm^3 h^{-1}, cycles at 60-110 °C, Table 6.9) did not substantially affect the efficiency of the CO_2 capture. The same results were obtained in the experiments carried out with BUMEA at 50-100 °C, 50-110 °C and 60-120 °C.

By varying the gas flow rate or CO_2 percentage, the experiment results (Table 6.9) clearly indicated that 40 % CO_2 was more efficiently captured than 15 % CO_2, most likely because of the increased partial pressure of CO_2 that enhanced its solubility and the reaction rate. As expected, the efficiency decreased if the gas flow rate was increased from 12.0 to 29.0 dm^3 h^{-1}, due to the reduced residence time of the gas in the absorber.

Based on the efficiency and the highest boiling temperature (i.e. the lowest vapour pressure at the highest operational temperature), as well as on the reasonable viscosity values (Tables 6.7 and 6.9), BUMEA seems to be the most suitable absorbent for its implementation in a full-scale CO_2 capture process. As such, the efficiency of BUMEA was measured under the reduced liquid circulation from 0.300 to 0.100 dm^3 h^{-1}. The reduction of the liquid circulation resulted in a decrease of the CO_2 capture efficiency, but in most experiments (15 % CO_2 and flow rate 12 dm^3 h^{-1} of the gas mixture) it was over 90 % (Table 6.9).

For comparison purposes we carried out experiments of CO_2 capture with 30% aqueous MEA under the same operational conditions of BUMEA. The 91.2 % efficiency of 0.250 dm^3 of neat BUMEA (Table 6.10, entry 1) by far overcomes the 49% efficiency of 0.390 dm^3 of aqueous MEA (Table 6.10, entry 3) by virtue of its higher neat amine circulating

rate (0.76 mol h^{-1}) compared to that of aqueous MEA (0.49 mol h^{-1}), the absorbent circulation rate (0.100 dm^3 h^{-1}) being the same in the two experiments and notwithstanding the much lower viscosity of aqueous MEA. It was necessary to increase the circulation rate of aqueous MEA up to 0.300 dm^3 h^{-1} (Table 6.10, entry 4; 1.46 mol h^{-1}), to attain an efficiency (91.8 %) comparable to that of 0.100 dm^3 h^{-1} BUMEA.

Table 6.10. *Absorption efficiency and working capacity of BUMEA and 30% aqueous MEA; the fixed operational conditions are: one absorbent column; gas flow rate 12.0 dm^3 h^{-1}, 15 % CO$_2$, absorption and desorption temperatures 50 °C and 100 °C.*

amine	entry	vol (dm^3)	mass[a] (kg)	mol[b]	liq flow (dm^3 h^{-1})	abs (%)[c]	CO$_2$ abs[d] (mol h^{-1})	amine flow[e] (mol h^{-1})	working capacity[f] (mol kg^{-1})
BUMEA	1	0.250	0.226	1.90	0.100	91.2	0.068	0.76	0.75
	2	0.150	0.136	1.14	0.300	94.1	0.070	2.28	0.26
30% MEA	3	0.390	0.417	1.90	0.100	49.0	0.036	0.49	0.34
	4	0.390	0.417	1.90	0.300	91.8	0.068	1.46	0.21
	5	0.500	0.535	2.44	0.300	96.6	0.072	1.46	0.22

[a] the density of the carbonated absorbents in the absorber at 50°C is: BUMEA 0,904 kg dm^{-3}; 30% aqueous MEA 1,070 kg dm^{-3}; [b] amount of the amines; [c]CO$_2$ absorption efficiency; [d] mol of absorbed CO$_2$; [e] flow rate of recirculated absorbents; [f] [absorbed CO$_2$ (mol h^{-1})]/[absorbent mass (kg h^{-1})]

In summary, the results here focused on CO$_2$ absorption indicate that a mass of aqueous MEA about 1.8 times greater and a threefold circulation rate were necessary to get the same CO$_2$ capture efficiency of neat BUMEA (Table 6.10, entry 1). It must be pointed out that the higher is the absorbent circulation rate, the greater is the energy required by the CO$_2$ desorption process [15]. The experiments of absorption-desorption we carried out with neat MEA in the same experimental conditions of these used with BUMEA gave absorption efficiency in the range 50-54%. The low absorption efficiency of solvent free MEA was due to the very high viscosity of the carbonated species (458 cP measured at 50 °C). To have a better comparison of the efficiency of neat BUMEA and aqueous MEA, we have defined the working capacity of the two absorbents as (mol of CO$_2$ captured)/(mass of circulating absorbent). This definition seemed to us more appropriate as the working capacity of aqueous MEA based on the amount of the sole amine (mol CO$_2$ captured/mol of circulating amine) would completely neglect the presence of water that must be pumped and heated in the desorption step. The results reported in Table 6.10 (entries 1 and 4) provided compelling evidences of the disadvantages of aqueous MEA which attained the same CO$_2$ capture efficiency of neat

BUMEA at the expense of a much lower working capacity because of its greater circulation rate. A volume increase of aqueous MEA (0.500 dm^3) had a negligible effect on its working capacity (Table 6.10, entry 5). By decreasing the BUMEA volume from 0.250 dm^3 to 0.150 dm^3 (from 1.90 mol to 1.14 mol) and increasing the absorbent flow rate from 0.100 to 0.300 dm^3 h^{-1}, the working capacity was greatly reduced (Table 6.10, entry 2) and was not compensated by the slight increase of the absorption efficiency. The working capacity of any absorbent is enhanced by increasing the ratio (gas flow rate)/(liquid flow rate), but the increased gas flow rate from 12.0 dm^3 h^{-1} to 29.0 dm^3 h^{-1} and, at the same time, the reduced absorbent flow rate from 0.300 dm^3 h^{-1} to 0.100 dm^3 h^{-1} were unfavourable to the absorption efficiency under any absorption-desorption temperature (Table 6.9, BUMEA).

With the purpose of increasing the working capacity without depressing the absorption efficiency, we designed a different equipment configuration with two packed columns for the CO_2 capture and absorption-desorption temperatures set at 50-105 °C. The results of the experiments performed with 0.250 dm^3 of either neat BUMEA or aqueous MEA, different liquid flow rates and flow rate of the gas mixture (15 % CO_2) fixed at 29 dm^3 h^{-1}, are reported in Table 6.11.

Table 6.11. Absorption efficiency and working capacity of BUMEA and 30% aqueous MEA; the fixed operational conditions are: two absorbent columns, absorbent volume 0.250 dm^3; gas mixture flow rate 29.0 dm^3 h^{-1} 15 % CO_2; absorption and desorption temperatures of 50 °C and 105 °C.

amine	entry	liquid flow rate			abs %	CO_2 abs [c] (mol h^{-1})	working capacity [d] (mol kg^{-1})
		dm^3 h^{-1}	kg h^{-1} [a]	mol h^{-1} [b]			
BUMEA	1	0.060	0.054	0.456	70.1	0.124	2.29
	2	0.090	0.081	0.684	80.3	0.143	1.76
	3	0.120	0.108	0.912	93.5	0.168	1.56
30% MEA	4	0.060	0.064	0.295	67.3	0.121	1.88
	5	0.090	0.096	0.443	85.7	0.154	1.60
	6	0.100	0.107	0.492	93.5	0.168	1.57

[a] density as in Table 6.10; [b] neat amine; [c] amount of absorbed CO_2; [d] defined as in Table 6.10.

As a general consideration, the configuration with two absorbent columns gave a neat advantage in terms of CO_2 absorption efficiency. As a matter of fact, we can compare the 80.3% absorption efficiency of 0.090 dm^3 h^{-1} flow rate of BUMEA at 50/105 °C (Table 6.11, entry 2) with 52.0% and 76.3% efficiencies obtained in the experiments

carried out with one absorbent column and 0.100 dm^3 h^{-1} flow rate at 50/100 °C and, respectively, 50/110 °C (Table 6.9), the gas flow rate of 29 dm^3 h^{-1} being the same in the two different experiments. Moreover, at comparable CO_2 absorption efficiency (Table 6.11, entry 3 and Table 6.10, entry 1), the working capacity of BUMEA was increased by a factor of 2.1. The comparison between the performances of BUMEA and aqueous MEA gives some unexpected results, if we consider the different properties of the two absorbents. In particular, if we take into account the same mass of circulating liquid (0.108 and 0.107 kg h^{-1}), the two absorbents have the same CO_2 absorption efficiency (93.5%, Table 6.11, entries 3 and 6), and the same working capacity (1.56 and 1.57). Presumably, the lower viscosity of aqueous MEA compensates the lower flow rate of the neat amine compared to BUMEA. By reducing the absorbent flow rate below 0.100-0.120 dm^3 h^{-1}, the working capacity of neat BUMEA and aqueous MEA progressively increased but CO_2 capture efficiency were below the target value of 90%.

Notwithstanding the two absorbents displayed the same good performances in terms of rate of CO_2 uptake, absorption efficiency and working capacity, the absence of water in neat BUMEA is the key advantage over aqueous MEA. The energy required by the amine regeneration comprises the sensible heat to increase the absorbent temperature from the absorption to the desorption steps, the heat of vaporization of the absorbent and the heat to decompose the carbonated species, the opposite of the reaction (1) enthalpy. Even if the reaction enthalpy of neat BUMEA with CO_2 is not available, notwithstanding some qualitative considerations could be drawn. In spite of the presence of water, the ^{13}C NMR spectrum of carbonated MEA did not give any evidence of bicarbonate formation. Consequently, the reaction enthalpy of both BUMEA and MEA with CO_2 depends on the relative stability of their carbamates. As we could safely assume that BUMEA carbamate is not more stable of MEA carbamate, the energy required to decompose the two carbamates could be not substantially different to each other. As such, the possible energy saving of BUMEA must come from its lower sensible heat (about 40 % less, see experimental) because of the absence of water. Additionally, the vaporization heat of BUMEA is negligible, compared to water, by virtue of its high boiling temperature (198-200 °C). An experiment of water evaporation of aqueous MEA from the desorber (set at 105 °C) in the continuous cycle of absorption-desorption experiment gave a water loss of 80.4 g/mol CO_2 captured.

As a final remark, it should be pointed out that, as the combustion gases contain water, our solvent free alkanolamines were found to be tolerant towards moisture as the flux of

moisture saturated gas mixture lasted 36 h did not gave a detectable amount of HCO_3^-, as evidenced by ^{13}C NMR spectra of carbonated absorbents (Figure 6.3), neither gave loss of efficiency. The thermal stability of the neat alkanolamines was tested by their heating at 110 °C for 40 days: the ^{13}C NMR spectra revealed unidentified decomposition products in the range 1.5-5 % (on molar scale) for all the amines except MMEA where 11 % of by-products were detected.

6.5.   Conclusions

Unlike traditional aqueous amines, neat secondary amines capture CO_2 with high efficiency while avoiding great volumes of water and do not suffer of the dramatically increase of viscosity upon carbonatation of the ionic liquid-based absorbents. The potential advantages of the solvent-free over the aqueous alkanolamines are:

a) a reduced mass of the absorbent (water accounts for about 70% by weight of aqueous amines) that must be circulated at a lower rate; a reduced size of the equipment;

b) no energy is wasted to heat superfluous water in the desorption step;

c) negligible absorbent evaporation by virtue of the high boiling temperature at room pressure;

d) the relatively small difference between absorption and desorption temperatures;

e) the lower operational temperatures and the absence of a remarkable amount of water are expected to reduce the amine decomposition and the rate of equipment corrosion.

By considering their absorption efficiency, high boiling temperature, thermal stability and moisture tolerance, neat DPEA, DHEA, DOCA and BUMEA are the most attractive options and should be the most promising absorbents as possible substitutes for aqueous alkanolamines.

Finally, in the processes of CO_2 separation from non-acidic gases (H_2, CH_4, N_2, O_2), the selectivity is as important as the solubility. In this contest, our solvent-free absorbents displayed a high selectivity towards acidic gases, like CO_2, without featuring an appreciable physical adsorption, at least at room pressure.

In spite of the much greater viscosity of the solvent-free amine (in particular neat alkanolamines) compared to that of aqueous MEA, the rate of CO_2 absorption is substantially the same in the two absorbents.

6.6.   References

[1] M. Ramdin, T.W. de Loos, T.J.H. Vlugt, State-of-the-Art of CO2 Capture with Ionic Liquids. Ind. Eng. Chem. Res., 2012, 51, 8149-8177.

[2] L.M. Galán Sánchez, G.W. Meindersma, A B. de Haan. Solvent properties of functionalized ionic liquids for CO_2 absorption. Chem. Eng. Res. Des., 2007, 85, 31-39.

[3] E.D. Bates, R. D. Mayton, I. Ntai, J. H. Davis Jr. CO_2 capture by a task-specific ionic liquid. J. Am. Chem. Soc., 2002, 124, 926-927.

[4] D.J. Heldebrant, P.K. Koech, M.T.C. Ang, C. Liang, J. E. Rainbolt, C. R. Yonker, P. G. Jessop. Reversible zwitterionic liquids, the reaction of alkanol guanidines, alkanol amidines, and diamines with CO_2. Green Chem., 2010, 12, 713-721.

[5] C. Wang, X. Luo, H. Luo, D. Jiang, H. Li, S. Dai. Tuning the Basicity of Ionic Liquids for Equimolar CO_2 Capture. Angew. Chem., Int. Ed., 2011, 50, 4918-4922.

[6] C. Wang, H. Luo, X. Luo, H. Li, S. Dai. Equimolar CO_2 capture by imidazolium-based ionic liquids and superbase systems. Green Chem. 2010, 12, 2019-2023.

[7] V. Blasucci, R. Hart, V. Llopis-Mestre, D.J. Hahne, M. Burlager, H. Huttenhower, B.J.R. Thio, P. Pollet, C.L. Liotta, C.A. Eckert. Single component, reversibile ionic liquids for energy applications. Fuel, 2010, 89, 1315-1319.

[8] R. Hart, P. Pollet, D.J. Hahne, E. John, V. Llopis-Mestre, V. Blasucci, H. Huttenhower, W. Leitner, C.A. Eckert, C.L. Liotta. Benign coupling of reactions and separations with reversible ionic liquids. Tetrahedron, 2010, 66, 1082–1090.

[9] M.S. Shannon, J.M. Tedstone, S.P.O. Danielsen, M.S. Hindman, J.E. Bara. Properties and Performance of Ether-Functionalized Imidazoles as Physical Solvents for CO_2 Separations. Energy Fuels, 2013, 27, 3349-3357.

[10] X. Han, D.W. Armstrong. Ionic Liquids in Separations. Acc. Chem. Res., 2007, 40, 1079-1086.

[11] R.J. Hook. An investigation of some sterically hindered amines as potential carbon dioxide scrubbing compounds. Ind. Eng. Chem. Res., 1991, 36, 1779–1790.

[12] E. Breitmaier, W. Voelter, Carbon-13 NMR Spectroscopy, 3rd ed., 1990, VCH-Weinheim, Germany.

[13] J.R. Switzer, A.L. Ethier, K.M. Flack, E.J. Biddinger, L. Gelbaum, P. Pollet, C.A. Eckert, C.L. Liotta. Reversible Ionic Liquid Stabilized Carbamic Acids: A Pathway Toward Enhanced CO_2 Capture. Ind. Eng. Chem. Res., 2013, 52, 13159-13163.

[14] A. Danon, P.C. Stair, E. Weitz. FTIR Study of CO_2 Adsorption on Amine-Grafted SBA-15: Elucidation of Adsorbed Species. J. Phys. Chem. C, 2011, 115, 11540-11549.

[15] L. Raynal, P.A. Bouillon, A. Gomez, P. Broutin. From MEA to demixing solvents and future steps, a road map for lowering the cost of post-combustion carbon capture. Chem. Eng. Journal. 2011, 171(3), 742-752.

7. Biphasic Systems in the CO_2 Capture Processes

7.1. Introduction

In an effort to circumvent the high energy demand of conventional absorbents for CO_2 capture, biphasic systems have been considered as a viable alternative. In such technique, the absorbent solution, after the reaction with CO_2, separates into two phases (liquid/liquid or solid/liquid) that comprise the solvent and, separately, the carbonatated species. In this way it is possible to desorb the sole carbonatated phase, preventing the energy wasted by solvent heating. After its thermal regeneration, the absorbent is mixed again with the solvent to get back the starting absorbent solution. Exploiting this possibility, the CO_2 absorption was accomplished with Na_2CO_3 or K_2CO_3, solutions. Solid $NaHCO_3$ and $KHCO_3$, which separate out from the absorbed solutions, are decomposed at 200 and 250 °C, respectively, to regenerate the carbonates for their reuse. In a different series of experiments, the CO_2 capture was investigated in non-aqueous solutions of either AMP or PZ (2.0 M) in 2-ethoxyethanol (ethylene glycol monoethyl ether; EGMEE) and 2-(2-methoxyethoxy)ethanol (diethylene glycol monomethyl ether; DEGMME), respectively. After the solid carbamate of each amine was obtained, the resulting slurries were decomposed at 80–110 °C to regenerate the free amines for their reuse. Finally it was started a study concerning the use of liquid/liquid biphasic systems, with a solution of 2-(ethylamino)ethanol (EMEA) in bis(2-ethoxyethyl)ether (diethylene glycol diethyl ether, DEGDEE). The study is still under development, and the preliminary results are here reported.

7.2. General Experimental Information

7.2.1. Solid/Liquid Biphasic Systems

The absorber (Figure 7.1 A) was charged with 0.400 dm^3 of 2.0 mol dm^{-3} solution of Na_2CO_3 in a water/1,2-propanediol mixture 7:1 (v/v) or 2.0 mol dm^{-3} K_2CO_3 solution in an analogous solvent mixture 3:1 (v/v). The absorbent solution was kept at any designed temperature (40, 50 and 60 °C) by a thermostatted bath. To mimic the flue gas, a gas mixture containing 12 vol % CO_2 in air was continuously fed into the bottom of the absorber through a sintered glass diffuser with a flow rate of 14 $dm^3 h^{-1}$ (CO_2, 0.0689

mol h^{-1} at 24 °C). The cyclic absorption-filtration device (Figure 7.1 B) allowed the absorbed slurry and the filtered solution to circulate continuously in a closed loop between the absorber and the filtration unit. Any absorption experiment lasted 90 min, afterwards the solid $NaHCO_3$ and $KHCO_3$, which separated out from the respective solution, were decomposed at the appropriate temperature of 200 and 250 °C, respectively, until no more CO_2 was desorbed (60 min). The regenerated alkali metal carbonate was re-dissolved into the filtrate-saturated solution for its reuse in the absorption step. It was found that three complete absorption-desorption cycles are required to attain constant results; the results of these preliminary cycles were discarded. In the AMP and PZ experiments, the solid compounds quickly obstructed the sintered glass diffuser into the absorber, thus hindering further gas flux. Consequently, the absorption of CO_2 by either AMP or PZ was tested in a gas-liquid contactor column packed with glass rings. As this device did not allow to separate the solid from the saturated solution, the gas-liquid contactor column operated alternatively as the CO_2 absorber, set at 20–50 °C, and as the regeneration unit, set at 80–110 °C. The column was a home-built glass cylinder with an internal diameter of 56 mm and height of 400 mm, equipped with a jacket and packed with glass rings. The reactor was charged with 0.35 dm^3 of 2.0 mol dm^{-3} of either AMP or PZ solution in EGMEE and DEGMME, respectively.
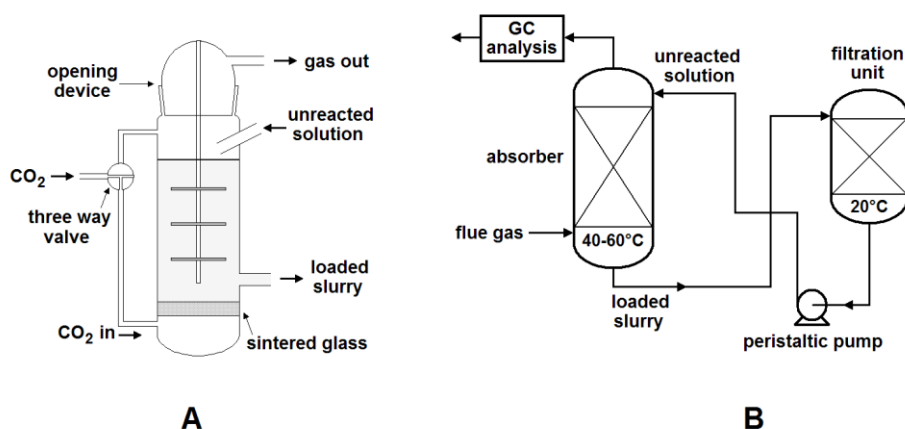

Figure 7.1. (A) Simplified sketch of the CO_2 gaseous solvent absorber; (B) simplified flow diagram of the absorber-filtration cyclic configuration.

The temperature of the internal contactor was maintained at the appropriate value by circulating a thermostatted liquid through the jacket. The gas mixture was continuously fed below the packed rings. The overhead vapor from the desorber was cooled by a water condenser and refluxed to the stripper. In this batch process, the reactor operated as the absorption device at 20–50 °C in the first stage and, after the absorption run lasting 90 min has been completed, as the stripper at 80–110 °C. The desorption-regeneration procedure was stopped after 60 min, when no more CO_2 was released.

7.2.2. Liquid/Liquid Biphasic Systems

The solution of EMEA in DEGDEE was at overall concentration 3.0 mol dm^{-3}.

The saturation of the solution with pure CO_2 was carried out at thermostatted 40 °C as described in Section 3.2.1. The closed cycle absorption-desorption apparatus (Figure 7.2) is quite similar to that previously described in Section 3.2.3, with the addition of a decanter right next the absorption column, to allow the separation of the two phases.
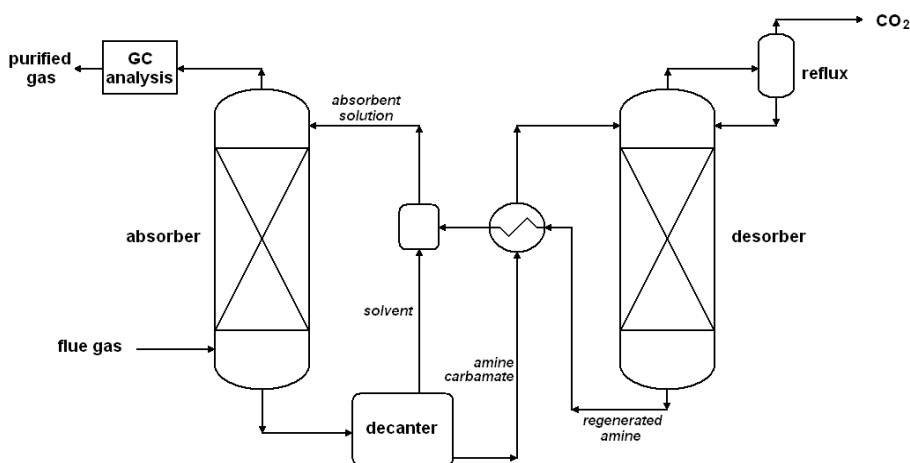
Figure 7.2. Simplified flow diagram of the absorber–desorber cyclic configuration.

In this way only the liquid carbonatated phase was sent to the desorber. After its thermal regeneration, the amine is mixed again with the solvent to get back the starting absorbent solution. The entire apparatus was charged with 0.300 dm^3 of the solution which has been circulated continuously between the absorber and the desorber at the rates of 0.100 and 0.300 dm^3 h^{-1}. To mimic the flue gas, we used 15% (v/v) CO_2 in air (overall pressure of the gas mixture set at 1.0 bar) which was water saturated before being injected into the absorber at a flow rate of 29.0 dm^3 h^{-1} (0.180 mol h^{-1} at 22 °C).

7.3. Solid/Liquid Systems: Results

7.3.1. CO$_2$ Captured as Alkali (Na$^+$, K$^+$) Bicarbonates in the Solid State

The main reaction in aqueous solution between CO$_2$ (K$_a$(20°C) = 4.08·10^{-7}) and CO$_3^{2-}$ ion (K$_b$ (20°C) = 2.1·10^{-4}) is [1] :

$$CO_2 + CO_3^{2-} + H_2O \rightleftharpoons 2HCO_3^- \quad Keq\ (20°C) = 8.6·10^3 \qquad (1)$$
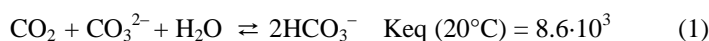
To overcome the solubility of NaHCO$_3$ (9.6 g/100 g at 20 °C; 16.5 g/100 g at 60 °C) and KHCO$_3$ (33.7 g/100 g at 20 °C; 60.0 g/ 100 g at 60 °C) in water, the CO$_2$ capture experiments aiming at obtaining alkali bicarbonates in the solid state were carried out with a 2.0 mol dm^{-3} solution of Na$_2$CO$_3$ in a water/1,2-propanediol mixture 7:1 (v/v) or 2.0 mol dm^{-3} K$_2$CO$_3$ solution in an analogous solvent mixture 3:1 (v/v). Reaction (1) exhibits a favourable equilibrium to the formation of bicarbonate when comparable amounts of CO$_2$ and CO$_3^{2-}$ are reacted. However, the rate of CO$_2$ absorption by carbonate is slow compared with the similar reaction involving NH$_3$ or amines. Each experiment was at least repeated in triplicate showing high reproducibility of the results, after the precipitation regeneration-dissolution process had reached the steady state. The results of typical absorption processes are reported in Table 7.1 and highlighted in Figure 7.3; they indicate that the average CO$_2$ capture efficiency is significantly affected by the absorption temperature, as expected. As a matter of fact, even if the CO$_2$ solubility decreases and the reaction equilibrium of reaction (1) is disfavoured as the temperature increases, the increasing rate of reaction (1) at higher temperature allows more CO$_2$ to react.

Table 7.1. CO$_2$ absorption efficiency of 2.0 M solution of alkali carbonate (Na$_2$CO$_3$ or K$_2$CO$_3$). Absorption and desorption times fixed at 90 and 60 min, respectively.

	T$_{abs}$ (°C)	T$_{des}$ (°C)	Absorption %			
			Step 1	Step 2	Step 3	Aver.[a]
	40	200	85.4	83.5	85.5	84.8
Na$_2$CO$_3$	50	200	88.4	90.5	90.1	89.7
	60	200	81.7	79.9	77.9	79.8
+ 5% PZ [b]	50	200	94.0	93.4	93.7	93.7
+ 5% AMP [c]	50	200	82.1	78.4	78.8	79.8
	40	250	86.5	87.8	88.5	87.6
K$_2$CO$_3$	50	250	88.2	87.4	88.6	88.1
	60	250	79.0	80.9	77.8	79.2

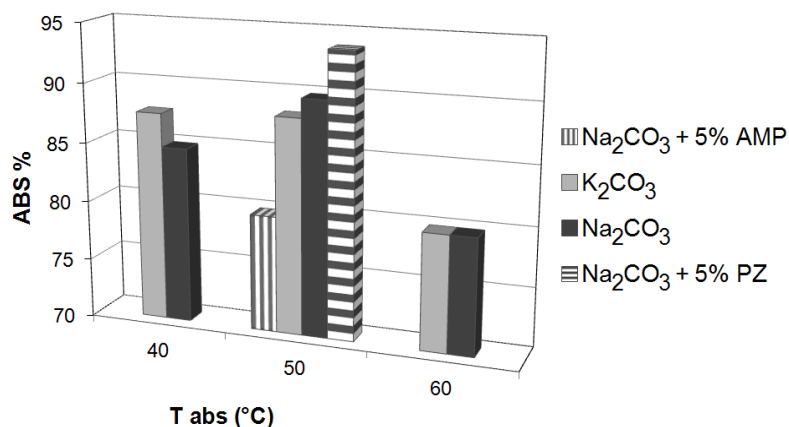[a] Average values; [b] PZ added, molar scale; [c] AMP added, molar scale.

Figure 7.3. CO$_2$ absorption efficiency of 2.0 M sodium and potassium carbonates as a function of the absorption temperatures and reaction promoters. Desorption temperatures are fixed at 200°C (Na$_2$CO$_3$) and 250°C (K$_2$CO$_3$).

Interestingly, replacing Na$_2$CO$_3$ for K$_2$CO$_3$ shows a slight but significant efficiency increase from 88.1 to 89.7 %. This result represents an appreciable advantage in terms of cost saving, in view of the half organic solvent used and lower cost of Na$_2$CO$_3$ with respect to K$_2$CO$_3$. The use of cheap Na$_2$CO$_3$ could compensate, at least in part, the major initial capital investment due to 1,2-propanediol which is anyway completely recycled.

Addition of PZ to an aqueous solution of K$_2$CO$_3$ was reported to considerably increase the CO$_2$ absorption efficiency [2-4]. Thus, a series of absorption-desorption experiments with a 2.0 M Na$_2$CO$_3$ solution in the presence of 5.0% (on molar scale) PZ was carried out. In the 50–200 °C cycle, the absorption efficiency of such mixed solution increased from 89.7% for single Na$_2$CO$_3$ to 93.7% (Table 7.1 and Figure 7.3). Trying to shed light on the role of PZ in enhancing the CO$_2$ absorption by Na$_2$CO$_3$, both CO$_2$-rich and regenerated solutions were monitored by ^{13}C NMR spectroscopy. Beside the high-intensity peaks due to 1,2-propanediol, the ^{13}C NMR spectra showed an intense peak at 164.4–165.1 ppm due to the fast equilibrating HCO$_3^-$/CO$_3^{2-}$ pair and peaks of mono-carbonated PZ at 162.86 (PZ-CO$_2^-$), 43.97 (CH$_2$ of PZ/PZH$^+$), 43.63 [NH(CH$_2$)$_2$(CH$_2$)$_2$NCO$_2^-$], and 42.70 ppm [NH(CH$_2$)$_2$(CH$_2$)$_2$NCO$_2^-$]. The chemical shifts were practically unchanged in both absorbed and regenerated solutions. Noticeably, there was no peak attributable to the bis-carbamate of PZ.

To verify whether the formation of the amine carbamate is compulsory to increase the efficiency of the mixed Na$_2$CO$_3$-PZ solution with respect to the pure carbonate solution, some CO$_2$ capture experiments were run with Na$_2$CO$_3$ solution also containing 5.0% (on

molar scale) of AMP that does not form carbamate in aqueous solution due to steric constraints [5]. In these experiments, the efficiency of CO_2 absorption decreased from 89.7 to 79.8 %.

7.3.2. CO_2 Captured as AMP and PZ Carbamates in the Solid State

The absorption of CO_2 (12 vol% in air) by either AMP or PZ in EGMEE and DEGMME, respectively, at 20–50 °C, produced solid compounds. . After the precipitation of the amine carbamate was completed (90 min), the column was heated to 80–110 °C to regenerate the free amine and to desorb pure CO_2. Nearly complete CO_2 desorption occurred in 60 min at the highest temperature investigated. The best results are reported in Table 7.2.
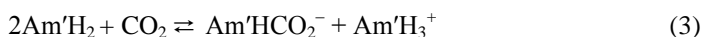
Even if close comparisons between the two amines cannot be carried out due to the different absorption and desorption temperatures, the performances of 2.0 mol dm^{-3} PZ appear to be superior to those of equimolar AMP. In the absence of water, CO_2 reacts with excess AMP forming the otherwise unstable carbamate in the solid state (reaction 2; AmH denotes the secondary amine AMP):

$$2AmH + CO_2 \rightleftarrows AmCO_2^- + AmH_2^+ \qquad (2)$$

Table 7.2. CO_2 absorption efficiency of 2.0 M solutions of either AMP or PZ. Absorption and desorption times fixed at 90 and 60 min, respectively..

	T_{abs} (°C)	T_{des} (°C)	Absorption %			
			Step 1	Step 2	Step 3	Average values
AMP	20	80	88.0	88.9	88.6	88.5
PZ	50	110	95.1	94.9	95.1	95.0

The cyclic diamine PZ can produce the mono carbamate derivative (reaction 3, Am'H$_2$ denotes PZ) and, albeit at a lower extent, the bis-carbamate derivative (reaction 4):

$$2Am'H_2 + CO_2 \rightleftarrows Am'HCO_2^- + Am'H_3^+ \qquad (3)$$

$$Am'HCO_2^- + CO_2 + Am'H_2 \rightleftarrows Am'(CO_2)_2^{2-} + Am'H_3^+ \qquad (4)$$

The ^{13}C NMR spectra of both carbonated and regenerated AMP solutions, besides the intense signals due to EGMEE (singlets at 72.30; 67.00; 61.36, and 15.51 ppm), display resonances in the range of 69.18–71.12 (CH_2–OH), 52.44–52.94 (C–NH$_2$), and 25.11–25.60 ppm (CH_3) readily assigned to the carbon atoms of both protonated and free AMP that are rapidly exchanging on the NMR scale. The corresponding resonances of the

106

AMP carbamate are at 71.73, 52.96, and 20.98 ppm while a weaker resonance at 164.23 ppm identifies the carbamate carbonyl AMP-CO_2^-. The crystalline compound that separates from the solution has been authenticated as the carbamate derivative [(AMPH$^+$)(AMP-CO$_2^-$)] on the basis of its solid state ^{13}C NMR spectrum [6].

The ^{13}C NMR spectra of carbonated PZ solutions, apart for the intense signals due to DEGMME, show four –CH_2– resonances assigned to the mono- (44.6 and 45.5 ppm) and bis-carbamate of PZ (45.0 ppm) as well as to the free PZ fast equilibrating with the protonated species (45.1 ppm). Quite similar resonances in the range of 44.9–45.7 ppm have been ascribed to the regenerated solutions. Furthermore, a couple of low-field resonances identifies the carbamate carbonyl of mono-(PZ-CO_2^- 163.35 ppm) and bis-carbamate of piperazine (PZ-$(CO_2)_2^{2-}$ 163.54 ppm).

The greater efficiency of PZ compared to AMP as CO_2 absorbent (Table 7.2) can be justified with the presence of two amine functionalities that allow a greater theoretical absorption capacity (molar ratio 3:2; reaction (3) and (4)) as compared to AMP (molar ratio 2:1; reaction 2). Moreover, the PZ carbamate is more stable than the AMP carbamate. This is roughly indicated by the substantially greater regeneration temperature of carbonated PZ (110 °C) compared to carbonated AMP (80 °C). As a matter of fact, the desorption reactions are the opposite of those of carbamate formation (reactions 2–4). With the objective of reducing as much as possible the difference between absorption and desorption temperatures, the absorption temperature of PZ solution has been increased up to 50 °C without any significant reduction of efficiency (Table 7.2). When comparing AMP and PZ performances, it is worth stressing that the lower CO_2 capture efficiency and capacity of AMP could be compensated by the lower regeneration temperature. Additionally, it can be noticed that the much lower regeneration temperature of both AMP and PZ carbamates (80–110 °C) compared to NaHCO$_3$ and KHCO$_3$ (200–250 °C) could compensate the energy wasted to heat EGMEE and DEGMME which, however, have heat capacities and evaporation enthalpies lower than water.

7.4. Liquid/Liquid Systems: Preliminary Results

As previously reported in Section 6.4, 2-(ethylamino)ethanol (EMEA) reversibly react with CO_2 to give carbonated species in the liquid phase notwithstanding the absence of

any dilution with an added solvent. A solution of EMEA in diethylene glycol diethyl ether (DEGDEE) separates into two liquid phases after the reaction with CO_2.

To measure the experimental loading capacity of EMEA in DGDEE, pure CO_2 was flowed through 0.100 dm^3 of the solution maintained at 40 °C until no more CO_2 was absorbed. The loading capacity measured by gravimetry is 0.52.

In order to check whether the EMEA-DGDEE system was capable of successfully working in a continuous absorption-desorption cycle (Section 7.2.2), the absorbent was continuously circulating in a closed cycle between the absorber (set at 40 °C) and the desorber (set at 110 °C). The gas mixture of 15% (v/v) CO_2 in air (overall gas pressure set at 1.0 bar) was continuously feeding into the base of the absorber where comes in contact with the liquid getting down off the top. The gas flow rate was 29.0 dm^3 h^{-1} The entire apparatus was charged with 0.300 dm^3 of solution. In order to verify how the absorption efficiency depends on the circulation rate of the absorbent, the experiments were carried out at increasing liquid flow rate (0.100–0.300 dm^3 h^{-1}). Each experiment was stopped when the reactions of CO_2 capture and amine regeneration reached the steady state and the absorption efficiency did not change with time. A summary of the operating conditions is reported in Table 7.3 while the results of the experiments with the different liquid flow rate are reported in Table 7.4.

Table 7.3. Operating conditions employed in the absorption-desorption AMP-blended experiments.

Solution volume	0.300 dm^3
Amine concentration	3.05 mol dm^{-3}; 29.9 wt%
Absorption temperature	40 °C
Desorption temperature / pressure	110 °C / 1 bar
Liquid flow rate	0.300 – 0.100 dm^3 h^{-1}
Gas flow rate and composition	29 dm^3 h^{-1}; CO_2 15% (v/v) in air

Table 7.4. CO_2 absorption efficiency at decreasing liquid flow rate.

Entry	Liquid Flow Rate (dm^3 h^{-1})	Absorption efficiency %
1	0,300	97,6%
2	0,240	82,6%
3	0,200	74,5%
4	0,140	60,7%
5	0,100	< 50%

108

As expected, increasing the liquid flow rate enhances the absorption efficiency (percentage of CO_2 absorbed/CO_2 flowed).

These preliminary results are very promising, particularly when compared with the experiments reported in the previous chapters with the same gas flow rate. Further experiments will be carried out with different solutions of other amines.

7.5. Conclusions

The CO_2 capture in a biphasic system combines the advantages of wet absorption with desorption in the absence of water or of any liquid at all. In particular, the performance of 2.0M Na_2CO_3 activated by 5.0% (on molar scale) PZ combines high efficiency of 93.7% at 50 °C with a nearly complete decomposition of solid $NaHCO_3$ at 200 °C. Obviously, the alkaly carbonates are quite stable species and avoid the environmental problems associated with the amine degradation and the dangerous admission of the degradation products in the environment [7-11]. The CO_2 capture by either AMP or PZ in organic solvents as amine carbamates in the solid state takes advantage from the relatively low temperatures (80–110 °C) of regeneration step and from the reduced evaporation and sensible heat of EGMEE and DEGMME with respect to aqueous absorbents [12-14]. It should be noticed that strictly anhydrous conditions are not necessary as the system is tolerant to small amounts of water which do not affect the results obtained under strictly anhydrous conditions.

Finally, the good preliminary results obtained in a continuous cycle of absorption/desorption with liquid/liquid biphasic systems stimulate for future developments of this technique.

7.6. References

[1] W.H. Austin. CO_2 solubility, pK' and related factors in acid-base balance. NBS Special Publication (USA) 1977, 450, 143–151.
[2] Carbon Dioxide Capture by Absorption with Potassium Carbonate, U.S. Department of Energy, Pittsburgh, PA 2010.
[3] J.T. Cullinane, G.T. Rochelle. Kinetics of Carbon Dioxide Absorption into Aqueous Potassium Carbonate and Piperazine. Ind. Eng. Chem. Res. 2006, 45, 2531–2545.
[4 A.L. Shier, P.V. Danckwerts. Carbon Dioxide Absorption into Amine-Promoted Potash Solutions. Ind. Eng. Chem. Fundam., 1969, 8, 415–423.
[5] G. Sartori, D.W Savage. Sterically hindered amines for CO_2 removal from gases. Ind. Eng. Chem. Fundam. 1983, 22, 239-249.

[6] F. Barzagli, F. Mani, M. Peruzzini. Efficient CO_2 absorption and low temperature desorption with non-aqueous solvents based on 2-amino-2-methyl-1-propanol (AMP). Int. J. Greenh. Gas Control, 2013, 16, 217–223.

[7] G.S. Goff, G.T. Rochelle. Oxidation Inhibitors for Copper and Iron Catalyzed Degradation of Monoethanolamine in CO_2 Capture Processes. Ind. Eng. Chem. Res., 2006, 45, 2513 –2521.

[8] M. Karl, R.F. Wright, T.F. Bergien, B. Denby. Worst case scenario study to assess the environmental impact of amine emissions from a CO_2 capture plant. Int. J. Greenh. Gas Control, 2011, 5, 439-447.

[9] B.R. Strazisar, R.R. Anderson, C. White. Degradation Pathways for Monoethanolamine in a CO_2 Capture Facility. Energy Fuels, 2003, 17, 1034-1039.

[10] T. Supap, R. Idem, P. Tontiwachwuthikul, C. Saiwan. Analysis of Monoethanolamine and Its Oxidative Degradation Products during CO_2 Absorption from Flue Gases: A Comparative Study of GC-MS, HPLC-RID, and CE-DAD Analytical Techniques and Possible Optimum Combinations. Ind. Eng. Chem. Res, 2006, 45, 2437-2451.

[11] K. Veltman, B. Sing, E. G. Hertwich. Human and Environmental Impact Assessment of Postcombustion CO_2 Capture Focusing on Emissions from Amine-Based Scrubbing Solvents to Air. Environ. Sci. Technol., 2010, 44, 1496–1502.

[12] B.A. Oyenekan, G.T. Rochelle. Energy performance of stripper configurations for CO_2 capture by aqueous amines. Ind. Eng. Chem. Res., 2006, 45, 2457-2464.

[13] N. McCann, M. Maeder, M. Attalla. Simulation of Enthalpy and Capacity of CO_2 Absorption by Aqueous Amine Systems. Ind. Eng. Chem. Res. 2008, 47, 2002–2009.

[14] J. Oexmann, A. Kather, S. Linnenberg, U. Liebenthal. Post-combustion CO_2 capture: chemical absorption processes in coal-fired steam power plants. Greenhouse Gases: Sci. Technol. 2 (2012) 80–98.

8. CO$_2$ Capture and Utilization: Production of Urea and 1,3-Disubstituted Ureas

8.1. Introduction

As an alternative to traditional processes of CO$_2$ capture and sorbent regeneration, in our laboratory has been developed a new concept of CO$_2$ capture technology which combines the CO$_2$ abatement with the production of commercially valuable products [1,2]. Turning carbon dioxide into useful chemicals in relatively mild conditions would indeed circumvent most of the drawbacks of the energy consuming steps of CO$_2$ desorption, absorbent regeneration as well as of CO$_2$ transporting and ultimate disposal.

As reported in a previous experimental study [3], the carbon dioxide capture with ammonia in both aqueous and non-aqueous solutions was fast and efficient and produced solid mixtures of ammonium carbamate, bicarbonate and carbonate in different molar ratio depending on the experimental conditions. In non-aqueous solvents pure ammonium carbamate was recovered in the solid state that was subsequently converted into urea (50% yield, average) at 120–140 °C in the presence of copper(II) promoters. This process avoid the serious hurdles due to the ammonia loss and to the costs of NH$_3$ separation from concentrated CO$_2$ in the regeneration step, but it was unsuitable for a commercial application, due to the anhydrous conditions, low rate of conversion (two-three day heating) and to the unavoidable separation of the reaction mixtures from the catalyst which must be recovered and reused.

By going on with these studies, in this chapter are reported the results focused on the fast urea production (average yield, 48%) by heating to 165 °C for 60-90 min mixtures of ammonium carbamate and bicarbonate, obtained from CO$_2$ capture with ammonia. Besides the advantage of an efficient CO$_2$ capture, this unconventional process could circumvent the high energy costs of the commercial processes of urea production carried out with an excess of ammonia (NH$_3$/CO$_2$ molar ratio up to 4) at high temperature (180-240 °C) and pressure (150-250 bar).

An analogous concept has been used for the CO$_2$ uptake by the non-aqueous solutions of some amines as solid carbamates and for their thermal conversion into the corresponding substituted 1,3-disubstituted ureas. The selected absorbents are solution of 1-aminobutane (*n*-butylamine NBA), 1-amino-2-methylpropane (isobutylamine IBA), 2-

amino-2-methylpropane (*tert*-butylamine TBA), aminocyclohexane (cyclohexylamine, CHA) in bis(2-ethoxyethyl)ether (diethylene glycol diethyl ether, DEGDEE), 1,4-diazacyclohexane (piperazine, PZ) in 2-ethoxyetanol (ethylene glycol monoethyl ether, EGMEE) and 1-aminooctane (*n*-octylamine, NOA) in 3-pentanone (diethyl ketone, DEK).

The 1,3-disubstituted ureas are valuable products with a wide range of application as intermediates in agrochemical, pharmaceutical, dye chemicals and recently as precursors of isocyanates and raw materials of polyurethanes [4-8]. Their traditional synthesis required unsafe chemicals such as phosgene or carbon oxide and Au or Pt catalysts [9-12]. In recent years the direct synthesis of substituted ureas has been accomplished with the non toxic and cheap carbon dioxide in the presence of different catalysts and dehydrating agents to increase the yield of reaction [13-16]. Ionic liquids in conjunction with a base (CsOH) or transition metal (Fe, Co, Ni, Cu, Zn) acetates were also employed as reaction medium and catalysts to obtain 1,3-disubstituted ureas in good yield [17-20]. However, most catalysts can be reused no more than 3-4 times.

The unconventional technology devised in this study combine the efficient CO_2 uptake from anthropogenic activities with the thermal conversion of the amine carbamates obtained in the solid state into substituted 1,3-disubstituted ureas without any catalyst, dehydrating agent or external pressure, yet with acceptable yields.

8.2.   General Experimental Information

The cyclic absorption–filtration device consisted of the absorber and the filtration units that are connected to each other by means of a peristaltic pump that allows the absorbent slurry and the filtered solution to circulate continuously in a closed loop between the absorber and the filtration unit (Figures 8.1). The temperature of the absorbent solution was kept constant by a thermostatted water bath. The NH_3 absorbent solution was made by mixing $20 \cdot 10^{-3}$ dm^3 of 15.2 mol dm^{-3} aqueous NH_3 with $270 \cdot 10^{-3}$ dm^3 of ethanol. Both CO_2 (12% v/v in air) and NH_3 were simultaneously and continuously introduced at the bottom of the absorbent solution through two separate gas diffuser (Figure 8.2 A). The CO_2/NH_3 flow ratio was 1/1.5 v/v with a flow rate of 14 $dm^3 h^{-1}$.
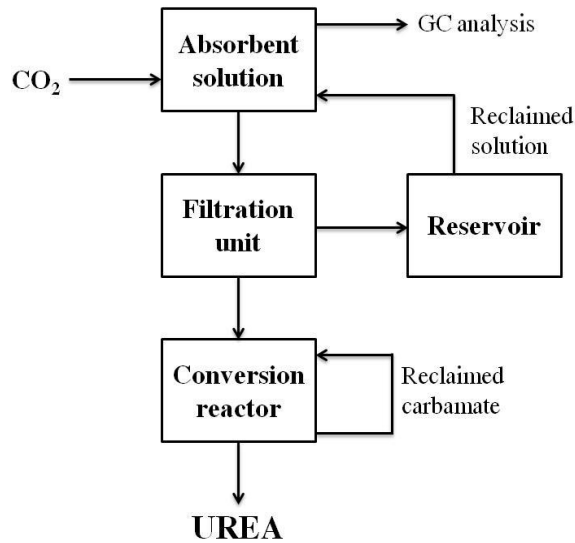
Figure 8.1. Simplified flow diagram of the cyclic process configuration. Gaseous ammonia was used in conjunction with CO_2 absorption by water-ethanol NH_3.

The outlet gas from the top of the absorber was dried by flowing in turn through a condenser cooled at -5 °C, a concentrated H_2SO_4 solution and a gas purification tower filled with P_2O_5, before being analysed with a gas chromatograph which measured the percentage of the CO_2 absorbed at intervals of 10 minutes. At the end of the experiment fixed at eight hours, the solid collected by filtration was washed with CO_2 saturated ethanol and diethyl ether in turn before being dried at room temperature in a stream of pure CO_2 to avoid the decomposition of both ammonium carbamate and bicarbonate.
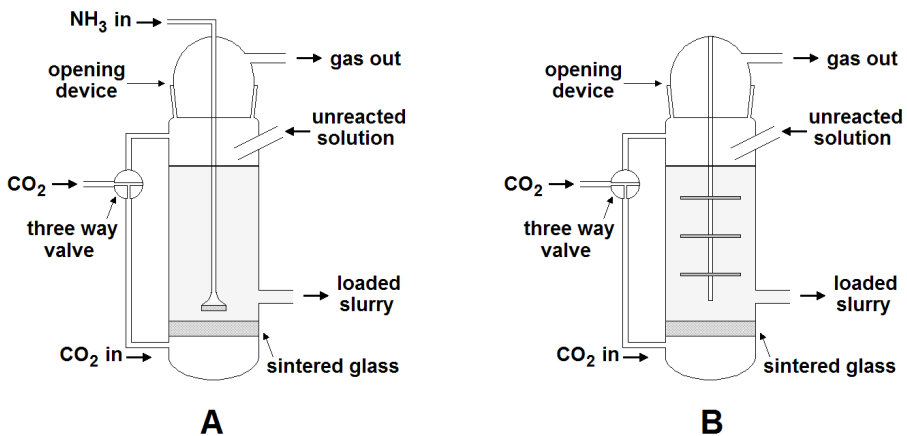

Figure 8.2. Simplified sketch of the absorbers used.

Analogous equipment (Figure 8.1 and 8.2 B) and procedure were used to capture CO_2 by non aqueous amines and to collect the corresponding solid amine carbamates. The absorber device was charged with 0.300 dm^3 of 3.0 mol dm^{-3} solutions of the different amines in bis(2-ethoxyethyl)ether (NBA, IBA, TBA), in 2-ethoxyetanol (PZ), or in 3-pentanone (NOA). The temperature of the absorbent solution was kept constant at 20 °C by a thermostatted water bath. The gas mixture containing 15% (v/v) CO_2 in air was continuously fed into the bottom of the absorber with a flow rate of 14 dm^3 h^{-1}. The outlet gas, exited from the top of the absorber, was analyzed by the gas chromatograph. A complete experiment lasted 150-660 min and it was stopped when the CO_2 absorption efficiency at the end of the experiment was reduced to about 50% (average absorption efficiency in the range 91-97%). The solid was collected by filtration unit, washed with a 1/1 mixture of ethanol and diethyl ether and pure diethyl ether in turn before being dried at room temperature in a stream of N_2.

The batch experiments aimed at measuring the loading capacities of the different amine solutions were carried out as described in Section 3.2.1.

The conversion of ammonium salts into urea was carried out in a stainless steel reactor (PARR MOD. 4791) with a volume of 0.025 dm^3 equipped with a thermocouple and pressure gauge (Figure 8.3). The reactor was heated to the appropriate temperature (165 °C) by means of a silicone oil heating bath (IKA HB4). In each experiment, the reactor

Figure 8.3. PARR reactor used for the conversion of ammonium and amine carbamate into ureas.

is charged with 12.0 g of the mixture of ammonium carbamate and bicarbonate in slightly different ratio (65-75% of carbamate, in molar ratio). For comparison purposes, blank experiments were carried with pure ammonium bicarbonate. Each conversion experiment comprised six separate heating times, 30, 45, 60, 75, 90, 105 min, aimed at measuring the urea yield as a function of heating time. After each heating time was completed, the reactor was water cooled to room temperature and a sample of the mixture, recovered from the vessel, was dissolved in D_2O and analysed by ^{13}C NMR spectroscopy.

Each experiment was repeated ten times showing a sufficient reproducibility of the results with changes in the percentage of each species never higher than 4 units.

The conversion of amine carbamate salts into the corresponding 1,3-disubstituted ureas was carried out in the same PARR reactor by heating 10.0-14.0 g of the salt to 150 °C. In some experiments, the amine carbamate and protonated amine ion pairs were mixed with 1% (molar scale) of either CuCl or $CuCl_2 \cdot 2H_2O$. The reaction mixtures were analysed by ^{13}C NMR technique in either D_2O or $CDCl_3$ as described in Section 3.3. The integration of the signals due to HCO_3^-/CO_3^{2-} (δ = 160.22-163.73 ppm), $-NHCO_2^-$ (δ = 163.83-164.30 ppm), $(NH_2)_2CO$ (δ = 161.92-163.26 ppm), $-CH_2-$ (δ = 19.08–49.06 ppm), CH_3- (δ = 13.31–19.88 ppm) and $>C=O$ (1,3-disubstituted ureas, δ = 158.83–159.27 ppm), allowed us to quantify the molar ratio of the different species. Despite some unavoidable uncertainty in comparing the different integrals, the method provides an estimation of the relative percentage of the different species (estimated error 5%).

The Cu(I) and Cu(II) catalysts employed in some amine carbamate dehydration increased the spin-lattice T_1 relaxation time of the carbon atoms of the amine carbamate and of protonated amine with respect to the corresponding carbon atoms of 1,3-didisubstituted ureas and, consequently, the integrated signals of the carbon atoms of the two species cannot be used to quantify their relative amount. To avoid this unwanted effect on ^{13}C NMR analysis, after the dehydration experiments were completed, the copper catalyst was precipitated with Na_2S and the reaction mixtures were separated from CuS by extraction either with $CDCl_3$ or D_2O and the solutions analysed by ^{13}C NMR spectroscopy.

8.3.   From NH_3 to Urea

The urea manufacture at industrial scale is carried out with an excess of ammonia and pure carbon dioxide at 180-240 °C and 150-250 bar. Pure CO_2 is obtained by the conventional process of aqueous amine scrubbing and thermal stripping, in turn. In the commercial plants, the yield of the reaction is in the order 30-55 % on NH_3 basis (60-70 % on CO_2 basis) and strongly depends on reaction temperature, pressure, time and NH_3/CO_2 ratio.
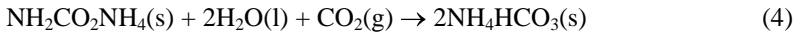
The urea synthesis from gaseous CO_2 and NH_3 involves the intermediate formation of ammonium carbamate

$$2NH_3 + CO_2 \rightarrow NH_2CO_2NH_4 \qquad\qquad (1)$$

that is successively dehydrated to form urea

$$NH_2CO_2NH_4 \rightarrow (NH_2)_2CO + H_2O \qquad\qquad (2)$$
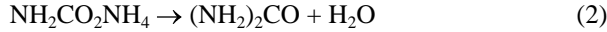
While reaction (1) is fast and exothermic ($\Delta H° = -151$ kJ mol^{-1}), reaction (2) is slow and endothermic ($\Delta H° = 32$ kJ mol^{-1}) [21-22] and even if the latter should be substantially right hand shifted at high temperature, it does not go to the completion due to the low reaction rate. Moreover, the reaction (2) is an oversimplification of the several equilibria occurring at high temperature and pressure. For example, the carbamate could be hydrolysed by the water produced in the reaction (2) (reactions 3 and 4).

$$NH_2CO_2NH_4(s) + H_2O(l) \rightarrow NH_4HCO_3(s) + NH_3(g) \qquad\qquad (3)$$

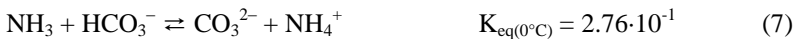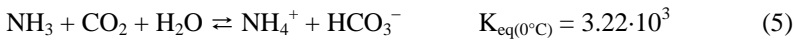$$NH_2CO_2NH_4(s) + 2H_2O(l) + CO_2(g) \rightarrow 2NH_4HCO_3(s) \qquad\qquad (4)$$

Therefore, the final yield of urea is the result of the competition between the conversion reactions of carbamate into urea and its decomposition reactions, mainly, to bicarbonate. In this study, the urea synthesis was accomplished in two separate steps:
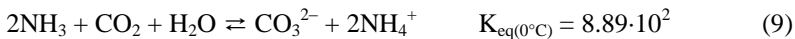
1) the CO_2 capture by NH_3 in aqueous-ethanol at room pressure aimed at obtaining solid mixtures of ammonium carbamate and bicarbonate;

2) the thermal dehydration of the solid ammonium salts into urea.

Due to the low solubility of both ammonium carbamate and bicarbonate in ethanol, the CO_2 capture experiments were carried out in ethanol–water ammonia solutions (see experimental).
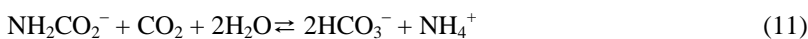
The equilibria which describe the reaction of CO_2 with aqueous NH_3 are [23]:

$$NH_3 + CO_2 + H_2O \rightleftharpoons NH_4^+ + HCO_3^- \qquad K_{eq(0°C)} = 3.22 \cdot 10^3 \qquad (5)$$

$$NH_3 + HCO_3^- \rightleftharpoons NH_2CO_2^- + H_2O \qquad K_{eq(0°C)} = 7.30 \qquad (6)$$

$$NH_3 + HCO_3^- \rightleftharpoons CO_3^{2-} + NH_4^+ \qquad K_{eq(0°C)} = 2.76 \cdot 10^{-1} \qquad (7)$$

If an excess of NH_3 is maintained in the system, the overall reactions can be rewritten as

$$2NH_3 + CO_2 \rightleftharpoons NH_2CO_2^- + NH_4^+ \qquad K_{eq(0°C)} = 2.35 \cdot 10^4 \qquad (8)$$

$$2NH_3 + CO_2 + H_2O \rightleftharpoons CO_3^{2-} + 2NH_4^+ \qquad K_{eq(0°C)} = 8.89 \cdot 10^2 \qquad (9)$$

The concentration of both $NH_2CO_2^-$ and CO_3^{2-} decreases by increasing CO_2 absorption; meanwhile, a simultaneous increase of bicarbonate occurs according to the equilibria (10) and (11)

$$CO_3^{2-} + CO_2 + H_2O \rightleftharpoons 2HCO_3^- \qquad\qquad (10)$$

$$NH_2CO_2^- + CO_2 + 2H_2O \rightleftharpoons 2HCO_3^- + NH_4^+ \qquad\qquad (11)$$

116

On the contrary, a greater ammonia concentration increases the efficiency of CO_2 removal and the formation of ammonium carbamate, but lowers the loading capacity and increases the loss of NH_3 from the scrubbing solution.

The solids recovered at the end of the absorption experiments were different mixtures of NH_4HCO_3 and $NH_2CO_2NH_4$. In order to estimate the composition of the solid obtained after the absorption process, ^{13}CNMR spectra were recorded in D_2O and compared with those of standard solutions of NH_4HCO_3 and $NH_2CO_2NH_4$ in the same solvent [23]. The accurate integration of the signals of the carbon atoms of carbamate ($\delta = 163.83$-164.30 ppm) and of the fast exchanging carbonate and bicarbonate ions ($\delta = 160.22$-163.73 ppm) gave a mixture composition comprised between 67 % and 73 % (on molar scale) of ammonium carbamate.

The conversion of ammonium bicarbonate into urea (reaction 12) is less efficient than that of the ammonium carbamate (reaction 2), having a theoretical 50% limit

$$2NH_4HCO_3 \rightarrow (NH_2)_2CO + CO_2 + 3H_2O \qquad (12)$$
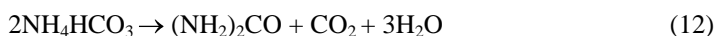
Consequently, the starting ammonium carbamate-bicarbonate mixture must contain at least 50% of carbamate to produce significant yields of urea.

The conversion of ammonium carbamate-bicarbonate mixtures (12 g, 66.6-72.9% carbamate, on molar scale) has been performed in a pressure stainless steel reactor heated to 165 °C for times ranging from 30 to 105 minutes. At the end of each experiment the ^{13}C NMR analysis in D_2O (urea carbon, $\delta = 161.92$-163.26 ppm) allowed us to identify and quantify the composition of the mixtures. Each experiment was repeated ten times. The average results of the experiments are reported in Table 8.1 and summarized in Figure 8.4.

Table 8.1. Average yields of the conversion of ammonium carbamate/ bicarbonate mixtures into urea as a function of heating time.

time (min)	P max (bar)	Reagents (%) [a]		Products (%) [b]		
		HCO_3^-	$NH_2CO_2^-$	Urea	HCO_3^-	$NH_2CO_2^-$
30	38	33.4	66.6	13.5	31.3	55.2
45	34	27.1	72.9	36.2	11.0	52.8
60	35	28.8	71.2	46.6	6.9	46.5
75	36	29.9	70.1	48.0	6.7	45.3
90	33	30.6	69.4	48.7	6.0	45.3
105	38	28.0	72.0	46.2	10.4	46.2

[a] percentage (molar scale) in the reagent mixtures; [b] average values (percentage, molar scale) in the urea mixtures.

After 90 min heating to 165 °C, the average yield of urea was 48.7% (percentage in mol) respect to the amount of carbamate and bicarbonate mixture (maximum yield 52%). The pressure generated *in situ* by the mixture decomposition and by the excess of CO_2 was at most 38 bar at 165 °C. The comparative analysis based on ^{13}C NMR spectra has shown that more than 80% of the bicarbonate contained in the reacting mixture was converted into urea and into carbamate (reactions 12 and 13).

$$2NH_4HCO_3 \rightarrow NH_2CO_2NH_4 + CO_2 + 2H_2O \qquad (13)$$

Because of the contribution of the reactions (12) and (13), there is not a clear relationship between the urea yield and what's more the composition of the starting reactants that comprised no less than 70 % of carbamate (on molar scale) in most experiments.
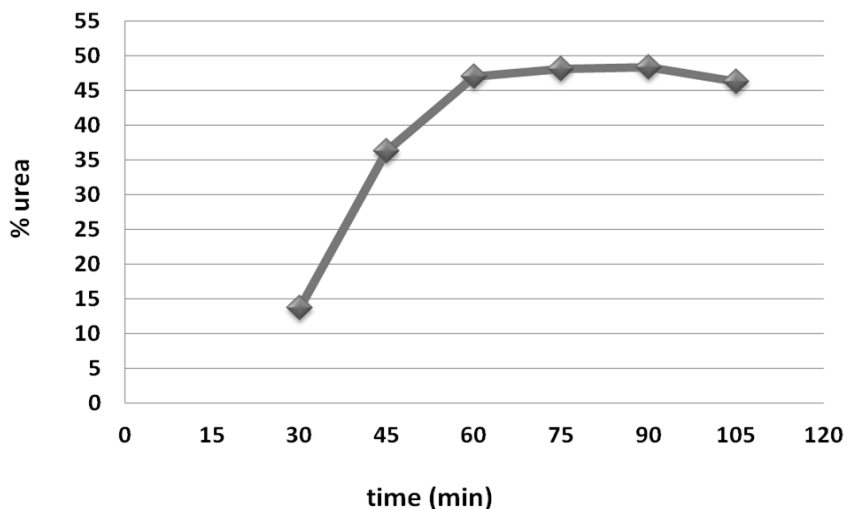

Figure 8.4. Percentage of urea formation as a function of heating time (T=165°C).

As the kinetic constraints overcame the equilibrium requirements, the yield of urea increased with heating time and temperature. At this respect, it is worth of noting that the conversion shows an initial delay of about 30 min, this being the time taken by the mixture inside the reactor to reach 140-150 °C and to start the dehydration process at a sufficient rate. On the contrary, increasing the heating times besides 90 min, at the expense of more energy consumed, does not increase the urea yield (Table 8.1 and Figure 8.4) as a prolonged heating time has the opposite effect, probably due to secondary reactions of urea, for instance due to guanidine formation:
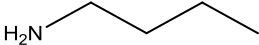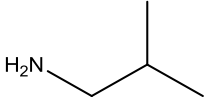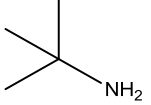
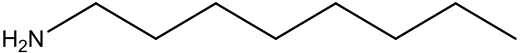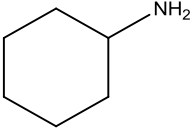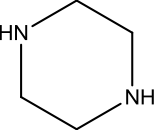$$NH_2CONH_2 + NH_3 \rightarrow (NH_2)_2CNH + H_2O$$
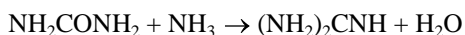
The best compromise between the maximum urea yield and the minimum heating time (*i.e.* the minimum energy consumption), is the 46.6% (average value, ±2) yield after 60 min heating. At the end of each reaction, ^{13}C NMR analysis in D_2O showed no other product besides urea, unreacted carbamate and bicarbonate/carbonate mixture. In particular, no trace of biuret (δ = 158.08 ppm) was found. Presumably, dimerization of urea to biuret requires more time and/or higher pressure than those of our experiments. Pure urea can be easily recovered after the gaseous H_2O, NH_3 and CO_2 were completely removed by heating the reaction mixtures (60 °C) to constant weight. Both gaseous NH_3 and CO_2 obtained from the decomposition of the unreacted reagents can be recovered and recycled. Blank experiments carried out with pure ammonium bicarbonate gave no more than 10% urea, irrespective of heating times in the range 60-120 min.

8.4. From Amines to 1,3-Disubstituted Ureas

The experiments of CO_2 capture by non-aqueous amines were performed with 3.0 mol dm^{-3} solutions of the amines reported in Table 8.2 in bis(2-ethoxyethyl)ether (diethylene glycol diethyl ether, DEGDEE), 2-ethoxyetanol (ethylene glycol monoethyl ether, EGMEE) or 3-pentanone (diethyl ketone, DEK).

Table 8.2. Abbreviation, name and formula of the tested amines.

NBA	*n*-butylamine	
IBA	isobutylamine	
TBA	*tert*-butylamine	
NOA	*n*-octylamine	
CHA	cyclohexyl amine	
PZ	piperazine	

The choice of the diluents was due to fulfil the main requirement of the insolubility of the carbonated compounds.

In anhydrous solvents, CO_2 reacts with an excess of the primary amines NBA, IBA, TBA, CHA and NOA, forming the corresponding carbamates (in equation 14) AmH denotes the amine)

$$2AmH + CO_2 \rightarrow AmCO_2^- + AmH_2^+ \qquad (14)$$
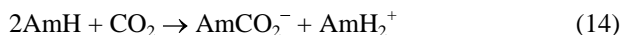
with a theoretical loading capacity of 0.5.

The loading capacity measured by gravimetry (see Section 3.2.1) ranges between 0,48 of NOA to 0.58 of IBA (Table 8.3), near to the expected theoretical value. The experimental values slightly greater than 0.5 may be ascribed to a small physical absorption by the organic solvents. The much lower loading of TBA, 0.27, was likewise due to the to the steric hindrance of the *tert*-butyl group at the amine function that is disadvantageous to the insertion of CO_2 and to the carbamate stability, thus disfavouring the reaction rate and the carbonatation equilibrium; the same occurs, but at a lower extent, to CHA featuring a 0.42 loading. The considerably greater value of 0.96 loading of PZ was ascribed to the two secondary amine groups which promoted a different reaction mechanism (see later). The ^{13}C NMR spectra of the different carbamates of the primary amines dissolved in $CDCl_3$, display couples of resonances ascribed to the same carbon atoms of amine carbonate and protonated amines in the range 13.31-49.06 ppm. The low intensity resonance of the carboxylated group, $-CO_2^-$, was found in the range 162.28-164.30 ppm. As an example, we report here the ^{13}C NMR spectrum of the NBA carbamate compared to that of pure amine (Figure 8.5 A and 8.5 B). As shown in Figure 8.5 B, the couple of resonances at 12.96 and 13.19 ppm ($-CH_3$), 19.37 and 19.53 ppm, 29.81 and 32.27 ppm, and 38.64 and 40.88 ppm ($-CH_2$) are ascribable to the carbon atom of both carbamate and protonated *n*-butylamine. The low intensity resonance at 163.05 ppm is readily assigned to the carbon atom of the $-CO_2^-$ group.

Table 8.3. CO_2 loading capacity and average absorption rate of the different amines at 20 °C.

Amine	Solvent	Absorption			Loading [c]
		t (min)	mol CO_2 [a]	rate[b](mol/min)	
NBA	DEGDEE	40	0.49	0.012	0.54
IBA	DEGDEE	70	0.52	0.074	0.58
TBA	DEGDEE	100	0.24	0.0024	0.27
NOA	DEK	40	0.43	0.011	0.48
CHA	DEGMME	150	0.38	0.0025	0.42
PZ	EGMEE	120	0.86	0.0072	0.96

[a] mol CO_2 absorbed; [b] average rate of CO_2 absorption; [c] molCO_2/mol amine
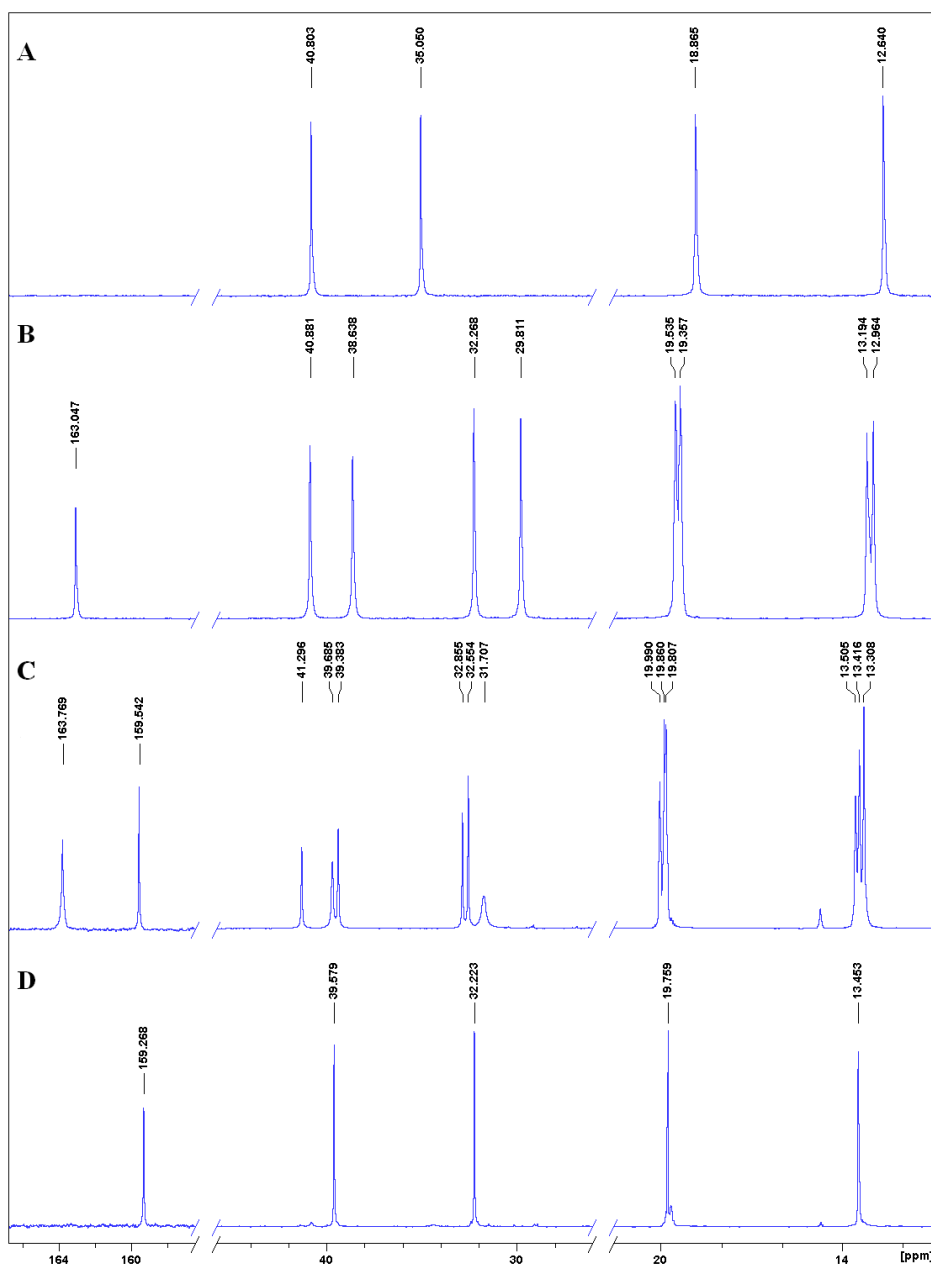
Figure 8.5. ^{13}C NMR spectra of: A) pure NBA; B) NBA carbamate; C) reaction mixture (in D_2O) obtained by heating NBA carbamate for 16 h at 150 °C; D) 1,3-dibutylurea recovered from the reaction mixture by extraction with CHCl$_3$. The intensity of the signals at about 160 ppm are not in scale.

The average rate of carbonatation reaction of the different amines decrease in the order NBA ≈ NOA > IBA > CHA > TBA (Table 8.3) in the same order of the increasing steric hindrance at the amine functionality. The rate of carbonatation of 1,4-diazacyclohexane

(piperazine, PZ) cannot be compared because of the different mechanism of amine carbonatation. The secondary amine PZ contains two basic nitrogen atoms ($pk_b(1)$ = 5.35; $pk_b(2)$ = 9.73 at 20 °C) and, consequently, it may give rise to more equilibria by the reaction with CO_2 (AmN_2H_2 stand for piperazine).

$$2AmN_2H_2 + CO_2 \rightarrow [AmN_2H(CO_2^-)] + [AmN_2H_3^+)] \qquad \text{loading 0.5} \qquad (15)$$

$$3AmN_2H_2 + 2CO_2 \rightarrow [AmN_2(CO_2^-)_2] + 2[AmN_2H_3^+] \qquad \text{loading 0.67} \qquad (16)$$

$$AmN_2H_2 + CO_2 \rightarrow [AmN_2H(CO_2H)] \qquad \text{loading 1} \qquad (17)$$
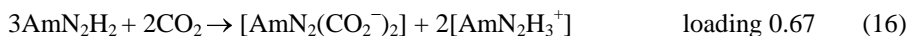
The formation of diprotonated PZ ($AmN_2H_4^{2+}$) should be negligible, on account of the weak acidity of CO_2 (pka = 6.4) as well as of the weak basicity of monoprotonated PZ ($pk_b(2)$ = 9.73). The experimental value of CO_2 loading, 0.96, can be accounted for on the basis of reaction (17), with a much minor contribution of reactions (15) and (16) (overall, less than 10%). The formation of carbamic acid by the reaction of an amine and an excess of CO_2 is quite uncommon, but it has been previously reported in the absence of water (see Chapter 6).

The ^{13}C NMR spectrum in D_2O of the carbonated PZ with an excess of pure CO_2 is reported in Figure 8.6. The spectrum displays four resonances of CH_2 carbon atoms of PZ backbone in the range 40.68 ppm and 43,79 ppm and two much less intense signals at 160.13 ppm and 161.75 ppm. The latter is due to the carbon atom of the fast exchanging $-CO_2^-/-CO_2H$ pair and the signal at 160.13 ppm should be ascribed to HCO_3^- species originating from the hydrolysis of the carbamate in D_2O.
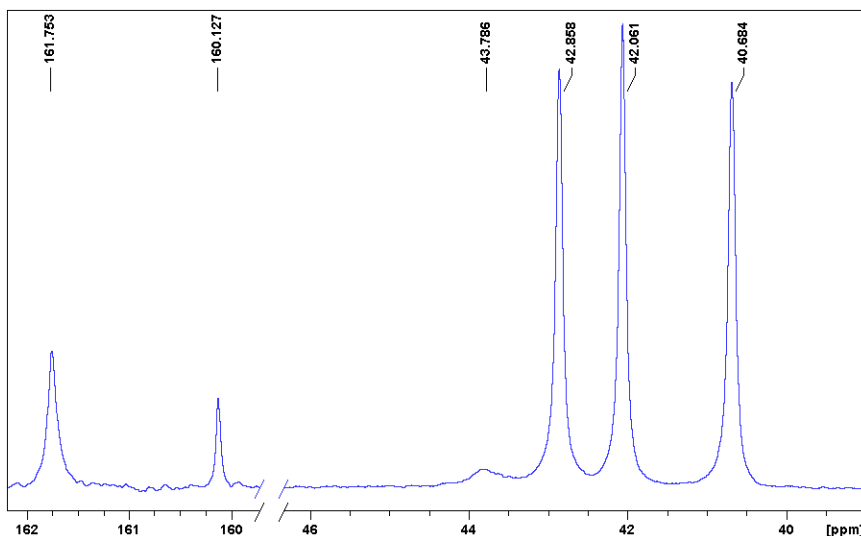

Figure 8.6. ^{13}C NMR spectrum in D_2O of the solid recovered by the PZ carbonatation with an excess of pure CO_2. The intensity of the signals at 160-161 ppm are not in scale.

The two signals at 40.68 and 42.86 ppm (integrated signals in 1/1 molar ratio) are assigned to the two couples of CH_2 carbon atoms of the neutral carbamic acid [$AmN_2H(CO_2H)$] (equation 17), presumably fast exchanging with the zwitterionic form [$AmN_2H_2^+(CO_2^-)$]. The resonance at 43.79 ppm is assigned to the CH_2 carbon atoms of a small amount (about 7%) of the symmetrically substituted bis-carbamate of piperazine. To complete the NMR analysis, the signal at 42.06 ppm is assigned to the carbon atoms of the protonated piperazine. The carbonated PZ was not soluble in the common deuterated organic solvents and, consequently, it was not possible to prevent its hydrolysis in D_2O in the ^{13}C NMR analysis.

The absorption efficiency of the amines was measured with the 15% CO_2 mixture in air and the cyclic absorption-filtration device (Figure 8.1) which allowed the carbonated slurry to be continuously transferred from the absorber to the filtration unit and the filtered liquid to be reclaimed to the absorber. During the experiments of CO_2 absorption no new amine was added to the absorbent solution. Most of the experiments lasted 150-360 min (660 min with the diamine piperazine) and were stopped when no more than 50% of CO_2 was still absorbed by the residual amines in excess with respect to flowed CO_2. The average CO_2 removal efficiency by the different amines in the entire experiment was comprised between 91 and 97% (Table 8.4).

Table 8.4. CO_2 absorption efficiency and percentage of carbamate formation for different amines.

amine	absorption efficiency [a]		CO_2 abs [b] (mol)	carbamate [c] (%)
	t (min)	abs %		
NBA	360	95.8	0.431	95.8
IBA	210	94.9	0.248	55.1
TBA	150	90.5	0.169	37.6
NOA	300	95.6	0.358	79.6
CHA	260	96.0	0.311	69.2
PZ	660	97.1	0.799	88.8

[a] average absorption efficiency of CO_2 and experiment time; [b] mol of CO_2 absorbed; [c] yield of carbamate with respect to the 0,90 mol of starting amine.

At the end of each absorption experiment, the solid recovered by filtration was washed and dried before being analysed by ^{13}C NMR spectroscopy that confirmed the formation of the amine carbamates.

The noticeable different absorption times in comparison with similar absorption efficiencies are inversely correlated to the amount of absorbed CO_2 that decreased in the order PZ >> NBA > NOA > IBA > TBA. As the average rate of CO_2 absorption by the different amines was the same (0.0011-0.0012 mol/min), the different amount of

absorbed CO_2 was a consequence of the reaction (14) equilibrium of the different amines. In this respect, NBA exhibits the most favourable equilibrium as the formation of the amine carbamate, computed from the amount of absorbed CO_2, was nearly quantitative with respect to starting amine (Table 8.4). As a matter of fact, when the reaction was stopped, 0.431 mol of CO_2 were absorbed by 0.900 mol of NBA: based on the stoichiometry of reaction (14), 95.8% of the amine was converted into the corresponding carbamate. As expected the least favourable equilibrium occurred with TBA which gave a 37.6 % of amine carbamate.

We looked for the possibility to obtain substituted ureas by the thermal dehydration of amine carbamates with a procedure quite similar to that successfully used for the conversion of ammonium carbamate into urea. To this purpose, 10.0-14.0 g of each amine carbamate and protonated amine ion pair was heated to 150 °C for 5-16 h in a stainless steel sealed reactor equipped with a pressure gauge and a thermocouple. The pressure generated *in situ* by the dehydration (in the reaction (18), R stands for an aliphatic group) and/or decarboxylation of the reagents (reactions inverse to 8-10) was in the range 34–40 bar (Table 8.5).

$$[R-NH-CO_2^-][R-NH_3^+] \rightarrow [R-NH]_2C=O + H_2O \quad (18)$$
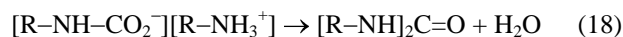
The identification of the species recovered at the end of each reaction was accomplished by ^{13}C NMR analysis. As an example, the ^{13}C NMR spectrum in D_2O of the reaction mixture obtained by heating NBA carbamate for 16 h to 150 °C is reported in Figure 8.5 C. Besides the resonances assigned to the unreacted amine carbamate and protonated amine quite similar to those of the pure compound (Figure 8.5 B), four distinct signals due to the carbon backbone of the dibutyl substituted urea were found at 39.69 ppm, 31.71 ppm, 19.99 ppm ($-CH_2-$) and 13.51 ($-CH_3$). The less intense signal at 159.54 ppm is easily assigned to the carbonyl group ($>C=O$) of substituted urea. Pure 1,3-dibutylurea was recovered from the reaction mixture by extraction with $CHCl_3$, as confirmed by the ^{13}C NMR spectrum in $CDCl_3$ (Figure 8.5 D).

Table 8.5. Average yields of the amine carbamate conversion into the corresponding 1,3-disobstituted urea.

Carbamate of amine	Dehydration reaction			Catalysed dehydration reaction			
	t (h)	P (bar)	Disubstituted Urea (%)	t (h)	P (bar)	Urea (%) CuCl	Urea (%) CuCl$_2$ hydr
NBA	16	34	39	5	40		42
IBA	15	42	30	5	40		
NOA	16	36	31	5	42	44	

To evaluate the relative percentage of the unreacted carbamate and of the substituted urea at the end of the dehydration experiments on the basis of ^{13}C NMR analysis, we carefully integrated the quaternary carbon resonances falling in the range 163.30-164.28 ppm (R$-$CO$_2^-$) and 158.66-159.54 ppm (R$_2$C=O). The percentage of carbamate conversion into the corresponding substituted ureas decreases in the order NBA > NOA ≈ IBA. (Table 8.7). Noticeably, the selectivity of the conversion reaction was 100% as no by-product could be detected from the ^{13}C NMR spectra, besides 1,3-disubstituted ureas and unreacted carbamates. Pure 1,3-disubstituted ureas, as checked by ^{13}C NMR analysis in CDCl$_3$, were recovered from the dehydration mixtures by extraction with CHCl$_3$ and solvent evaporation. In the absence of any solvent and catalyst, the mechanism of amine carbamate conversion into urea should be quite simple and it is depicted in Scheme 8.1.
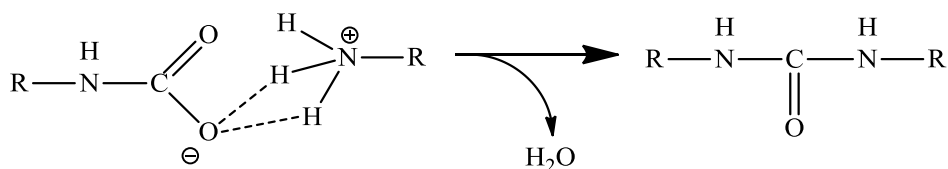
Scheme 8.1. *Proposed mechanism of amine carbamate conversion into the corresponding 1,3-disobstituited urea.*

The dehydration of the TBA and CHA carbamates gave products not sufficiently soluble in the common deuterated solvents to be identified by the ^{13}C NMR analysis. Presumably, the steric hindrance at the amino functionality disfavours the stability of both carbamate and substituted urea and a different reaction could have occurred. No corresponding 1,3-disubstituted urea was recovered from the piperazine carbamate that remained substantially unchanged after 16 h heating at 150 °C. The reaction of two molecules of the neutral carbamic acid of piperazine should likewise have a much greater activation energy than the reaction between one carbamate and one protonated amine depicted in Scheme 8.1 and, consequently, a higher temperature and/or heating time should be necessary to increase the rate of conversion of carbamic acid of piperazine. In our previous study we reported that the thermal conversion of pure ammonium carbamate into urea at relatively low pressure (14 bar at most) was improved by copper(II) catalysts [3]. Therefore, we exploited the feasibility of the thermal conversion of the NBA, NOA and IBA carbamates in the presence of CuCl or

CuCl$_2$·2H$_2$O catalysts. The catalyst (1% on molar scale) substantially decreased the heating time from 15-16 h to 4-5 h, yet attaining a significant increase of the conversion yield (Table 8.5). Each 1,3-disubstituted urea can be easily separated from the catalysed reaction mixture by extraction with a common organic solvent whereas the mixture of unreacted carbamate and the catalysts, after water evaporation and the addition of new carbamate, is ready to be recycled.

8.5.   Conclusions

The non-conventional concept of CO$_2$ capture combined with the production of valuable commodity chemicals such as urea and 1,3-disubtituded ureas provides a technique that should have the potential of circumventing the main disadvantages of traditional CO$_2$ absorption processes based on either aqueous amines or ammonia, namely the high-energy consumption of amine regeneration and the costs associated to avoid the ammonia loss and its separation from CO$_2$ in the regeneration step. The efficient absorption of CO$_2$ by water-ethanol ammonia or by some non-aqueous amines and the recovery of solid mixtures of either ammonium carbamate and bicarbonate or carbamates of the protonated amines, make their thermal conversion into urea and, respectively, 1,3-disubstituted ureas a feasible process with reasonable yields (30-50%). This procedure could offer potential advantages in terms of energy saving in urea manufacture as it avoids the energy penalty of the high pressure (150-250 bar) and temperature (180-240 °C) reactions, and of CO$_2$ purification by amine scrubbing affecting the conventional processes of urea production. The thermal conversion of amine carbamates into 1,3-disubstituted ureas is a milder and greener route to the synthesis of these valuable intermediates as it avoids the unsafe chemicals or the expensive catalysts of the conventional syntheses. Quite interestingly, the use of inexpensive copper catalysts increased the yield of the 1,3-disubstituted ureas.. We must admit that the conversion of CO$_2$ into commercial products does not significantly reduce the anthropogenic CO$_2$ emissions (billions of metric tons for year) but it can contribute to reduce the cost of biogas and natural gas cleaning, hydrogen and ammonia production, and of all the processes where the separation of CO$_2$ from other gases is unavoidable.

8.6.   References

[1] F. Mani, M. Peruzzini, P. Stoppioni. Combined Process of CO_2 Capture by Potassium Carbonate and Production of Basic Zinc(II) Carbonates: CO_2 Release from Bicarbonate Solutions at Room Temperature and Pressure. Energy & Fuels, 2008, 22, 1714–1719.

[2] F. Mani, M. Peruzzini, F. Barzagli. The Role of Zinc(II) in the Absorption-Desorption of CO_2 by aqueous NH_3, a Potentially Cost-Effective method for CO_2 Capture and Recycling. ChemSusChem, 2008, 1, 228-235.

[3] F. Barzagli, F. Mani, M. Peruzzini. From greenhouse to feedstock : formation of ammonium carbamate from CO_2 and NH_3 in organic solvents and its catalytic conversion into urea under mild conditions. Green Chem., 2011, 13, 1267-1274.

[4] F. Bigi, R. Maggi, G. Sartori. Selected syntheses of ureas through phosgene substitutes. Green Chem., 2000, 2, 140–148.

[5] B. Gabriele, G. Salerno, R. Mancuso, M. Costa. Efficient Synthesis of Ureas by Direct Palladium-Catalyzed Oxidative Carbonylation of Amines. J. Org. Chem., 2004, 69, 4741–4750.

[6] J.A. Shimshoni, M. Bialer, B. Wlodarczyk, R.H. Finnell, B. Yagen. Potent Anticonvulsant Urea Derivatives of Constitutional Isomers of Valproic Acid. J. Med. Chem., 2007, 50, 6419–6427.

[7] H.Q. Li, T.T. Zhu, T. Yan, Y. Luo, H.L. Zhu. Design, synthesis and structure–activity relationships of antiproliferative 1,3-disubstituted urea derivatives. Eur. J. Med. Chem., 2009, 44, 453–459.

[8] D.W. Kim, E.S. Huh, S. Do Park, L.V. Nguyen, M.D. Nguyen, H.S. Kim, M. Cheong, D.Q. Nguyen. Methoxycarbonylation of Aliphatic Diamines with Dimethyl Carbonate Promoted by in situ Generated Hydroxide Ion: A Mechanistic Consideration. Adv. Synth. Catal. 352 (2010) 440–446.

[9] H. Babad, A.G. Zeiler. Chemistry of phosgene. Chem. Rev., 1973, 73, 75–91.

[10] A.F. Hegarty, L.J. Drennan, Comprehensive Organic Functional Group Transformations, Pergamon, New York (1995).

[11] D.J. Dìaz, A.K. Darko, L.McElwee-White. Transition Metal-Catalyzed Oxidative Carbonylation of Amines to Ureas. Eur. J. Org. Chem., 2007, 27, 4453-4465.

[12] A.G.M. Barrett, T.C. Boorman, M.R. Crimmin, M.S. Hill, G. Kociok-Kohn, P.A. Procopiou. Heavier group 2 element-catalysed hydroamination of isocyanates. Chem. Comm., 2008, 5206-5208.

[13] F. Shi, Y.Q. Deng, T.L. SiMa, J.J. Peng, Y.L. Gu, B.T. Qiao. Alternatives to Phosgene and Carbon Monoxide: Synthesis of Symmetric Urea Derivatives with Carbon Dioxide in Ionic Liquids. Angew. Chem., Int. Ed., 2003, 42, 3257-3260.

[14] F. Shi, Q.H. Zhang, Y.B. Ma, Y.D. He, Y.Q. Deng. From CO Oxidation to CO_2 Activation: An Unexpected Catalytic Activity of Polymer-Supported Nanogold. J. Am. Chem. Soc., 2005, 127, 4182-4183.

[15] A. Ion, V. Parvulescu, P. Jacobs, D. De Vos. Synthesis of symmetrical or asymmetrical urea compounds from CO_2 via base catalysis. Green Chem., 2007, 9, 158-161.

[16] D-L. Kong, L-N. He, J-Q. Wang. Synthesis of Urea Derivatives from CO_2 and Amines Catalyzed by Polyethylene Glycol Supported Potassium Hydroxide without Dehydrating Agents. Synlett., 2010, 1276-1280.

[17] T. Jiang, X.M. Ma, Y.X. Zhou, S.G. Liang, J.C. Zhang, B. X. Han. Solvent-free synthesis of substituted ureas from CO_2 and amines with a functional ionic liquid as the catalyst. Green Chem., 2008, 10, 465-469.

[18] L. Han, S.W. Park, D.W. Park. Silica grafted imidazolium-based ionic liquids: efficient heterogeneous catalysts for chemical fixation of CO_2 to a cyclic carbonate Energy Environ. Science, 2009, 2, 1286–1292.

[19] Y.N. Shim, J.K. Lee, J.K. Im, Q.N. Dinh, M. Cheong, H.S. Kim. Ionic liquid-assisted carboxylation of amines by CO_2: a mechanistic consideration. Phys. Chem. Chem. Phys., 2011, 13, 6197–6204.

[20] Z-Z. Yang, Y-N. Zhao, L-N. He. CO_2 chemistry: task-specific ionic liquids for CO_2 capture/activation and subsequent conversion. RCS Advances, 2011, 1, 545-567.

[21] B. Rumpf, F. Weyrich, G. Maurer. Enthalpy Changes upon Partial Evaporation of Aqueous Solutions Containing Ammonia and Carbon Dioxide. Ind. Eng. Chem. Res., 1998, 37, 2983-2995.

[22] O. Brettschneider, R. Thiele, R. Faber, H. Thielert, G. Wozny. Experimental investigation and simulation of the chemical absorption in a packed column for the system NH_3–CO_2–H_2S–$NaOH$–H_2O. Separ. Purific. Tech., 2004, 39, 139-159.

[23] F. Mani, M. Peruzzini, P. Stoppioni. CO_2 absorption by aqueous NH_3 solutions: speciation of ammonium carbamate, bicarbonate and carbonate by a ^{13}C NMR study. Green Chem., 2006, 8, 995–1000.

9. The Chemistry of Resorcinol Carboxylation and its Possible Application to CO_2 Removal from Exhaust Gases

9.1. Introduction

In this section are reported the results of the experimental studies addressed to investigate the chemistry and the efficiency of the CO_2 reaction with resorcinol (1,3-dihydroxy benzene) in different operational conditions. The insertion of CO_2 into the aromatic ring has been reported to occur in refluxing aqueous potassium bicarbonate and CO_2 at atmospheric pressure affording the β-resorcylic acid (2,4-dihydroxy benzoic acid) [1,2]. Moreover, the carboxylation reaction of resorcinol was reported to be reversible [3]. The β-resorcylic acid is an useful intermediate for the industrial production of pharmaceuticals, cosmetic preparations, reprographic materials, dyestuffs and fine chemicals, and experimental studies have been recently addressed to improve the production of the β-resorcylic acid [4,5].

Two different experimental procedures were designed: *i*) batch experiments of CO_2 absorption as a function of the different experimental conditions in order to investigate the chemistry of resorcinol carbonatation and to maximize the conversion efficiency into β-resorcylic acid; *ii*) continuous cycles of simultaneous CO_2 absorption and resorcinol regeneration aimed at exploiting the CO_2 absorption efficiency from a simulated flue gases. The CO_2/resorcinol equilibria were analyzed by ^{13}C NMR spectroscopy to identify and quantify the carbonated species in solution originated from resorcinol carbonatation. The capacity of CO_2 uptake by resorcinol upon oxidation was also investigated.

9.2. General Experimental Information

All reagents were reagent grade. Resorcinol, β-resorcylic acid, glycerol, KOH, KHCO$_3$, K$_2$CO$_3$ (Sigma-Aldrich) were used as received without further purification. Pure CO_2, 12% CO_2 in N$_2$, 15% CO_2 in air were used to simulate flue gas.

Most of the experiments were performed by using solutions of resorcinol 2.0 mol dm^{-3} and either single KOH, KHCO$_3$, K$_2$CO$_3$ or their mixtures in a mixture of glycerol (1,2,3-propantriol) and water 1:1 (v/v) and CO$_2$ 100%, 15% or 12% (v/v). The choice of the solvent was dictated by two main constraints: *i)* solubility in water of both the reagents and the products, otherwise a mixture of the potassium salts of the carbonated compounds would crystallize; *ii)* the high temperatures of the experiments up to 170 °C required the high boiling temperature of glycerol.

The batch experiments were carried out at room pressure with the apparatus already described in Section 3.2.1. The absorber was charged with 0.100 dm^3 of 2.0 mol dm^{-3} resorcinol solution in a 1/1 (v/v) glycerol/water mixture. KOH, KHCO$_3$ or K$_2$CO$_3$, separately, were used with a resorcinol/base molar ratio in the range 1/1-1/2. Pure CO$_2$ or a gas mixture containing 12% (v/v) CO$_2$ in N$_2$ at 1.0 bar flowed continuously through the gas diffuser at the bottom of the absorber at a flow rate of 14 dm^3 h^{-1}.

The release of pure CO$_2$ during the desorption processes was followed using a gastight apparatus as described in Section 3.2.2.

In order to test the carboxylation efficiency of the oxidized resorcinol, pure CO$_2$ and air were alternatively introduced into the alkaline solution heated at 130 °C. Each flux lasted 1 h and was repeated four times.

The apparatus and the technique used for continuous absorption-desorption cycles has been already described in the Section 3.2.3. The desorption of CO$_2$ and the resorcinol regeneration were performed in a 0.500 dm^3 flask where the solution was stirred with a magnetic stirring to accelerate the CO$_2$ release and was maintained at 170 °C using a thermostatted silicone oil bath. Both absorber and desorber were equipped with a water cooled condenser to reflux the possible overhead vapor. The entire apparatus was charged with 0.400 dm^3 of the alkaline resorcinol solution. The gas mixture (15% CO$_2$ in air) was continuously fed into the bottom of the absorber with a flow rate of 12.2 dm^3 h^{-1} (0.0750 mol of CO$_2$ at 24 °C). The vent gas exited from the top of the absorber. The outlet gas was purified before being analyzed by the gas chromatograph. A complete cyclic experiment lasted 24-36 h and it was stopped when the reactions of CO$_2$ capture and resorcinol regeneration were equilibrated to each other. The ^{13}C NMR spectra of the solutions were obtained as previously described in Section 3.3.

9.3. Batch Experiments of CO$_2$ Absorption and Desorption

The experiments of CO$_2$ (1 bar) capture were performed with 0.100 dm^3 of the 2.0 mol dm^{-3} solution of resorcinol in a 1/1 (v/v) glycerol/water mixture and, separately, KOH, KHCO$_3$ or K$_2$CO$_3$ with a base/resorcinol molar ratio 1, 1.5, 2. The exothermic reaction of resorcinol with CO$_2$ in alkaline solution (in equation 1 the base is K$_2$CO$_3$) is slow at room temperature and, consequently, the reactions were performed at temperatures in the range 90-140 °C.

$$+ \; CO_3{}^{2-} + CO_2 \; \rightleftharpoons \qquad\qquad + \; HCO_3{}^{-} \qquad (1)$$
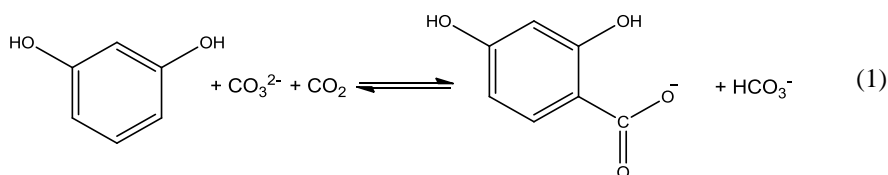
The results of the reaction (1) at 90 °C with the different bases as a function of resorcinol/base molar ratio and reaction time are reported in Table 9.1. For the sake of simplicity, through the text β-resorcylic acid stands for the equilibrating protonated and deprotonated β-resorcylic acid.

Table 9.1. Yield of resorcinol conversion into β-resorcylic acid in the absorption step (1.0 bar of CO$_2$; 90 °C) with the different bases; percentage of β-resorcylic acid (Res-CO$_2^-$) that was left in solution after desorption (150 °C), as a function of the base/resorcinol ratio and of the reaction time. The resorcinol concentration was 2.0 mol dm^{-3} and the percentages are referred to the starting resorcinol.

Base	Base/Res[a] molar ratio	conversion % absorption [b]			% Res-CO$_2^-$ desorption [c]		
		1h	2h	3h	1h	2h	3h
KOH	1	16	23	29	16	6	4
	1.5	12	24	31	18	14	12
K$_2$CO$_3$	1	9	26	38	28	20	17
	1.5	37	50	57	40	33	27
	2	40	49	56	48	43	42
KHCO	1	3,6	8,5	16	16	11	9
	1.5	8	22	35	30	20	16
	2	11	28	41	36	25	21

[a] molar ratio between the base and resorcinol
[b] percentage of resorcinol conversion at the end of each hour
[c] percentage of β-resorcylic acid at each desorption step

The carbonated species in solution were analysed by means of ^{13}C NMR spectroscopy displaying resonances in the range 172-105 ppm easily ascribed to the carbon atoms of the aromatic ring of both resorcinol and β-resorcylic acid.

The low-intensity resonance at about 176 ppm was assigned to the fast exchanging $-CO_2^-/CO_2H$. of both protonated and deprotonated β-resorcylic acid that are fast exchanging on NMR scale. To complete the ^{13}C NMR picture the two resonances at 72.09 and 63.53 ppm were ascribed to the carbon atoms of glycerol backbone and the resonance in the range 161-165 ppm to the fast exchanging CO_3^{2-}/HCO_3^-. No other product was detected in the NMR spectra, and no appreciable amount of either γ-resorcylic acid (2,6-dihydroxy benzoic acid) or glycerol carbonate was found. In particular, the $R-OCO_2^-$ resonance of the glycerol carbonate expected at 159 ppm [6] was not detected. As an example, the spectrum of CO_2 saturated solution of 1.5 K_2CO_3/resorcinol is reported in Figure 9.1.
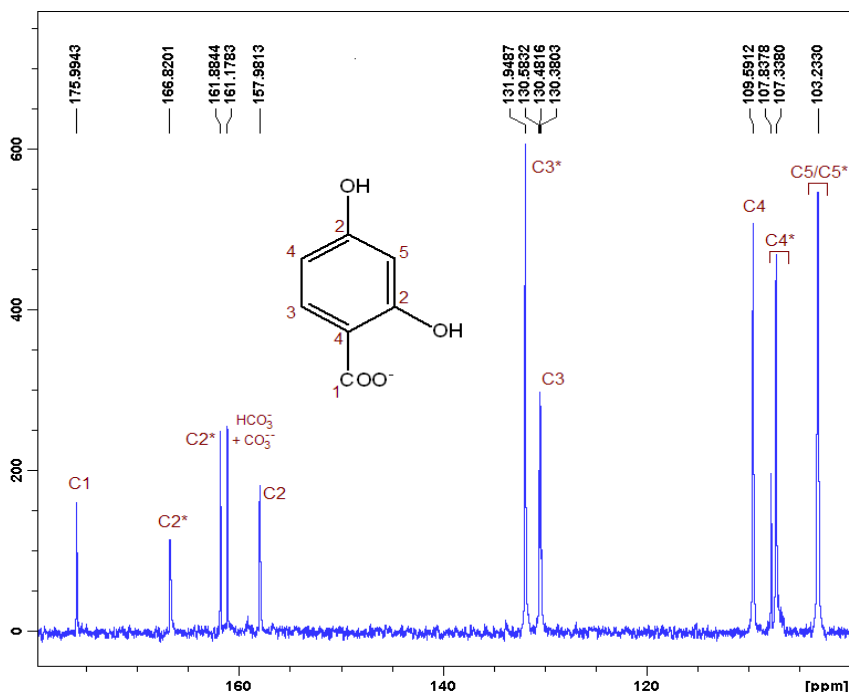

Figure 9.1. ^{13}C NMR spectrum of the CO_2 saturated (3 h) solution of resorcinol/K_2CO_3.1/1.5 molar ratio. The asterisks denote the chemical shifts of the ring carbons of the fast exchanging protonated and deprotonated β-resorcylic acid. The assignment refers to the arbitrary numbering of the ring carbon atoms in the inset. $HCO_3^- + CO_3^{2-}$ indicates the resonance of the carbon atoms the two fast exchanging species; the resonances of the carbon atoms of glycerol backbone were omitted.

The relative amounts of unreacted resorcinol and β-resorcylic acid have been determined by careful integration of the $C(3)$ corresponding signals (see inset of Figure 3 for carbon numbering) in the range 130-132 ppm. These carbon atoms have the same number of hydrogen directly attached and similar chemical environmental, so that they likely exhibit similar T_1 relaxation times (estimated error 5%) [6-9].The efficiency of the resorcinol carboxylation increased in the order $K_2CO_3 > KHCO_3 \approx KOH$, with increasing the base/resorcinol ratio and reaction time.

The decarboxylation reaction was carried out at 150 °C and its efficiency had an opposite feature with respect to that of the forward reaction (1) (except with time, obviously), as the increased base/resorcinol ratio sets an unavoidable limit to the decarboxylation equilibrium. The efficiency of resorcinol carboxylation as a function of temperature in the range 90–140 °C with the decarboxylation carried out at 150 °C was measured in the systems K_2CO_3/resorcinol and $KHCO_3$/resorcinol 1.5. The results are reported in Table 9.2. Once again, the carboxylation efficiency in the presence of K_2CO_3 is higher than that of $KHCO_3$, for any reaction time and temperature. The increasing yield of β-resorcylic acid with reaction temperature and time indicates that the kinetic constraints of reaction (1) prevail over the thermodynamic ones at temperatures up to 120–130 °C.

Table 9.2. Percentages of resorcinol conversion into β-resorcylic acid formed in the absorption step (90-140 °C; 1.0 bar of CO_2) and of residual β-resorcylic acid (Res–CO_2^-) after desorption (150 °C) as a function of the absorption temperature and the reaction time. The resorcinol concentration was 2.0 mol dm^{-3} and the base/resorcinol molar ratio was fixed at 1.5.

Base	Tabs (°C)	Tdes (°C)	convers. % absorption [a]			% Res-CO_2^- desorption [b]		
			1h	2h	3h	1h	2h	3h
K_2CO_3	90	150	37	50	57	40	33	27
	100	150	37	49	58	50	37	32
	110	150	54	60	61	46	37	35
	120	150	57	58	60	48	37	31
	130	150	58	60	59	39	27	24
	140	150	57	56	57	37	29	26
$KHCO_3$	90	150	8	22	35	30	20	16
	100	150	12	34	44	24	19	15
	110	150	26	43	45	27	19	15
	120	150	35	43	45	27	18	14
	130	150	40	40	40	28	19	15
	140	150	41	42	40	27	18	15

[a] percentage of resorcinol conversion at each one hour step
[b] percentage of residual β-resorcylic acid at each desorption step

In this connection, 58% of β-resorcylic acid was obtained by flowing CO_2 into the resorcinol/K_2CO_3 solution either at 100 °C for 3 h or at 130 °C for 1 h. The reaction rate at 140 °C was sufficient to reach the equilibrium in one hour and the percentage of the carboxylic acid did not substantially change with reaction time.

The decreased carboxylation efficiency of resorcinol/K_2CO_3 from 61% to 57% after 3 hours by increasing the temperature from 110 to 140 °C, was due to the decreasing equilibrium constant of the exothermic reaction (1). The results referred to the resorcinol/K_2CO_3 solution are reported in Figure 9.2.
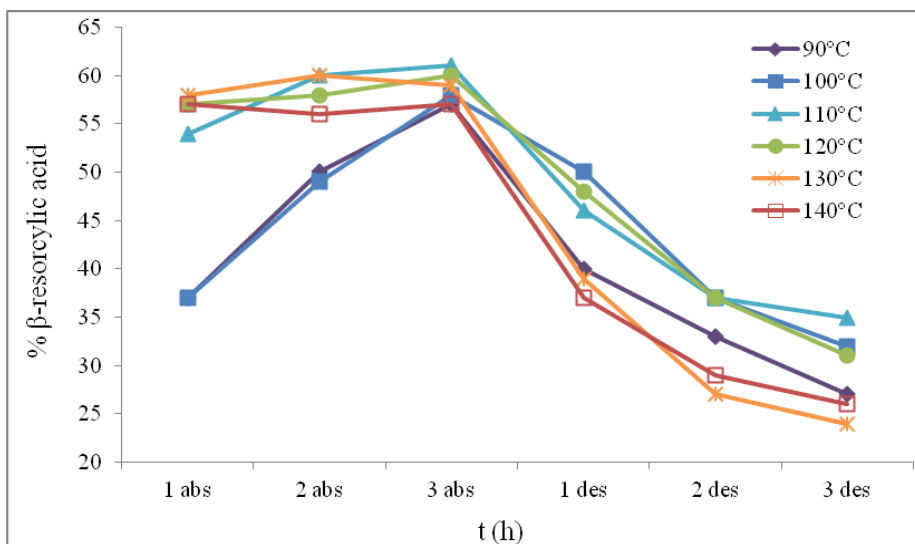

Figure 9.2. Yield of resorcinol conversion into β-resorcylic acid (percentage in mol) at each absorption step (abs; 90-140 °C; 1.0 bar of CO_2) and percentage of residual β-resorcylic in the desorption steps (des) at 150 °C. Absorption and desorption steps are in hours. The resorcinol concentration was 2.0 mol dm^{-3} and the K_2CO_3/resorcinol molar ratio was 1.5.

The figure clearly shows the kinetic constrains of the carboxylation reaction at the lower temperatures (90 and 100 °C) that required more time to attain nearly the same efficiency of the reactions performed at higher temperatures. For comparison purposes with the above mentioned results obtained with 100% CO, the carboxylation efficiency was also investigated either with CO_2 12% (N_2 for balance) or in the absence of CO_2. The experiments were performed with resorcinol 2.0 mol dm^{-3}, base/resorcinol molar ratio 1.5 (base, K_2CO_3 or $KHCO_3$).

The absorption temperature was set at 90, 130 and 170 °C and reaction time 1-5 h. The results are reported in Tables 9.3 and 9.4 and Figures 9.3 and 9.4. As expected, the carboxylation efficiency increased with the increased CO_2 concentration (Table 9.3), but

the β-resorcylic acid was obtained even in the absence of CO_2. Experiments in the absence of CO_2 were carried out at a fixed temperature as a function of heating time (Table 9.4) and at a fixed time as a function of the temperature.

Table 9.3. Carboxylation efficiency at 130 °C (3h heating) as a function of CO_2 concentration. Base/resorcinol 1/1.5.

base	% CO_2		
	100[a]	12	0
	conversion %		
K_2CO_3	59	45	29
$KHCO_3$	40	34	20

[a] values from Table 9.2.

Table 9.4. Carboxylation efficiency at 130 °C as a function of the heating time in the absence of CO_2. Base/resorcinol 1/1.5.

	time, h				
	1	2	3	4	5
	conversion %				
K_2CO_3	34	32	30	28	25
$KHCO_3$	24	22	19	16	14

The carboxylation efficiency at 90 °C increased with time (Figure 9.3) because of the low reaction rate that required more than 3 h for the equilibrium to be reached. At 130 °C the reaction is fast and the equilibrium was reached within 1 h. By further increasing the reaction time, the decarboxylation overcomes the carboxylation and the yield of β-resorcylic acid progressively decreased by emitting CO_2.

The results of the carboxylation experiments in the absence of CO_2 with increasing the temperature, the heating time being fixed at 1 h, are reported in Figure 9.4.
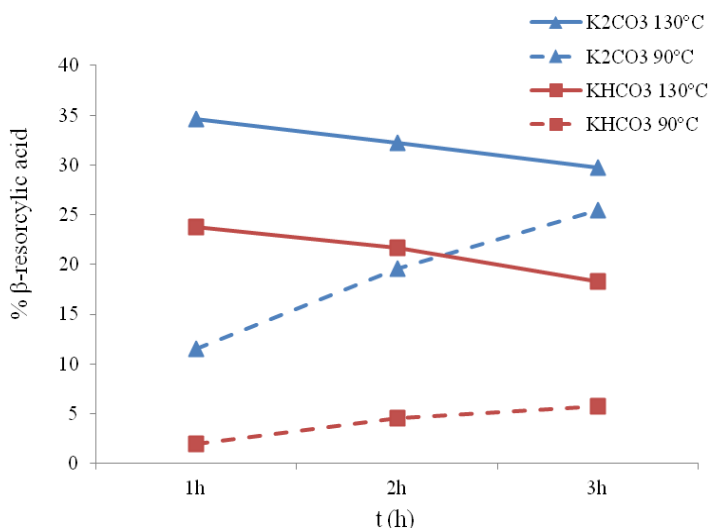

Figure 9.3. Resorcinol conversion into of β-resorcylic acid (percentage in mol) as a function of heating time at 90 and 130 °C in the absence of CO_2. Resorcinol concentration 2.0 mol dm^{-3}, K_2CO_3/resorcinol and $KHCO_3$ resorcinol molar ratio 1.5.
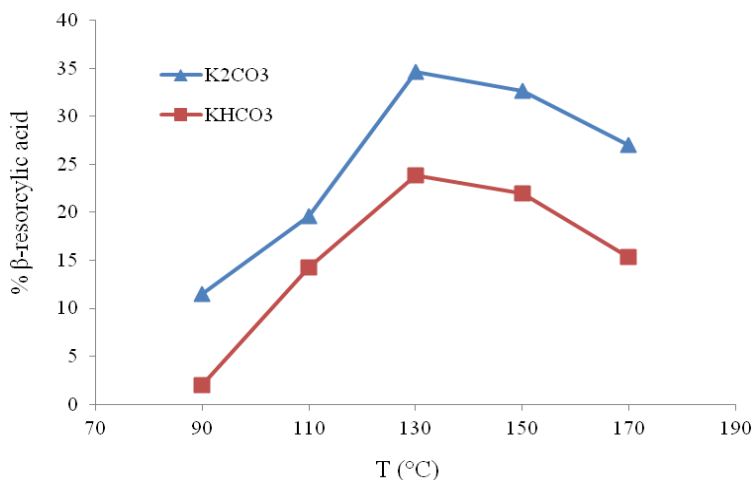
Figure 9.4. Resorcinol conversion into β-resorcylic acid (percentage in mol) as a function of the heating temperature in the absence of CO_2. Heating time fixed at 1 h.

Between 90 and 130 °C the increased rate of carboxylation reaction prevailed over the exothermic equilibrium. At temperatures over 130 °C the equilibrium became increasingly left hand shifted, the percentage of β-resorcylic acid decreased and CO_2 was evolved. Notwithstanding, it should be noticed that about 27% of β-resorcylic acid occurred in the resorcinol/K_2CO_3 solution heated at 170 °C.

9.3.1. The Proposed Mechanism of Resorcinol Carboxylation by K_2CO_3

On the basis of the results previously reported, in particular those obtained with K_2CO_3 in the absence of CO_2, the following pathway of resorcinol carboxylation seems the most plausible, and was reinforced by further experiments (see later).
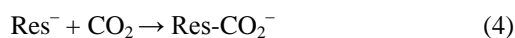
The CO_2 introduction into the aromatic ring was initiated by the resorcinol deprotonation [in eq. (2) ResH stands for the neutral resorcinol]

$$ResH + CO_3^{2-} \rightarrow Res^- + HCO_3^- \qquad (2)$$
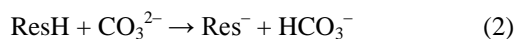
At 90–130 °C the decomposition of HCO_3^- occurred

$$2HCO_3^- \rightarrow CO_3^{2-} + CO_2 + H_2O \qquad (3)$$
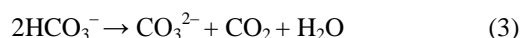
Once formed, CO_2 (at least in part) reacted with deprotonated resorcinol

$$Res^- + CO_2 \rightarrow Res\text{-}CO_2^- \qquad (4)$$

The reaction (3) is endothermic and is favored by the increasing temperature that has an opposite effect on the exothermic equilibrium (4), even if its rate is increased. When the amount of CO_2 formed by reaction (3) overcomes that consumed by the carboxylation

136

reaction (4), the unreacted CO_2 exited from the solution. The overall efficiency of resorcinol carboxylation is a subtle balance of the temperature as high as possible to produce both the maximum amount of CO_2 from the reaction (3) and to enhance the rate of the reaction (4), without too much depressing the reaction equilibrium (4). In summary, the best compromise between the thermodynamic and kinetic constraints accounts for the maximum efficiency of resorcinol carboxylation. According to proposed pathway, the reacting species is CO_2 produced *in situ* by reaction (3) by means of an electrophilic attack to the carbon(−) of the deprotonated resorcinol (Scheme 9.1).

This mechanism explains the lower carboxylation efficiency of resorcinol/KOH with respect to resorcinol/K_2CO_3 in the presence of CO_2 (Table 9.1), despite KOH is much more basic than K_2CO_3. In this experiment, resorcinol was deprotonated by KOH, no CO_2 was produced *in situ* and the gaseous CO_2 introduced into the solution has to be dissolved before to react. Obviously, a higher carboxylation was obtained if the gaseous CO_2 was added to the carbonating HCO_3^- (equation 3 and Table 9.3).
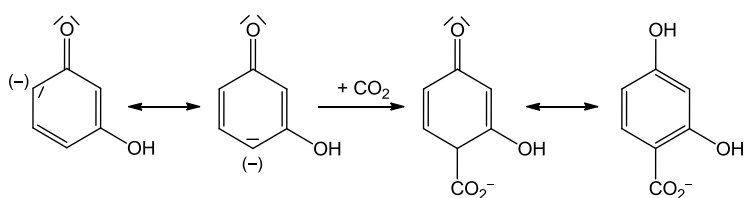
Scheme 9.1. The CO_2 insertion into deprotonated resorcinol in alkaline solution and the formation of β-resorcylic acid.

The crucial role of the *in situ* formation of CO_2 was verified by further experiments in the absence of CO_2. A solution of resorcinol/K_2CO_3/KOH in 1/1/2 molar ratio was heated at 110 °C for 5 h and neither HCO_3^- nor CO_2 could be formed *in situ*: the ^{13}C NMR analysis of the solution did not reveal the formation of the β-resorcylic acid because resorcinol deprotonated by the more basic KOH cannot be carboxylated by CO_3^{2-}. If K_2CO_3 is replaced by $KHCO_3$, it was expected that the solution of resorcinol/$KHCO_3$/KOH would display analogous features of the resorcinol/K_2CO_3. This hypothesis was indeed verified in the cyclic systems of absorption-desorption (Section 9.4). Aqueous solutions of resorcinol undergoes fast aerial oxidation, but quite surprisingly the carboxylation efficiency was in the range 57-60% and did not change appreciably before and after the solution oxidation. The ^{13}C NMR spectra allowed us to identify the β-resorcylic acid (*C*(3), δ = 132.37 ppm) and a small amount (3-5%) of the

γ-resorcylic acid ($C(3)$, $\delta = 134.36$ ppm) that slightly increased with the time of the CO_2 absorption (Figure 9.5).

These results can be explained by the peculiar electronic features of oxidised resorcinol that can produce a nucleophilic carbon atom well suited to react with CO_2 affording β-resorcylic or γ-resorcylic acid.
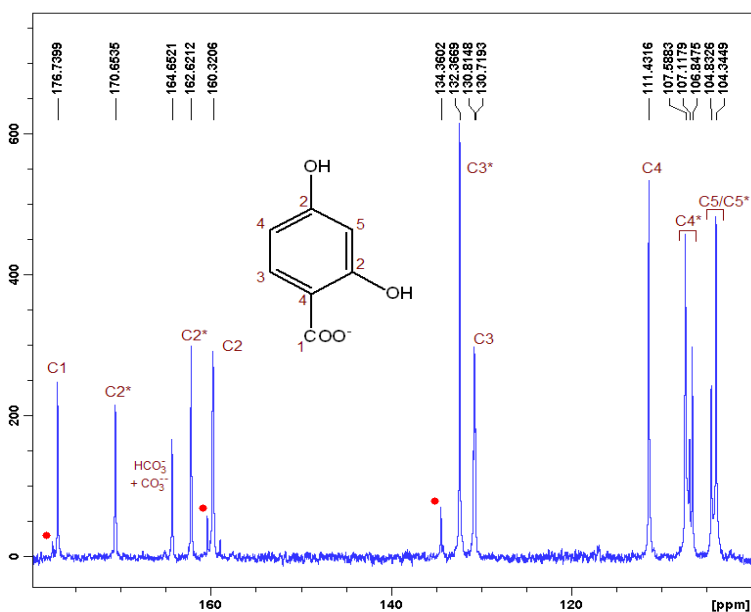

Figure 9.5. ^{13}C NMR spectrum of the CO_2 saturated solution of oxidized K_2CO_3/resorcinol, 1.5 molar ratio. The chemical shift assignment of the carbon atoms is the same of the Figure 3. The red asterisk denotes the chemical shifts of the carbon atoms of γ-resorcylic acid. The C4 and C5 chemical shifts are masked by the more intense signals of β-resorcylic acid.

9.4.   Continuous Cycles of CO_2 Absorption-Desorption

As the batch experiments carried out with a gas mixture of 12 % CO_2 gave a 45 % yield of resorcinol carboxylation, we decided to check whether the alkaline solutions of resorcinol could be feasible absorbents for CO_2 separation and removal from a simulated exhaust gas in continuous cycles of CO_2 absorption and resorcinol regeneration as previously described for alkanolamines [6-9]. In these experiments, the CO_2 loaded and the regenerated resorcinol solutions were continuously circulating at the same rate of 0.300 dm^3 h^{-1} in a closed cycle between the absorber and the desorber. The desorption of CO_2 and the resorcinol regeneration were performed in a flask maintained at 170 °C by a thermostatted silicone oil bath. The experiments were performed with resorcinol

concentration 2.0 mol dm^{-3} and the base/resorcinol 1.5 molar ratio that combines good carboxylation and decarboxylation efficiency. A summary of the operating conditions is reported in Table 9.5.

Table 9.5. Operating conditions in the continuous cycles of absorption-desorption

Resorcinol concentration	2.0 mol dm^{-3}
Base/resorcinol	1.5 on molar scale
Base	K_2CO_3; $KHCO_3$/KOH 1/1; $KHCO_3$/K_2CO_3 1.5/1 (mol/mol)
Solvent	Glycerol/Water 1/1 (v/v)
Volume solution	0.400 dm^3
Gas mixture	15% CO_2 (v/v) in air
Absorption temperature	70-110°C
Desorption temperature	170°C
Liquid flow rate	0.300 dm^3 h^{-1}
Gas flow rate	14 dm^3 h^{-1}

The results of the closed-cycle experiments with different bases and absorption temperatures are reported in Table 9.6. The maximum absorption efficiency was 82 % at 70 °C in the presence of the 1/1 mixture of $KHCO_3$/KOH, and, in general, the CO_2 absorption efficiency decreased on going from 90 °C to 110 °C.

The percentages of β-resorcylic acid contained in the absorber solutions was in the range 33-40 % (average values of four tests), well below those obtained in the batch experiments. The results of these closed-cycle experiments were mainly determined by the low rate of resorcinol carboxylation, as the continuous circulation of the liquid between the absorber and the desorber did not allow the reactions to reach their equilibria.

Table 9.6. CO_2 absorption efficiency and percentage of β-resorcylic acid in the absorber solution as a function of absorption temperature (T_{des} = 170 °C). Overall base/resorcinol molar ratio 1.5.

Base (molar ratio)	T_{abs} (°C)	abs % [a]	% [b] Res-CO_2^-
K_2CO_3	70	74	40
	90	78	37
	110	38	35
$KHCO_3$/KOH (1/1)	70	82	33
	90	79	33
	110	50	26
$KHCO_3$/K_2CO_3 (1.5/1)	70	80	37
	90	80	39
	110	73	27

[a] CO_2 absorption efficiency; [b] average values of four experiments.

Moreover, we should also bear in mind the reaction (3) that adds CO_2 to the 15% CO_2 introduced into the absorbent. Therefore, the lower CO_2 absorption efficiency and the reduced amount of β-resorcylic acid at 110 °C were the consequence of the increasing CO_2 evolution according to the reaction (3) and, respectively, of the reaction equilibrium (4) that was disfavored by higher temperatures. If the amount of CO_2 evolved by reaction (3) becomes greater than CO_2 captured by the reaction (4), the absorption efficiency becomes *negative* and CO_2 was emitted in the absorption step instead of to be captured. The lower absorption efficiency of resorcinol/K_2CO_3 compared to resorcinol/$KHCO_3$/KOH and resorcinol/$KHCO_3$/K_2CO_3 was, presumably, due to the rather inefficient decarboxylation of β-resorcylic acid in the presence of K_2CO_3 even at 170 °C. As a matter of fact, the resorcinol/K_2CO_3 solution once heated at 170 °C in the absence of CO_2 yet contained 27% of β-resorcylic acid (Figure 9.2).

9.5.   Conclusions

This study concerns the chemistry of the CO_2 uptake by resorcinol (1,3-dihydroxy benzene) in alkaline water/glycerol solutions under different experimental conditions with the purpose of unveil the reaction mechanism bridging to maximize the resorcinol conversion into β-resorcylic acid (2,4-dihydroxybenzoic acid). The β-resorcylic acid (mainly, in the deprotonated form) was the sole product of resorcinol carbonatation in alkaline solution and K_2CO_3 was found to be the most efficient base. Noteworthy, the aerial oxidation of resorcinol did not influence the yield of the β-resorcylic acid formation. The batch experiments of CO_2 capture from a 12% gas mixture with the formation of 34% β-resorcylic acid, could be a promising new technique that combines the CO_2 separation from industrial gas mixtures with the production of an useful product. A different approach to CO_2 capture and separation from exhaust gases was the CO_2 absorption and simultaneous thermal resorcinol regeneration carried out in closed cycles. The best result of CO_2 capture (82%) was obtained with the resorcinol/$KHCO_3$/KOH system well below the efficiency of alkanolamines (40-120 °C and 90% efficiency). The main advantages of the resorcinol-based absorbent are the negligible vapour pressure and to be unaffected by aerial oxidation.

9.6. References

[1] J. Thiele, K. Jaeger. Ueber Abkömmlinge des Oxyhydrochinons. Ber. Dtsch. Chem. Ges., 1901, 34, 2837-2842.

[2] D.K. Hale, A.R. Hawdon, I.J. Jones, D.I. Packham. The carboxylation of resorcinol and the separation of β-and γ-resorcylic acid by ion-exchange chromatography. J. Chem. Soc., 1952, 3503-3509.

[3] V.N. Khlebnikov, O.E. Kuznetsov, E.I. Gaitanova, A.Z. Vikkulov. Mechanism of carboxylation of resorcinol with potassium bicarbonate in aqueous-solution. Kinet. Catal., 1991, 32, 1-5.

[4] U. Krtschil, V. Hessel, D. Reinhard, A. Stark. Flow Chemistry of the Kolbe-Schmitt Synthesis from Resorcinol: Process Intensification by Alternative Solvents, New Reagents and Advanced Reactor Engineering. Chem. Eng. Technol., 2009, 32, 1774–1789.

[5] U. Krtschil, V. Hessel, H-J. Kost, D. Reinhard. Kolbe-Schmitt Flow Synthesis in Aqueous Solution – From Lab Capillary Reactor to Pilot Plant. Chem. Eng. Technol., 2013, 36, 1010-1016.

[6] V. Barbarossa, F. Barzagli, F. Mani, S. Lai, P. Stoppioni, G. Vanga. Efficient CO_2 capture by non-aqueous 2-amino-2-methyl-1-propanol (AMP) and low temperature solvent regeneration. RSC Adv., 2013, 3, 12349-12355.

[7] F. Barzagli, F. Mani, M. Peruzzini. A ^{13}C NMR study of the carbon dioxide absorption and desorption equilibria by aqueous 2-aminoethanol and N-methyl-substituted 2-aminoethanol. Energy Environ. Sci., 2009, 2, 322-330.

[8] F. Barzagli, F. Mani, M. Peruzzini. Continuous cycles of CO_2 absorption and amine regeneration with aqueous alkanolamines: a comparison of the efficiency between pure and blended DEA, MDEA and AMP solutions by ^{13}C NMR spectroscopy. Energy Environ. Sci., 2010, 3, 772-779.

[9] F. Barzagli, F. Mani, M. Peruzzini. A ^{13}C NMR investigation of CO_2 absorption and desorption in aqueous 2,2'-iminodiethanol and N-methyl-2,2'-iminodiethanol. Int. J. Greenh. Gas Contr. 2011, 5, 448-456.

List of Abbreviation

AMP	2-amino-2-methyl-1-propanol
BUMEA	2-(butylamino)ethanol
BZMEA	2-(benzylamino)ethanol
CCS	Carbon Capture & Storage
CCU	Carbon Capture & Utilization
CHA	Cyclohexylamine
CP-MAS	Cross Polarization Magic Angle Spinning
DBUA	dibutylamine
DEA	2,2'-iminodiethanol / diethanolamine
DEGDEE	bis(2-ethoxyethyl)ether / diethylene glycol diethyl ether
DEGMME	diethylene glycol monomethyl ether
DEK	diethyl ketone
DGA	2-(2-aminoethoxy)ethanol / diethyleneglycolamine
DHEA	dihexylamine
DIPA	1-(2-hydroxypropylamino)propan-2-ol / diisopropanolamine
DOCA	dioctylamine
DPEA	dipentylamine
DPRA	dipropylamine
EBUA	N-ethylbutylamine
EG	Ethylene Glycol
EGMEE	2-ethoxyethanol / ethylene glycol monoethyl ether
EGR	Enhanced Natural Gas Recovery
EMEA	2-(ethylamino)ethanol
EOR	Enhanced Oil Recovery
GHG	Greenhouse Gas
IBA	1-amino-2-methylpropane / isobutylamine
IPMEA	2-(isopropylamino) ethanol
MEA	2-aminoethanol / monoethanolamine
MDEA	N-methyl-2,2'-iminodiethanol / methyldiethanolamine
MMEA	N-methyl-2-aminoethanol / methylethanolamine
NBA	1-aminobutane / *n*-butylamine
NMR	Nuclear Magnetic Resonance
NOA	1-aminooctane / *n*-octylamine
PrOH	1-propanol
PZ	1,4-diazacyclohexane / piperazine
RET	Renewable Energy Target
RTIL	Room Temperature Ionic Liquid
TBA	2-amino-2-methylpropane / *tert*-butylamine
TBMEA	2-(*tert*-butylamino) ethanol
TEA	Triethanolamine
TPES	Total Primary Energy Supply

List of Publications

F. Barzagli, F. Mani, M. Peruzzini. *Efficient CO_2 absorption and low temperature desorption with non-aqueous solvents based on 2-amino-2-methyl-1-propanol (AMP).* Int. J. Greenh. Gas Contr. 2013, 16, 217-223.

V. Barbarossa, **F. Barzagli**, F. Mani, S. Lai, P. Stoppioni, G. Vanga. *Efficient CO_2 capture by non-aqueous 2-amino-2-methyl-1-propanol (AMP) and low temperature solvent regeneration.* RSC Adv., 2013, 3, 12349-12355.

F. Barzagli, S. Lai, F. Mani. *CO_2 capture by liquid solvents and their regeneration by thermal decomposition of the solid carbonated derivatives.* Chem. Eng. Technol., 2013, 36, No. 11, 1847–1852.

F. Barzagli, S. Lai, F. Mani, P. Stoppioni. *Novel Non-aqueous Amine Solvents for Biogas Upgrading.* Energy Fuels, 2014, 28, 5252-5258.

F. Barzagli, S. Lai, F. Mani. *Novel non-aqueous amine solvents for reversible CO_2 capture.* Energy Procedia, 2014, 63, 1795 – 1804.

F. Barzagli, S. Lai, F. Mani. *A New Class of Single-Component Absorbents for Reversible Carbon Dioxide Capture under Mild Conditions.* ChemSusChem, 2015, 8, 184 – 191.

V. Barbarossa, **F. Barzagli**, F. Mani, S. Lai, G. Vanga. *The chemistry of resorcinol carboxylation and its possible application to the CO2 removal from exhaust gases.* Journal of CO_2 Utilization, 2015, 10, 50–59.

F. Barzagli, F. Mani, M. Peruzzini. *Carbon Dioxide Uptake as Ammonium Carbamates in the Solid State and their Efficient Thermal Conversion into Urea and 1,3-disubstituted Ureas.* Journal of CO_2 Utilization. (Submitted)

F. Barzagli, F. Mani, M. Peruzzini. *A comparative study of the CO_2 absorption in some solvent-free alkanolamines and in aqueous monoethanolamine (MEA).* Int. J. Greenh. Gas Contr. (Submitted)

Acknowledgments

This work would not have been possible without the valued contribution of a number of persons, to whom I would like to express my gratitude.

Especially I would like to express my sincerest gratitude to my "mentor", Professor Fabrizio Mani. I have enormously benefited from his invaluable scientific support, suggestions, comments and continuous encouragement throughout my work with him, and in the writing of this thesis.

A special mention with sincere gratefulness goes to Dr. Maurizio Peruzzini for his continuous suggestions, interesting discussions, support and for giving me the opportunity to work for ICCOM CNR.

To all the other friends and colleagues, who in one way or another have contributed to the success of this work, I would like to express my gratitude.

Lastly, but certainly not least, I express my gratitude to my family for all the support and the permanent encouragement to reach my goals. I dedicate this thesis to you.

For the financial support, I would like to thank DSCTM CNR (Rome), ENEL Ricerca (Rome), Agenzia Nazionale per le Nuove Tecnologie, l'Energia e lo Sviluppo Economico Sostenibile (ENEA, Rome) and STM Technologies (Calvenzano (BG)). Thanks are also expressed to Florence Hydrolab (ECRF) and ENOTRIA CNR projects for supporting this research activity.